



UNIVERSITEIT VAN PRETORIA
UNIVERSITY OF PRETORIA
YUNIBESITHI YA PRETORIA

RAILWAY WHEEL SQUEAL AS A RESULT OF UNSTEADY LONGITUDINAL AND SPIN CREEPAGE

DANIËL JOHANNES FOURIE

A thesis submitted in partial fulfilment of the requirements for the degree of

PHILOSOPHIAE DOCTOR (ENGINEERING)

In the

**FACULTY OF ENGINEERING, THE BUILT ENVIRONMENT & INFORMATION
TECHNOLOGY**

UNIVERSITY OF PRETORIA

November 2018

THESIS SUMMARY

RAILWAY WHEEL SQUEAL AS A RESULT OF UNSTEADY LONGITUDINAL AND SPIN CREEPAGE

DJ FOURIE

Supervisor:	Professor PJ Gräbe
Co-Supervisor:	Professor PS Heyns
Co-Supervisor:	Doctor RD Fröhling
Department:	Civil Engineering
University:	University of Pretoria
Degree:	Philosophiae Doctor (Engineering)

Railway wheel squeal is an unresolved noise challenge facing the railway industry. Of all the noise sources originating from railways, tonal curve squeal is one of the loudest and most disturbing. Wheel squeal results from frictional self-excited vibration occurring in the wheel-rail contact. Solving the problem of squeal requires researchers to work towards an engineering squeal model that can predict squeal comprehensively and in every situation. This will allow for squeal to be resolved during the design stages of new railway systems and railway system components.

In South Africa tonal curve squeal originates from the leading outer and trailing inner wheel-rail contacts of Scheffel self-steering bogies underneath empty freight wagons whilst traversing a 1000 m radius curve. Squeal emanating from the trailing inner wheels is especially problematic, occurring at frequencies between 3.8 and 6.5 kHz with very high intensity. Vehicle dynamics simulations have shown that the combination of worn wheel and rail profiles caused by a wheelset tracking error in the bogie cause affected self-steering bogies to over-steer in the test curve. Over-steering causes both wheelsets of the bogie to displace laterally towards the outside of the curve causing high levels of longitudinal creepage. In agreement with on-track measurements, vehicle dynamics simulations showed that the squealing wheels are subject to predominantly longitudinal creepage with little lateral creepage. In contrast, squeal emanating from the leading outer wheel making contact between the flange throat of the wheel and the rail gauge corner occurs at frequencies above 12 kHz reaching into the ultrasonic range. More familiar in the noise environment, the leading outer wheel in some instances also emitted broadband flanging noise. Experimental evidence suggests that the rubbing

between the wheel flange face and rail gauge face that causes broadband flanging noise provides positive damping to flange contact squeal, reducing the amplitude of the tonal squeal or eliminating it completely.

Mitigation of squeal due to unsteady longitudinal creepage was achieved using a new outer rail profile design. The designed rail profile prevents over-steering of the affected self-steering bogies, eliminating the large longitudinal creepages at the trailing inner wheel necessary for vibrational self-excitation of this wheel.

Modelling the longitudinal creep force and spin creep moment as a feedback loop and testing it for stability using the Nyquist criterion showed that both squeal due to unsteady longitudinal creepage and flange contact squeal can be attributed to mode-coupling instability. Crucial to identifying the instability, was modelling the dynamics of a wheel including the effects of wheel rotation subject to moving load excitation; this captures the cross-coupling dynamics between the normal/longitudinal and normal/spin degrees of freedom that is zero for a stationary wheel. In contrast to the current body of knowledge that does not consider longitudinal and spin creepage as sources of instability for squeal, this study shows that both are important sources of instability for squeal. Thus, it is recommended that a future complete model for curve squeal should include longitudinal and spin creepage and the dynamics of a rotating wheel subject to moving load excitation.


DECLARATION

I, the undersigned hereby declare that:

- I understand what plagiarism is and I am aware of the University's policy in this regard;
- The work contained in this thesis is my own original work;
- I did not refer to work of current or previous students, lecture notes, handbooks or any other study material without proper referencing;
- Where other people's work has been used this has been properly acknowledged and referenced;
- I have not allowed anyone to copy any part of my thesis;
- I have not previously in its entirety or in part submitted this thesis at any university for a degree.

DISCLAIMER:

The work presented in this report is that of the student alone. Students were encouraged to take ownership of their projects and to develop and execute their experiments with limited guidance and assistance. The content of the research does not necessarily represent the views of the supervisor or any staff member of the University of Pretoria, Department of Civil Engineering. The supervisor is not responsible for any technical inaccuracies, statements or errors. The conclusions and recommendations given in the report are also not necessarily that of the supervisor, sponsors or companies involved in the research.

Signature of student:  _____

Name of student: **Danie Fourie** _____

Student number: **14460816** _____

Date: **22 November 2018** _____

Number of words in report: **42 730** _____ words

ACKNOWLEDGEMENTS

To God, Jesus Christ, all the glory! I hope that this research will help set people free that are suffering from the burden of excessive squeal noise.

If I think back on the research contained in this thesis, it has surely been an exciting journey of mixed emotions and continuous learning and unlearning. A journey that I could never have finished without the encouragement, support and dedication offered by many individuals in many different ways.

First and foremost, a special word of thanks to my supervisor Prof Hannes Gräbe, my co-supervisors Prof Stephan Heyns and Dr Robert Fröhling and my line-manager at Transnet Freight Rail Mr Georg Hettasch for the mentorship that they provided during the course of the study. “Mentoring is a brain to pick, an ear to listen and a push in the right direction”, John C. Crossby. Thank you for all of the above and more.

I would also like to express my gratitude for my colleagues at Transnet Freight Rail that assisted during the experimental phases of this study as well as for your words of encouragement. Also a word of heartfelt thanks to Dr Ulrich Spangenberg whom assisted me with the vehicle dynamics simulations for this study. Mechanical Technology within Transnet Freight Rail is without a doubt my home away from home. I am also very grateful for the support, believe and words of motivation offered by my family on a continuous basis.

Last, but not least thank you to my wife Lynnette Fourie and daughter Miané Fourie for being the most wonderful support system in those low moments and always believing in me. For this and much more I can never thank you enough.

TABLE OF CONTENTS

THESIS SUMMARY	I
DECLARATION	III
ACKNOWLEDGEMENTS	IV
LIST OF TABLES	IX
LIST OF FIGURES	X
LIST OF SYMBOLS	XIV
1 INTRODUCTION	1-1
1.1 Background.....	1-2
1.2 Curve squeal	1-3
1.3 Context of current study	1-5
1.4 Objectives of the study	1-6
1.5 Publications	1-7
1.6 Organisation of the dissertation.....	1-7
2 LITERATURE REVIEW.....	2-1
2.1 Mechanisms of frictional self-excitation	2-1
2.2 Railway wheel squeal	2-2
2.2.1 Bogie curving	2-2
2.2.2 Sources of instability responsible for squeal	2-3
2.2.3 Wheel dynamics.....	2-4
2.2.4 Mechanisms responsible for curve squeal	2-7
2.3 Modelling squeal	2-10
2.4 Parameters influencing squeal generation	2-13
2.4.1 Wheelset angle-of-attack	2-13
2.4.2 Wheelset lateral displacement	2-15
2.4.3 Contact friction law/Friction characteristic	2-17
2.5 Field measurements related to squeal	2-18
2.5.1 Key parameters accounted for during field measurements.....	2-19
2.5.2 Source identification of squealing wheel.....	2-20

2.5.3	Key findings of field measurement campaigns.....	2-21
2.6	Guidance from literature.....	2-23
3	EXPERIMENTAL CHARACTERISATION OF RAILWAY WHEEL SQUEAL OCCURRING IN LARGE RADIUS CURVES	3-1
3.1	Field measurements	3-1
3.1.1	Measurement setup	3-1
3.1.2	The Sishen-Saldanha railway line	3-3
3.2	Evaluation of field measurements	3-4
3.2.1	Source of squeal.....	3-4
3.2.2	Bogie curving characteristic	3-8
3.2.3	Longitudinal creepage present in wheel-rail contact of squealing wheel	3-15
3.3	Tracking condition of squealing bogies.....	3-22
3.4	Squeal frequency versus wheel diameter.....	3-28
3.5	Top-of-rail friction modification	3-30
3.6	Flange throat squeal.....	3-30
3.6.1	Flanging/squeal noise and bogie curving.....	3-32
3.7	Discussion.....	3-35
3.7.1	Inner wheel squeal	3-35
3.7.2	Outer wheel squeal	3-35
4	CURVING BEHAVIOUR OF “SQUEALING” BOGIES	4-1
4.1	Vehicle dynamics simulations	4-2
4.1.1	Bogie curving performance	4-5
4.2	Operating point of squealing wheel on Adhesion curve	4-7
4.3	Discussion.....	4-11
5	WHEEL EIGENMODES INVOLVED IN SQUEAL	5-1
5.1	Experimental modal analysis.....	5-1
5.2	Eigenmodes involved in squeal	5-3
5.2.1	Mode shape components of eigenmodes relevant to squeal	5-7
5.3	Finite element modal analysis	5-9
5.4	Discussion.....	5-11
6	FREQUENCY DOMAIN MODEL FOR RAILWAY WHEEL SQUEAL RESULTING FROM UNSTEADY LONGITUDINAL CREEPAGE	6-1
6.1	Frequency domain model using the Nyquist criterion.....	6-1
6.1.1	Unsteady longitudinal creepage.....	6-2

6.2	Wheel model.....	6-4
6.3	Rail model.....	6-7
6.4	Contact spring.....	6-8
6.5	Results	6-9
6.5.1	On-track measured squeal frequencies	6-9
6.5.2	Model results: $k_H = 8 \times 10^8$ N/m.....	6-10
6.5.3	Model results: $k_H = 6 \times 10^8$ N/m.....	6-12
6.6	Wheel type B	6-14
6.7	Discussion.....	6-14
6.8	Frequency domain model using complex eigenvalue analysis	6-15
6.8.1	Validity of model.....	6-19
6.9	Discussion.....	6-19
7	FREQUENCY DOMAIN MODEL FOR RAILWAY WHEEL SQUEAL	
	RESULTING FROM UNSTEADY SPIN CREEPAGE	7-1
7.1	Introduction	7-1
7.2	Modelling of wheel squeal due to unsteady spin creepage.....	7-2
7.2.1	Wheel model.....	7-3
7.2.2	Rail model.....	7-5
7.2.3	Contact spring.....	7-6
7.3	Results	7-6
7.4	Sensitivity Analysis	7-9
7.5	Discussion.....	7-11
8	SQUEAL MITIGATION	8-1
8.1	Improved curving behaviour – Site specific	8-2
8.1.1	Rail profiles	8-3
8.1.2	Bogie curving performance	8-4
8.2	Improved curving behaviour – Long term.....	8-6
8.2.1	Wheelset tracking error.....	8-6
8.2.2	Conformal wheel-rail pair.....	8-7
8.3	Changing wheel and/or track dynamic behaviour	8-10
8.3.1	Wheel damping.....	8-10
8.3.2	Rail damping.....	8-10
8.3.3	Rail pad properties.....	8-10
8.4	Discussion.....	8-11

9	CONCLUSIONS AND RECOMMENDATIONS	9-1
9.1	Conclusions	9-1
9.1.1	Source of instability for squeal	9-1
9.1.2	Mechanism of instability: Unsteady longitudinal creepage.....	9-2
9.1.3	Mechanism of instability: Unsteady spin creepage	9-3
9.1.4	Mitigation: Squeal due to unsteady longitudinal creepage.....	9-3
9.2	Recommendations.....	9-4
9.2.1	Mitigation	9-4
9.2.2	Squeal model	9-4
9.2.3	Future work.....	9-4
10	REFERENCES.....	10-1

LIST OF TABLES

Table 2-1: Key parameters accounted for during field experiments.....	2-19
Table 3-1: Percentage squeal events per trailing wheelset lateral displacement category.....	3-15
Table 4-1: Simulation configuration for scenarios considered	4-4
Table 4-2: Contact parameters from vehicle dynamics simulation.....	4-9
Table 5-1: Estimated squeal frequency versus measured eigenfrequencies	5-5
Table 5-2: Estimated squeal frequency versus eigenfrequencies of mounted wheelset	5-6
Table 5-3: Estimated squeal frequency versus eigenfrequencies of suspended wheelset.....	5-7
Table 6-1: Eigenfrequencies (measured and calculated) and damping ratios for wheel Type A	6-6
Table 7-1: Stability results for empty and loaded contact conditions.....	7-10
Table 8-1: Simulation scenarios	8-4

LIST OF FIGURES

Figure 2-1: Zero-nodal-circle axial modes	2-4
Figure 2-2: Zero-nodal-circle radial modes	2-5
Figure 2-3: Zero-nodal-circle circumferential modes	2-5
Figure 2-4: One-nodal-circle axial modes	2-5
Figure 2-5: Two-nodal-diameter spatially orthogonal axial mode pair	2-6
Figure 2-6: Typical cross sections of railway wheels	2-7
Figure 2-7: Creep force-creepage relationship showing positive, neutral and negative friction characteristics beyond creep saturatio	2-8
Figure 2-8: Observed frequency shift in acoustic signal due to the Doppler Effect	2-21
Figure 3-1: Test setup in test curve	3-2
Figure 3-2: Iron ore train compilation	3-3
Figure 3-3: Aerial image of Elands Bay including 342 wagon train	3-3
Figure 3-4: Identification of squealing wheel from simultaneously measured sound pressure and lateral forces	3-5
Figure 3-5: Estimated wagon speed vs. true wagon speed	3-6
Figure 3-6: Position of leading wheelset with respect to Doppler curve	3-8
Figure 3-7: Lateral force curving signatures	3-9
Figure 3-8: Angle-of-Attack notation	3-10
Figure 3-9: Force convention for lateral track force measurements in test curve	3-10
Figure 3-10: Example curving signatures of 6 randomly chosen inner trailer squeal events	3-12
Figure 3-11: Lateral displacement of bogie trailing wheels	3-13
Figure 3-12: Influence of vertical load on measured lateral load	3-14
Figure 3-13: Vertical force influence on lateral force circuit	3-14
Figure 3-14: Histogram of lateral displacement of squealing wheelsets	3-15
Figure 3-15: Δr vs. y functions of squealing wheelsets ($y \geq 8$ mm)	3-18
Figure 3-16: Contact distribution of target wheel-rail pair	3-19

Figure 3-17: Typical hollow worn shape of No 21 wheel profile on ore line.....	3-19
Figure 3-18: Typical outer wheel profile of squealing wheelset	3-20
Figure 3-19: Squeal outer (black) vs. No 23 wheel profile (red).....	3-20
Figure 3-20: Rolling radius difference functions of four different squealing bogies	3-21
Figure 3-21: Lateral force signature for a healthy bogie on tangent track.....	3-23
Figure 3-22: Bogie tracking error	3-23
Figure 3-23: Lateral force tracking signatures of six squealing bogies on tangent track	3-24
Figure 3-24: Rolling radius difference function mismatch due to + 4 mm TE.....	3-25
Figure 3-25: Prevalent curving signature of squealing bogies on tangent track.....	3-26
Figure 3-26: Wheelset curving positions in a left hand curve	3-26
Figure 3-27: Rolling radius difference functions of trailing bogie of wagon 60 257 881	3-27
Figure 3-28: Squeal frequency vs. wheel diameter for three wheel types used on line	3-29
Figure 3-29: Time/frequency analysis showing squeal for an empty ore train.....	3-31
Figure 3-30: Time/frequency analysis of a portion of a passing loaded ore train	3-32
Figure 3-31: Lateral force curving signature for bogie curving solely using creep forces (empty wagon).....	3-33
Figure 3-32: Lateral force curving signature with flange root contact of the leading outer wheel (empty wagon).....	3-33
Figure 3-33: Lateral force curving signature with flange contact of the leading outer wheel (empty wagon).....	3-34
Figure 3-34: Bogie curving signature for loaded wagon flange contact event	3-34
Figure 4-1: Model of MkV bogie	4-2
Figure 4-2: Graphical depiction of the connections between bodies of the MkV bogie model.....	4-3
Figure 4-3: Assembled CR-13 wagon with two MkV self-steering bogies.....	4-4
Figure 4-4: Bogie curving performance for different scenarios	4-6
Figure 4-5: Wheelset lateral displacement results	4-6
Figure 4-6: Angle-of-Attack results.....	4-7
Figure 4-7: Creepages at squealing wheel-rail contact.....	4-7

Figure 4-8: Adhesion curve assumed for current study	4-11
Figure 5-1: Measurement grid on wheel.....	5-2
Figure 5-2: Mass normalised sinusoidal mode shape components at wheel tread.....	5-3
Figure 5-3: Comparison between wheel eigenfrequencies and squeal frequencies.....	5-4
Figure 5-4: Magnitude of wheel receptances (vertical point and longitudinal point) on wheel tread measured for a 916 mm diameter wheel in relation to squeal frequencies for wheel type A.....	5-4
Figure 5-5: Magnitude of wheel receptances (vertical point and longitudinal point) on wheel tread measured for a 916 mm diameter wheel in relation to squeal frequencies for wheel type B.....	5-5
Figure 5-6: Radial and circumferential mode shape components of eigenmodes most likely to be relevant to squeal	5-8
Figure 5-7: Example mode shapes of the 3D wheel model of wheel type A.....	5-10
Figure 5-8: Modes of vibration of wheel Types A and B identified to be relevant to squeal.....	5-10
Figure 6-1: Feedback loop for squeal model	6-2
Figure 6-2: Sign conventions at wheel-rail interface	6-4
Figure 6-3: Contact point mobilities of wheel including the effects of wheel rotation	6-7
Figure 6-4: Trailing inner wheel, wheel load distribution	6-8
Figure 6-5: Measured squeal frequencies for modelled wheel	6-9
Figure 6-6: Stability chart for a contact position 105 mm from back of flange ($k_H = 8 \times 10^8$ N/m)	6-10
Figure 6-7: Instability regions as a function of the gradient of the adhesion curve.....	6-11
Figure 6-8: Mobility magnitude of Y_{33}	6-12
Figure 6-9: Stability chart for a contact position 105 mm from back of flange ($k_H = 6 \times 10^8$ N/m)	6-13
Figure 6-10: Mobility magnitude (Y_{33}) for different Hertzian contact stiffnesses	6-14
Figure 6-11: System mode involving (2,C) sine doublet mode	6-17
Figure 6-12: System mode involving (2,C) cosine doublet mode	6-17

Figure 6-13: Coalescing modes as a function of equivalent frictional stiffness	6-18
Figure 7-1: Sign conventions at wheel-rail interface: Normal and spin directions.....	7-3
Figure 7-2: Coordinate system: Global (FE model) vs. Local.....	7-4
Figure 7-3: Rotational receptance α_{66} of rotating wheelset at 60 km/h	7-5
Figure 7-4. Normal/Rotational cross receptance α_{36} of rotating wheelset at 60 km/h.....	7-5
Figure 7-5: Nyquist plot of open loop transfer function	7-7
Figure 7-6: Spectrum of real part of loop gain	7-7
Figure 7-7: Denominator of open loop transfer function.....	7-8
Figure 7-8: (3,1) Doublet modes.....	7-9
Figure 7-9: (7,2) Doublet modes.....	7-11
Figure 8-1: Ore line target vs. proposed conformal target.....	8-3
Figure 8-2: Rolling radius difference functions: Transnet Freight Rail No 21 wheelset.....	8-3
Figure 8-3: Bogie curving performance for different scenarios	8-5
Figure 8-4: Wheelset lateral displacement results	8-5
Figure 8-5: Angle-of-Attack results.....	8-5
Figure 8-6: Creepages at squealing wheel-rail contact	8-6
Figure 8-7: Distribution of wheelset tracking error for 342-wagon empty ore train	8-6
Figure 8-8: Contact distribution of TFR No 24 wheel profile and ore line target profile.....	8-7
Figure 8-9: Δr vs y functions for + 4 mm tracking error	8-8
Figure 8-10: Δr vs y functions for - 4 mm tracking error	8-9
Figure 8-11: Rolling radius difference functions: Transnet Freight Rail No 24 wheelset.....	8-9

LIST OF SYMBOLS

A	Ratio of limit friction coefficient at infinite slip velocity to maximum friction coefficient
B	Coefficient of exponential friction decrease
C_{11}	Kalker creepage coefficient
F_0	Quasi-static vertical contact force
G	Shear Modulus
$H(\omega)$	Nyquist contour
K_H	Normal Hertzian contact spring stiffness
K_{L1}	Longitudinal-tangential contact spring stiffness
Q	Wheel load
R	Curve radius
V_0	Rolling velocity
W	Bogie wheelbase
Y	Mobility
a	Contact area half axis of the assumed elliptical contact area in the longitudinal direction
b	Contact area half axis of the assumed elliptical contact area in the transverse direction
f_1	Dynamic longitudinal wheel-rail contact force
f_2	Dynamic lateral wheel-rail contact force
f_3	Dynamic normal wheel-rail contact force
f_a	Observed frequency from Doppler curve before passage of source
f_b	True squeal frequency
f_c	Observed frequency from Doppler curve after passage of source
k	Kalker reduction coefficient
k_A	Reduction factor for adhesion area
k_c	Normal contact spring stiffness
k_S	Reduction factor for slip area
l	Wheelset tapping-to-taping line distance
m	Number of nodal circles
m_3	Dynamic spin moment in wheel-rail contact
n	Number of nodal diameters
r_0	Wheel radius at wheel tapping line
v	Sliding velocity in wheel-rail contact

v	Speed of sound in air (Section 3.2.1)
v_2	Time varying lateral creep velocity
v_s	Source speed (Section 3.2.1)
y	Wheelset lateral displacement
α	Receptance
α	Wheelset angle-of-attack (Section 2.4.1)
β_3	Rolling friction coefficient in spin degree of freedom
ε_1	Gradient of the tangential stress in the contact longitudinal direction
ζ	Modal damping ratio
ζ_{mn}	Modal damping ratio of mode (m,n)
λ_1	Longitudinal creepage
μ	Coefficient of friction
μ_0	Maximum friction coefficient
μ_1	Adhesion coefficient for pure longitudinal creepage
μ_∞	Limit friction coefficient at infinite slip velocity
ν	Poisson's ratio
ψ_{mn}	Mode shape amplitude of mode (m,n)
ω	Circular frequency
ω_{mn}	Natural frequency of mode (m,n)
Δ_r	Wheelset rolling radius difference
Ψ_{mn}	Term in equation for rotating wheel
Ω	Rotational velocity of wheel

1 INTRODUCTION

The dawn of the modern railway age dates back to September 1825 when George Stephenson's Locomotion No. 1 hauled a load of 68 tons along the 34 km track between Shildon and Stockton, United Kingdom. During these early days of railway transport people had little trust in steam locomotion for passenger transit and it was not until September 1830 that the first genuine passenger carrying railway, the Liverpool & Manchester Railway, came into existence (Chant 2007).

Today the world's railways covers a distance in excess of 1 300 000 route-kilometres and is increasingly seen as a transportation mode with an important role to play in sustainable mobility. Sustainable mobility will require the world to break the transport system's dependence on oil by using less and cleaner energy without sacrificing efficiency, convenience and affordability (European Commission 2011).

Railways, being the most environmentally friendly mode of transport for both freight and passenger traffic (Oertli and Hübner 2010) are currently being promoted by European Union policy as well as by that of many other national governments including South Africa. The 2011 white paper on transportation issued by the European Commission (European Commission 2011) states that one of the key goals by 2050 is a 50 % shift of medium distance intercity passenger and freight journeys from road to rail and waterborne transport.

On own turf, South Africa, also realises the important role of rail transport in a sustainable, economical and efficient multi-model transportation system through the National Transportation Master Plan (NATMAP) 2050. 43 % of the total R751.739 billion NATMAP project value will be invested in rail infrastructure (Republic of South Africa Department of Transport 2010).

In spite of its environmentally friendly image, rail transport does influence the environment. The most significant environmental impact of the railways is noise (Oertli and Hübner 2010). In the European context rail transport encounters substantial public opposition to noise in many countries (Verheijen and Elbers 2015). It is therefore crucial that the environmental impact of railways in terms of noise be further reduced to promote the shift from road to rail towards sustainable mobility.

Of all the noise sources originating from railways, tonal curve squeal is one of the loudest and most disturbing. It thus comes as no surprise that the Australian and European rail industries

see squeal as one of their top noise mitigation priorities and an important area for future research (Anderson et al. 2008, Wiebe et al. 2011).

Treatments for squeal do exist. The most widely used methods are top-of-rail friction modification and wheel damping (UIC 2013). However, experience with such treatments show variable results from eliminating squeal, to reducing its amplitude and duration to having no effect at all. The inability to predict if a certain technical measure against squeal will eliminate squeal in a particular situation requires each of the measures to be tested on a trial and error basis. This is a costly exercise and doesn't guarantee that a measure will be obtained that completely eliminate squeal from occurring in a particular situation.

The inability to predict which technical measure, if any of the known measures, will be successful in eliminating squeal in a particular situation can be linked to the fact that an engineering model that can predict squeal comprehensively still eludes the railway fraternity. An engineering model that can predict squeal comprehensively on the other hand eludes the railway fraternity as all the parameters influencing squeal are still not fully understood. This is likely a result of the few detailed in-field studies that can be found in the literature describing curve squeal.

Dittrich and Jansen (2015) provide a rather complete list of the parameters which are known or expected to influence squeal. This includes parameters related to the vehicle, track and the environment. Vehicle parameters include speed, bogie wheel base, wheel tread profile, wheel and bogie dynamics as well as wheel damping. Track parameters include the curve radius, track cant and gauge, railhead profile as well as track dynamics. Environmental parameters include moisture, wheel and rail temperature and friction coefficient due to lubricants, dust and iron oxides.

Only a fundamental understanding of all the parameters and underlying mechanisms responsible for squeal will pave the way for avoiding squeal, if possible, by appropriate vehicle and/or track design – this is the ultimate goal.

1.1 BACKGROUND

The specific focus of the study was to identify the parameters and mechanisms influencing squeal generation in large radius curves. Squeal occurring in large radius curves was chosen as the unit of analysis, due to the existence of a noise ordinance between Transnet SOC Ltd. and the community of Elands Bay next to the Sishen-Saldanha railway line in South Africa. The noise ordinance is a result of squeal being emitted by some of the wagon wheels underneath heavy haul iron ore trains in the two 1000 m radius curves passing through the

town. In addition to squeal occurring in the 1000 m radius curves, the author has also observed squeal on the heavy haul line in curves of radii exceeding 1000 m. Squeal occurring in curves with radii of this magnitude is unheard of in literature and generally occurs exclusively in tight curves of radii smaller than 200 m (Thompson 2009).

In addition, self-steering bogies are used underneath the iron ore wagons. Self-steering bogies are often listed as a possible mitigation measure for squeal (Remington 1987, Thompson 2009, UIC 2013, Thompson et al. 2016).

This disconnect between the current state of the art and practice, sets forth the main argument for an in depth study concerned with identifying the parameters and mechanisms influencing squeal generation in large radius curves.

The aim of the current study is to increase the understanding of the parameters and underlying mechanisms responsible for squeal by experimentally characterising the phenomenon of squeal in field and subsequently developing an analytical/numerical model for its generation. Such a validated squeal model can be used to test alternate measures for squeal mitigation in large radius curves.

Before further contextualising the current study and giving the specific research objectives, a brief overview of squeal is given.

1.2 CURVE SQUEAL

Curve squeal is an instability phenomenon that results from the unstable response of a railway wheel subject to large creep forces in the region of contact between the wheel and rail. The instability is caused by the slip velocity dependent falling friction characteristic of the wheel-rail contact and/or modes coupling of the wheel and rail between different degrees of freedom in the wheel-rail contact (Pieringer 2011). The wheel is excited into vibration at frequencies corresponding to the wheel's normal modes of vibration (Thompson 2009). Predominantly, squeal is excited at the leading inner wheel of a four wheeled bogie subject to large lateral creepage, the squeal frequency corresponding to one of the wheel's axial modes of vibration. Most theoretical squeal models in literature (Rudd 1976, Fingberg 1990, Périard 1998, Heckl and Abrahams 2000, De Beer et al. 2003, Chiello et al. 2006, Pieringer 2011) account specifically for squeal due to unstable lateral creepage excited at the leading inner wheel.

Although the leading inner wheel accounts for most occurrences of squeal, in practice squeal is also excited at the other wheels of a four wheeled bogie (Vincent et al. 2006, Glocker et al. 2009, Fourie 2011, Jiang et al. 2012, Curley et al. 2015, and Jiang et al. 2015a). Some

researchers (Thompson and Monk-Steel 2003, Huang et al. 2008, and Pieringer et al. 2016) have extended the common lateral creepage models to include creepage in the longitudinal and/or spin directions to try and account for squeal occurring at other wheels. Such models have however generally been unsuccessful to account for squeal excited at wheels other than the leading inner. Thompson and Monk-Steel (2003) show that the leading inner wheel making flange contact, subject to large spin and lateral creepage, is most likely to squeal in its radial modes. However flange contact has generally been found to reduce the likelihood of stick-slip due to lateral creepage and that it most likely generates flanging noise (Thompson 2009). On the other hand experimental evidence also exists that shows how rail gauge face lubrication was able to eliminate squeal where the predominant source of instability was contact between the rail gauge corner and the wheel flange throat (Curley et al. 2015). Huang et al. (2008) demonstrate that the trailing wheels in a tight curve subject to large longitudinal creepage, but small lateral creepage are unstable in their fundamental circumferential mode. Because the fundamental circumferential mode generally occurs between 50 and 100 Hz (Grassie and Kalousek 1993), longitudinal creepage is not considered relevant to squeal. Instead longitudinal creepage is considered relevant to corrugation formation. Both models of Monk-Steel and Thompson (2003) and Huang et al. (2008) assume decreasing friction with increasing relative velocity. Pieringer et al. (2016) shows that for a model assuming constant friction that no instability is predicted when the resulting creep force acts in the longitudinal direction independent of the coefficient of friction.

Summarising the above, the conclusion can be drawn that researchers studying squeal are in agreement that unsteady lateral creepage is the dominant cause for squeal generation whilst longitudinal creepage is not considered relevant to squeal. Conflicting evidence exist regarding flange contact as a possible source of instability for squeal; here the exact contact conditions might be important i.e. contact between the rail gauge corner and wheel flange throat or additionally between the rail gauge and wheel flange faces.

Based on the conclusion that unsteady lateral creepage is the dominant cause for squeal generation, the author (Fourie 2011) previously conducted a wayside measurement campaign at Elands Bay based on the hypothesis that the impaired curving ability of self-steering bogies, and curving with excessive lateral creep forces/angles-of-attack, is responsible for the generation of squeal noise in the large radius curves. The results of this measurement campaign in terms of the simultaneous measurement of sound pressure levels and lateral wheel-rail forces subsequently proved this hypothesis invalid.

Instead the results proved that whilst some squeal events emanated from bogies curving with higher lateral forces than expected for the curve, most of the squeal events emanated from

bogies curving with lateral forces close to that expected for the 1000 m radius curve. In neither of the instances were the lateral forces of magnitude to lead to saturated lateral creep conditions.

The measurement results did however prove that the squealing in the 1000 m radius curve can be exclusively attributed to the trailing inner wheel of some bogies underneath empty wagons and that the squealing bogies all curved with the same distinct curving signature. The specific local contact conditions of the squealing wheel could however not be uniquely identified without knowing the lateral displacement of the trailing wheelset with respect to the inner and outer rails of the curve. The curving signature could be interpreted as either the trailing inner or trailing outer wheels making flange contact. If the trailing outer wheel is identified as making flange contact, the trailing inner wheel is subject to predominantly longitudinal creepage given the near radial alignment of the wheelset. Otherwise the trailing inner wheel is subject to flange throat/rail gauge corner contact. The current research is a continuation of the previous research by Fourie (2011) and aims to broaden the understanding of the parameters and mechanisms influencing squeal generation in large radius curves.

1.3 CONTEXT OF CURRENT STUDY

As indicated, a noise ordinance exist between Transnet SOC Ltd. and the community of Elands Bay in South Africa as a result of squeal being emitted by some of the wagon wheels underneath heavy haul iron ore trains in the two 1000 m radius curves passing through the town. This noise ordinance, if not resolved, could be detrimental to the expansion plans to increase the export capacity of South Africa's heavy haul iron ore line to 93 million tons per annum (mtpa) from the current export capacity of 67 mtpa. Expanding the capacity of the ore line is one of the five major investment programmes of Transnet SOC Ltd. and key to the success of its market demand strategy (MDS). The MDS is the centrepiece of the South African government's drive for an infrastructure investment-led economic growth strategy and was introduced on the 9th of February 2012 by South African President Jacob Zuma in his state of the nation address.

Being one of the key programmes of the MDS, it is crucial that the noise ordinance between Transnet SOC Ltd. and the community of Elands Bay doesn't become an Achilles heel to the expansion plans of the Sishen-Saldanha iron ore railway line. This in return makes identifying and subsequently eliminating the root cause of squeal occurring in the large radius Elands Bay curves paramount to the success of expanding throughput on the iron ore railway line.

1.4 OBJECTIVES OF THE STUDY

This thesis presents, (i) an experimental study of the key parameters that influence self-excitation of railway wheels in large radius curves, (ii) a vehicle dynamics model that captures the curving behaviour of squealing bogies, (iii) an analytical model that captures the mechanism of self-excitation responsible for the squeal and (iv) identifying mitigation measures that can successfully reduce or eliminate squeal in large radius curves.

The specific objectives of the study are the following:

- To establish a complete experimental characterisation of the phenomenon of squeal occurring in large radius curves and to identify the parameters that would warrant self-excitation of the wheels. The main parameters that are investigated include, but are not limited to the kinematic parameters and wheel dynamics influencing the generation of squeal in the 1000 m radius curves. This includes quantifying the exact contact conditions prevalent at the squealing wheel-rail contact which could previously not be determined by Fourie (2011) without knowing the lateral displacement of the trailing wheelset.
- The descriptive phase of the study also includes finite element modal analysis as well as vehicle dynamics simulations. Finite element modal analysis is included to ascertain if the wheel modes identified as being involved in squeal have significant out-of-plane vibration that can be linked to the high noise levels associated with squeal, whilst vehicle dynamics simulations are used in an attempt to capture the quasi-static curving behaviour of the “squealing” bogies in the test curves as per the experimental results. It is anticipated that an accurate representation of the quasi-static curving behaviour might yield valuable insights into possible mitigation measures that can eliminate squeal from the test curves.
- Following the descriptive phase of the research, is a modelling phase to capture the underlying mechanism of self-excitation (negative-friction or mode-coupling) that is responsible for squeal in the test curves. It is anticipated that the results of the descriptive phase of the research will influence the mechanism of self-excitation that is modelled in the analytical/numerical phase of the research. Known in advance is that the source of instability of squeal is either longitudinal creepage or wheel flange contact. Whilst longitudinal creepage is not considered relevant to squeal generation by the current state-of-the-art on the topic, different evidence exist in literature about the relevance of flange contact to squeal.

- The last phase of the study is to employ the squeal and vehicle dynamics models in a series of simulation studies to identify mitigation measures to reduce or eliminate squeal in large radius curves.

1.5 PUBLICATIONS

The thesis is based on the following publications. The order of the publications is not sorted according to the date of publication, but instead the order in which they were written.

Fourie, D.J. Gräbe, P.J. Heyns, P.S. and Fröhling, R.D. 2016. Experimental characterisation of railway wheel squeal occurring in large-radius curves. *J of Rail and Rapid Transit*, Vol 230, No. 6, pp 1561-1574.

Fourie, D.J. Gräbe, P.J. Heyns, P.S. and Fröhling, R.D. 2018. Analysis of railway wheel squeal due to unsteady longitudinal creepage using the complex eigenvalue method. Eds Anderson, D. et al. *Noise and Vibration Mitigation for Rail Transportation Systems, NNFM*. Vol 139, pp 57-69.

Fourie, D.J. Gräbe, P.J. Heyns, P.S. Fröhling, R.D. and Spangenberg, U. 2017. New insights into curve squeal mitigation measures. In: Proceedings of the 11th International Heavy Haul Association Conference, Cape Town, South Africa, September 2017: 705-712.

Fourie, D.J. Gräbe, P.J. Heyns, P.S. and Fröhling, R.D. 2018. Frequency domain model for railway wheel squeal resulting from unsteady longitudinal creepage. Manuscript submitted to *J Sound Vib* May 2018.

Fourie, D.J. Gräbe, P.J. Heyns, P.S. and Fröhling, R.D. 2018. Frequency domain model for railway wheel flange contact squeal resulting from unsteady spin creepage. Manuscript to be submitted.

1.6 ORGANISATION OF THE DISSERTATION

The general structure of the thesis is as follows:

Chapter 1 contextualises the current study and demonstrates the need for the study.

Chapter 2 provides guidance from literature for the current study based on the current state-of-the-art on railway squeal noise.

Chapter 3 provides a complete description of the key kinematic parameters influencing squeal generation in the test curve. This description covers both squeal occurring at the leading outer and trailing inner wheels.

Chapter 4 describes the vehicle dynamics simulations that capture the curving behaviour of inner wheel squealing bogies in the test curve using worn wheel and rail profiles. The chapter also presents the typical operating point of the simulated squealing wheel on an adhesion curve assumed for the study.

Chapter 5 identifies the wheel eigenmodes involved in inner wheel squeal and establishes a relationship between the kinematic parameters found to be important to squeal and such eigenmodes.

Chapter 6 presents a frequency domain model for the excitation of inner wheel squeal as well as a qualitative comparison between the model's results and measurements. In this model the time varying part of the creep force is modelled as a feedback loop and tested for stability with the Nyquist criterion. In addition Chapter 6 provides a brief overview of the complex eigenvalue squeal model described in Fourie et al. (2018) and discusses the limitations of such a model.

Chapter 7 presents a frequency domain model for the excitation of flange contact squeal. In this model the time varying part of the spin moment is modelled as a feedback loop and tested for stability with the Nyquist criterion.

Chapter 8 uses the validated squeal model due to unsteady longitudinal creepage and the vehicle dynamics model to evaluate alternate mitigation measures for inner wheel squeal and evaluates these alternates based on the economics and ease of implementation.

Chapter 9 contains the conclusions and recommendations of the study

2 LITERATURE REVIEW

The literature review commences with a broad overview of self-excited vibration. It then narrows down by discussing the creepages introduced during bogie curving and how these creepages act as sources of instability to activate squeal through either mode-coupling or decreasing friction with increasing relative velocity. After the mechanisms responsible for railway wheel squeal are introduced, modelling of squeal is discussed followed by a discussion on the parameters that have a significant influence on the excitation of squeal. Lastly the literature review looks at some studies that are devoted to field measurements of squeal. Conglomerating all of the above, the last section of the literature review provides the guidance for the current study.

2.1 MECHANISMS OF FRICTIONAL SELF-EXCITATION

Self-excited systems begin to vibrate on their own accord at a natural or critical frequency of the system, essentially independent of the frequency of any external stimulus to the vibrating system (Ehrich 2010). Essentially it is the motion of the system that creates or sustains the alternating force responsible for the vibration; when the motion stops the alternating force disappears. In the case of frictional self-excitation the alternating force is established by the friction forces acting between sliding surfaces.

Generally speaking, frictional instability occurs when the friction between sliding surfaces acts as a non-conservative force, providing more energy to a system than it can dissipate from the system. Such instabilities often result in sound radiation from one or both components of the friction pair or from other parts of the system to which the friction pair transmits energy (Akay 2002). A well-known example of the sound radiated due to frictional instability is that of the rubbing of the rim of a wine glass, preferably with a moist finger.

Instabilities in the response to friction usually develop through one of four mechanisms (Akay 2002): (i) geometric instabilities; (ii) material nonlinearities; (iii) thermo-elastic instabilities and (iv) instabilities due to decreasing friction with increasing relative velocity.

Geometric instabilities refer to instabilities caused by frictional coupling between specific dynamic modes of the system with respect to the contact. This is also referred to as mode-coupling instability. For mode-coupling instability it is characteristic that the oscillation frequencies of two structural modes of an undamped system, as a function of the control parameter, come closer and closer together until they merge and a pair of a stable and unstable mode results (Hoffman 2002). Because two normal modes of the system occurring at

different natural frequencies coalesce, the instability manifests itself at a frequency between these natural frequencies.

Frictional instabilities that develop due to material nonlinearities refer to cases where material properties exhibit nonlinear contact stresses which contribute to the instability mechanism.

Thermo-elastic instabilities occur in sliding systems with frictional heating, whereby the frictional heating tend to magnify contact pressure non-uniformity (Zagrodzki 2009). If either the initial temperature distribution is consistent with an unstable mode or there exists a transitional phase where a temperature distribution consistent with an unstable mode is formed, the temperature distribution and induced vibrations grow exponentially.

Instabilities due to decreasing friction with increasing velocity refer to the case where negative damping leads to mode lock-in of a specific fundamental frequency of the system and its harmonics. Only a single structural mode of the system is rendered unstable (Hoffman 2002). The instability manifests itself at a frequency corresponding to that of the structural mode of the system.

2.2 RAILWAY WHEEL SQUEAL

2.2.1 Bogie curving

During the passage of a vehicle through a curve the wheels/wheelsets do not align with the pure rolling position. This deviation from the kinematic rolling position results in the wheel continuously sliding across the railhead to ensure its rolling direction and its speed matches that of the forward motion of the train.

The relative velocities of such motions normalised by the rolling velocity of the wheel are denoted creepages. Creepages are defined in three degrees of freedom in the contact, namely lateral creepage, longitudinal creepage and spin creepage. Longitudinal creepage arises because the outer wheel of a rigid wheelset has a further distance to travel than the inner wheel in a curve and because the conicity of the wheels can only partly compensate for this difference in running distance. Lateral creepage results from curving of the wheel with an angle-of-attack relative to the rail. Spin creepage results when the contact is not perpendicular to the rolling direction. This causes the angular velocity to have a component normal to the inclined contact area.

In large-radius curves the equilibrium curving of bogies are achieved using only the creep forces set-up by such relative motions. Once the bogie loses the ability to steer around a curve by means of only utilising frictional (creep) forces due to exceeding the lateral free play

between the wheel flange and rail, it necessitates that the flange or flange throat of the leading wheel come in contact with the gauge corner of the outer rail to help steer the bogie around the curve.

Flange contact causes the wheel flange to slide over the rail gauge face in addition to the wheel sliding across the railhead due to creepage.

2.2.2 Sources of instability responsible for squeal

It is recognised that it is this relative motion (flange rubbing, lateral creepage and longitudinal creepage) between the wheel and rail during curving that provides the source of instability to develop and sustain the high amplitude tonal singing of a railway wheel referred to as railway wheel squeal (Rudd 1976). Of the three sources of instability, Rudd discounts longitudinal creepage and wheel flange rubbing as mechanisms for squeal, whilst he develops the concept of unsteady lateral creepage into a linear frequency domain model to describe the occurrence of squeal based on bogie wheelbase, curve radius and train speed.

Rudd's main hypothesis for discrediting longitudinal creepage and wheel flange rubbing as mechanisms for squeal was that the excitation forces associated with longitudinal creepage and flange rubbing excite the wheel in its own plane where it is a relatively inefficient radiator of sound. On the other hand lateral creepage excite the wheel normal to its plane where it is an efficient radiator of sound. In reality the wheel's mode shapes contain coupled in-plane and out-of-plane motions such that Rudd's hypotheses for discounting longitudinal creepage and flange rubbing as mechanisms for squeal is not entirely correct.

In addition to the hypothesis stated above, Rudd's conclusion for discrediting longitudinal creepage and flange rubbing as mechanisms for squeal was also based on the following experimental findings: Independently rotating wheels eliminating longitudinal creepage do not necessarily eliminate squeal and because it is the inner wheels in a curve that is responsible for squeal, flange rubbing occurring at the outer wheels is not considered relevant to squeal.

Other researchers have followed similar arguments to eliminate longitudinal creepage and flange rubbing as mechanisms for squeal. Remington (1987) concludes from roller rig tests by Bleedorn and Johnstone (1977 as cited in Remington (1987)) that flange contact reduces the level of squeal noise and that flange contact alone will not produce squeal. Field measurements by Vincent et al. (2006) have similarly shown that no squeal occurs at the outer wheel of the leading wheelset upon flange contact and once more that independent wheels not connected by a common rigid axle do squeal.

Today after almost four decades since Rudd's prediction model, unsteady lateral creepage is still thought to be the main cause of squeal noise (Thompson et al. 2016).

However, recent experimental observations that gauge face lubrication eliminated squeal occurring at the outer wheel in flange contact show that flange contact may contribute to squeal (Curley et al. 2015) although the conditions leading to this situation are still unknown. Here lubrication of the rail gauge corner, rather than just the gauge face was found to be important to eliminate squeal. In addition Zenzerovic (2017) showed that modelling two-point wheel-rail contact can actually be important to capture squealing of curve-outer wheels, although such a model was not validated against experimental results at the time. Here squeal is a result of the dynamic interaction of the two contact points and the presence of two closely spaced wheel modes. This is similar to the model of Squicciarini et al. (2015) who modelled flange-back contact squeal and validated it against on-track measurements.

2.2.3 Wheel dynamics

The normal modes of vibration of a flat circular disc or wheel is characterised by a number of nodal diameters (n) and nodal circles (m). These nodal circles and diameters (points of zero displacement) can occur in any combination for both the in-plane and out-of-plane motion of the circular disc. The disc sustains out-of-plane motion through its axial modes, whilst in-plane motion of the disc is sustained through its radial or circumferential modes.

Figure 2-1 to Figure 2-3 show some examples of the zero-nodal-circle axial, radial and circumferential mode shapes of a flat circular disc respectively, whilst Figure 2-4 introduces the concept of nodal circles by showing some examples of one-nodal-circle axial modes. Positive and negative signs indicate the relative phase of vibration in the different areas of the disc. For the axial modes in Figure 2-1 the vibration is normal to the area of the plate, for the radial modes in Figure 2-2 the vibration is normal to the periphery whilst the vibration is tangential to the disc periphery for the circumferential modes in Figure 2-3.

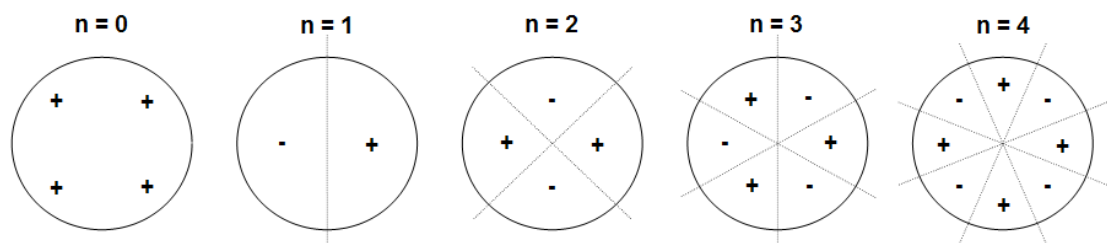


Figure 2-1: Zero-nodal-circle axial modes

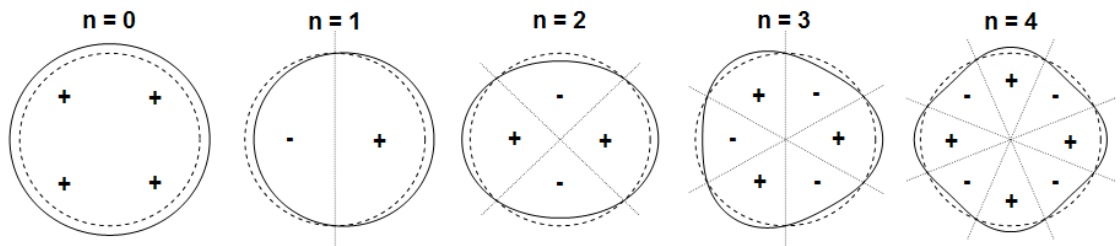


Figure 2-2: Zero-nodal-circle radial modes (--- undeformed shape, —deformed shape)

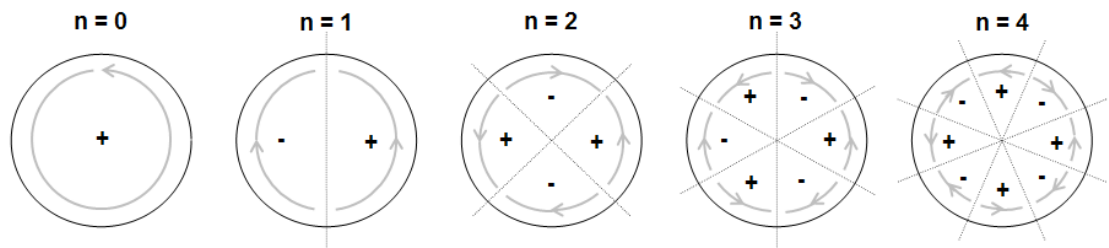


Figure 2-3: Zero-nodal-circle circumferential modes

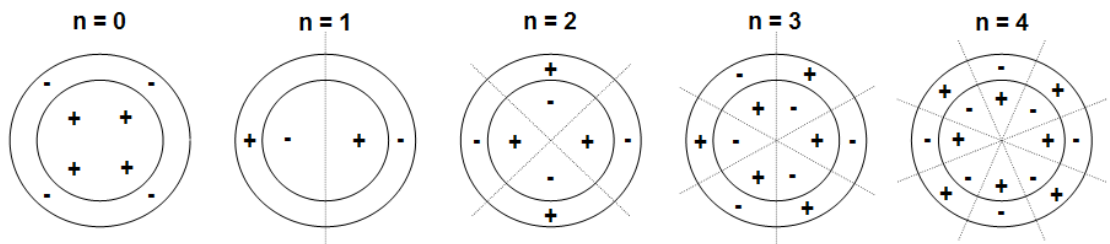


Figure 2-4: One-nodal-circle axial modes

For each mode shape with one or more nodal diameters the mode shapes occur as spatially orthogonal pairs (Stanbridge et al. 2001), with the nodal radii becoming the anti-nodes in the other, and vice versa. As an example, see Figure 2-5 illustrating the two-nodal-diameter orthogonal axial mode pair. It is important to note that the pair of doublet modes is two independent modes of the disc.

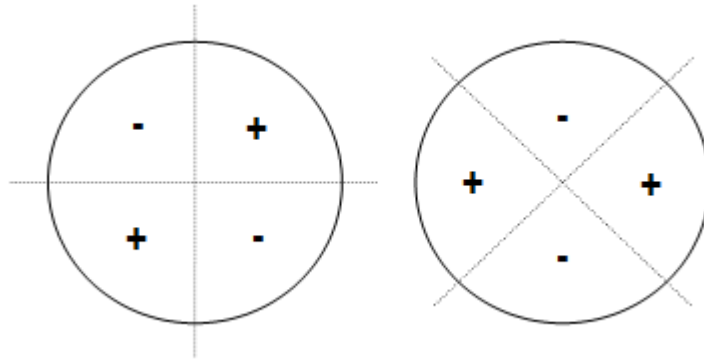


Figure 2-5: Two-nodal-diameter spatially orthogonal axial mode pair

In perfect axi-symmetric structures, the orthogonal mode pair will have identical natural frequencies and the location of nodal lines is arbitrary, being determined by the location of the applied excitation. If however, the axi-symmetry of the structure is broken, there are preferred locations for the nodal diameters and the pair of modes (doublet modes) occurs at slightly different frequencies (Thompson 2009). The symmetry of axi-symmetric structures can be broken when external forces or moments are applied to the structure, the structure is rotated or when features, such as bolt assemblies or geometric imperfections, destroy the rotational symmetry of the axi-symmetric structure (Kinkaid et al. 2003).

The biggest difference between a flat circular disc and a railway wheel is that the cross section of a railway wheel is not symmetric (see Figure 2-6 for typical cross sections of a railway wheel). This asymmetry causes the in-plane and out-of-plane motions to become coupled (Thompson 2009). For example, the one-nodal-circle axial modes and the radial modes are closest in frequency and so experience the greatest degree of coupling. It is thus intuitive that the one-nodal-circle axial modes contain some radial motion and the radial modes some axial motion. The modes of vibration of the wheel are classified according to their predominant motion. This includes axial, radial and circumferential modes, having n nodal diameters and m nodal circles. Axial modes are denoted (n,m) . Radial and circumferential modes with more than 0 nodal circles do not occur in the frequency range of interest (Thompson 2009) and are denoted (n,R) and (n,C) .

For a stationary (non-rotating) wheel in contact with a rail, each sine and cosine doublet mode pair consists of two independent modes of the wheel without coupling in the contact area. This is because the anti-nodes of the one doublet mode become the nodes of the other doublet mode and vice versa.

Thompson (1993) derived the dynamics of a rotating wheel due to the moving load nature of the wheel contact, ignoring gyroscopic effects and centrifugal stiffening. With the rotating wheel being exposed to moving loads, the doublet mode pairs become two complex modes which are rotating in opposite directions, and at frequencies of $\omega_{mn} \pm n\Omega$ (for $n > 0$). ω_{mn} is the rotational natural frequency of mode (n,m) and Ω the rotational velocity of the wheelset. The deformation vector of both these travelling waves are given by $\Psi_{mn} = \Psi_{mn}^I + i\Psi_{mn}^{II}$ in which I represents axial and radial displacements and rotation about the circumferential axis and II represents circumferential displacement and rotations about the radial and axial axis. Because a forward and backward travelling wave exists, the contact point mobility will have two resonance peaks for each natural frequency of the stationary wheel (ω_{mn}). For a non-rotating wheel no structural cross-coupling exists between type I and type II degrees of freedom.

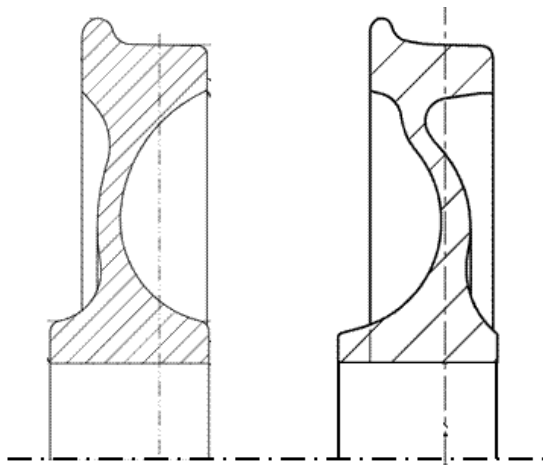


Figure 2-6: Typical cross sections of railway wheels

2.2.4 Mechanisms responsible for curve squeal

The literature describing the instability mechanism responsible for railway wheel squeal identifies two schools of thought, namely (i) negative damping and (ii) mode-coupling.

The classical squeal theory describes the instability mechanism through negative damping introduced to the wheel-rail contact by a negative friction characteristic of the creep force-creepage relationship as shown in Figure 2-7. A creep force-creepage relationship describes the relationship between the tangential forces transmitted by the contact patch and the relative sliding velocity between the wheel and rail. This relative sliding velocity which is normalised by the rolling velocity of the wheel is called creepage. The tangential force is transmitted between the wheel and rail through the simultaneous action of both adhesion and slip of the

wheel and rail over the contact patch. As the slip between the wheel and rail increases, the adhesion coefficient approaches the Coulomb limit and gross sliding occurs when the contact patch is saturated with slip.

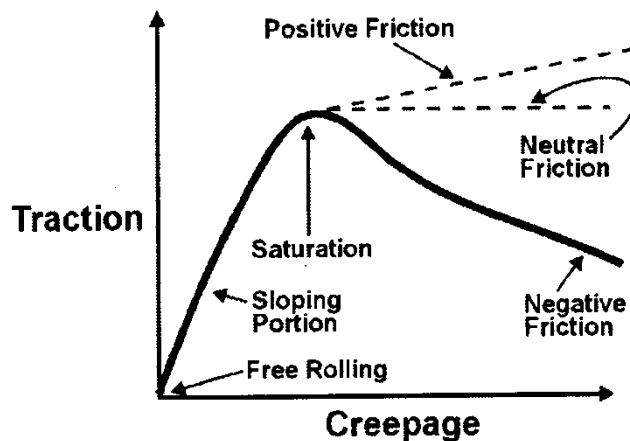


Figure 2-7: Creep force-creepage relationship showing positive, neutral and negative friction characteristics beyond creep saturation (Zakhrov 2001)

A negative slope of the friction characteristic beyond creep saturation is equivalent to negative damping and can result in self-excited oscillation if it exceeds the damping of a specific wheel mode. The negative damping squeal theory shows that especially the leading inner wheel of a four wheeled bogie subject to large lateral creepage is prone to squeal in its zero-nodal-circle axial modes (Thompson 2009).

This theory has been the main school of thought since the first prediction model for squeal was presented by Rudd (1976) and most theoretical models account specifically for this mechanism (Fingberg 1990, Périard 1998, Heckl and Abrahams 2000, De Beer et al. 2003, Thompson and Monk-Steel 2003, Chiello et al. 2006, Huang et al. 2008).

Before De Beer et al. (2003), all squeal models only considered tangential dynamics with respect to the contact zone. Such models of squeal can only exhibit self-excited vibration if a decreasing friction characteristic is present in the model. From literature it is however known that mechanical systems subject to dry friction can exhibit self-excited oscillation in the absence of a negative friction characteristic when the frictional contact exhibit coupling between the normal and tangential degrees of freedom (see for example the review article by Akay (2002)).

Whilst De Beer et al. (2003) include the variation of the normal contact force in their frequency domain squeal model, the motivation behind it was not to study mode-coupling instability. Instead the variation in the normal force was included to account for the influence that the lateral contact position on the wheel tread has on squeal noise due to lateral creepage with a negative friction characteristic. On the other hand Chiello et al. (2006) deliberately included both a negative friction-velocity relationship and the coupling between tangential and normal dynamics in their time domain squeal model with the aim to specifically study the effect of both parameters on the stability of the system. They concluded that only a negative friction characteristic, and not mode-coupling, is able to destabilise the system and induce wheel vibrations.

The literature up to Chiello et al. (2006) can thus be summarised as that the railway community believed that the negative dependency of the creep force-creepage characteristic with increasing relative velocity is the only mechanism that can initiate curve squeal.

This point of view changed when recent studies by Chen et al. (2008), Glocker et al. (2009) and Pieringer (2011) showed that squeal can be excited in the case of a constant friction curve (beyond creep saturation) when coupling between the vertical and tangential dynamics (with respect to the contact zone) is considered in the squeal model. Interestingly Pieringer's detailed high-frequency wheel-rail interaction model formulated in the time-domain and considering lateral creepage shows that for a specific squeal case that develops at 5235 Hz the lateral contact force stays below the traction limit at all times. Squeal in this specific case was associated with the coupling of the (7,0) and (2,C) modes of the modelled wheel. This suggests that creep saturation is not a necessary prerequisite for squeal due to mode-coupling where the squeal results from coupling between the vertical and tangential dynamics of the wheel. It is evident from the adhesion curve shown in Figure 2-7 that the initial linear slope of the adhesion curve transitions to a non-linear region with a significantly reduced slope before it reaches the point of creep saturation. This positive slope of the adhesion curve is equivalent to positive frictional damping. Judging from the shape of the adhesion curve in Figure 2-7 and knowing that creep saturation is not a pre-requisite for squeal due to mode-coupling (Pieringer 2011) it is postulated that the significantly reduced gradient of the adhesion curve leading up to the adhesion optimum might not provide enough positive damping to overcome the positive energy generation associated with mode-coupling instability and hence instability can occur even for a positive gradient of the creep force-creepage relationship.

In a more recent study Ding et al. (2016) investigated the effect that rail dynamics and the friction characteristic has on curve squeal using an extended version of the model by Huang et al. (2008). Results of this research show that more wheel modes can potentially become

unstable for the same wheel due to a falling friction characteristic, compared to mode-coupling instability in the case of constant friction. Mode-coupling occurred predominantly between a lightly damped wheel mode and a highly damped equivalent rail mode, but for one unstable frequency also between two lightly damped wheel modes. In addition it was found that rail dynamics modified the dominant squeal mode when it was included in the time-domain analysis for both falling and constant friction characteristics.

Presently researchers studying squeal realise the importance of both a creepage dependent falling friction characteristic of the wheel-rail contact and the vertical/lateral coupling of the wheel and rail, although it is still not clear to what extent each mechanism contributes to the development of squeal (Pieringer 2011, Zenzerovic et al. 2015, Jiang et al. 2015a, Ding et al. 2016, Thompson et al. 2016, Ding et al. 2018). Jiang et al. (2015a) are confident that the mode-coupling theory might explain the deficiencies of the classical squeal theory in explaining the experimental observations from some in-field and laboratory tests. These observations include (i) coupled vertical and lateral rail vibrations when a squealing wheel passes, (ii) squeal occurring in laboratory tests in the absence of a negative friction characteristic for high angles-of-attack (Koch et al. 2006, Collette 2012), (iii) the mixed results of field trials with friction modifiers (Oertli 2005, Anderson et al. 2008), (iv) squeal being excited at wheels other than the leading inner wheel of a bogie especially the outer wheels in flange contact (Oertli 2005, Curley et al. 2015), (v) the occurrence of squeal at frequencies higher than the wheel's lowest zero-nodal-circle axial mode frequencies predicted by the classical squeal models as well as (vi) the influence of the trackform on squeal occurrence (Jiang et al. 2015b).

The above mentioned deficiencies of the current squeal theory in explaining the experimental observations listed above exist in spite of all the progress made over the last couple of decades. The ultimate goal of the scientific community studying squeal, is a squeal model which can predict squeal comprehensively and that can explain all the experimental observations related to squeal. Such a model will allow for all phenomena to be accounted for during the design process. Currently squeal remains a difficult to predict phenomenon as all the parameters influencing the generation of squeal are not yet fully understood.

2.3 MODELLING SQUEAL

Squeal models use wheel dynamics, rail/track dynamics and contact dynamics to solve wheel-rail interaction at high frequencies in either the frequency or time domains. The friction law (falling or constant friction) is contained in the contact model. Most squeal models model a non-rotating, sliding wheel. Pieringer et al. (2015) were the first to include the effects of a

rotating wheel in a squeal model due to unsteady lateral creepage. They show that a non-rotating, sliding wheel is sufficient to capture the tendency to squeal although the rotation of the wheel delays the build-up of the stick-slip oscillation. It is important to take note that the cross-coupling between the vertical and lateral degrees of freedom (with respect to the contact) is similar for a rotating and non-rotating wheel as both belong to a type *I* degree of freedom. This is most likely the reason why a non-rotating wheel is sufficient to predict squeal due to unsteady lateral creepage arising from mode-coupling instability. However should wheel squeal arise from mode-coupling instability due to cross-coupling between either vertical (type I) and longitudinal or spin degrees of freedom (type II), modelling the moving load nature of the rotating wheel might prove important as cross-coupling between these degrees of freedom are zero for a non-rotating wheel. To date the dynamics of a rotating wheel has not been included in a squeal model arising from unsteady longitudinal or spin creepage.

Frequency domain models describe the instability of the linearised system, determining which wheel modes are prone to squeal. Not all modes with negative damping in the simulation results will be found in experimental squeal results. This is because the linear stability analysis only indicates the tendency to squeal and not which mode(s) will eventually grow into limit cycles (Ouyang et al. 2005). On the other hand, time domain models can include all non-linearities and can determine true squeal amplitudes, but at the expense of computational resources and time.

Two frequency domain methods are generally used to study railway wheel squeal instability, that is a complex eigenvalue analysis and the Nyquist criterion (Thompson et al. 2016).

Complex eigenvalue analysis calculates the eigenvalues of the contact coupled wheel-rail system and instability is identified when the real part of at least one eigenvalue becomes positive. The positive real part of the eigenvalue is mathematically equivalent to negative damping, feeding energy into the vibration. This approach was first considered by Chen et al. (2008) and later by Pieringer et al. (2016), Wang et al. (2016) as well as by Fourie et al. (2018). In these studies the positive real part of the eigenvalue is a consequence of a non-symmetric stiffness matrix and not related to negative frictional damping.

The Nyquist criterion can be used to test a system for stability if it can be represented by a control system with a feedback loop. The system is unstable for frequencies where the Nyquist contour $H(\omega)$ passes the real axis at the right side of $(+1,0)$ on the Nyquist (real vs. imaginary) plane (De Beer et al. 2000). This corresponds to a loop gain larger than one.

Finite element representation of the wheel allows for accurate determination of eigenfrequencies and corresponding eigenmodes, whilst modal damping ratios must be measured or assumed.

Generally modal damping ratios ζ are assumed based on the values proposed by Thompson (2009):

$$\zeta = \begin{cases} 10^{-3} & \text{for } n = 0 \\ 10^{-2} & \text{for } n = 1 \\ 10^{-4} & \text{for } n \geq 2 \end{cases} \quad (\text{Equation 1})$$

This approach has been followed by Chiello et al. (2006), Huang et al. (2008), Pieringer (2014), and Pieringer et al. (2016). Because these models are more concerned with modelling the mechanism behind squeal and not the investigation of a specific squeal problem in a specific curve, it suffices as a first approximation. Given the importance of wheel damping for the occurrence of curve squeal, measured modal damping ratios should be used to study the occurrence of squeal in curves with specific squeal problems.

The light damping of the wheel plays a pivotal role in the excitation of squeal. In many cases a slight increase in the level of damping of the wheel is sufficient to prevent the excitation of squeal (Thompson 2009). In contrast to the wheel being a finite and lightly damped structure with its vibration response strongly characterised by its resonance frequencies, the track is an infinite structure exhibiting a non-modal damped behaviour (Vincent et al. 2006, Thompson 2009). The track will thus have a significantly lower mobility at the wheel resonant frequencies which explains the difference in wheel and rail vibration response during squeal.

Although it appears as if track dynamics has little influence on the excitation of squeal, rail damping has been reported to be effective in reducing squeal noise in some instances (Thompson 2009). At other sites experience has also shown that curve noise issues can become more severe when curved track is upgraded from timber to concrete sleepers (Jiang et al. 2015b). More recently Ding et al. (2016) investigated the effect that rail dynamics has on curve squeal using an updated version of the model by Huang et al. (2008). Results of this research found that rail dynamics modified the dominant squeal mode from (3,0) to (4,0) when it was included in the time-domain analysis for both falling and constant friction characteristics. In addition, for constant friction the number of unstable frequencies was reduced significantly when the rail was assumed rigid in the model. The inclusion of the rail dynamics shows that mode-coupling instability can occur due to coupling between the tangential component and normal component of a single wheel mode. When the rail is assumed as rigid, instability only occurred as a coupling between two different wheel modes.

Because of the notion that track dynamics has no or only a minor influence on squeal occurrence, squeal models often neglected track dynamics and assumed the rail as rigid (Rudd 1976, Chiello et al. 2006, Glocker 2009). De Beer et al. (2000, 2003) as well as Thompson and Monk-Steel (2003) used two distinct analytical models to represent track dynamics, one to represent the vertical dynamics and another to represent the lateral and torsional dynamics. For the vertical direction a Timoshenko beam on a continuous two layer resilient support was modelled (see for example Thompson (2009)) whilst the dynamics in the lateral and torsional directions were based on two beams (the rail head and foot) connected by an array of springs representing the rail web and resting on a continuous two layer resilient support (Wu and Thompson 1999). Pieringer (2014) represented the track using a waveguide finite element (WFE) model of a continuously supported rail. WFE models overcome the difficulty of traditional finite element models in predicting the response of infinite structures by modelling the two dimensional cross-section whilst mathematically taking account of the wave number in the third dimension. Huang et al. (2008) represented the track in state-space form by fitting rational polynomial functions to drive point receptances in the vertical, lateral and longitudinal directions. Ding et al. (2016) represented the track dynamics in the vertical, lateral, longitudinal and spin directions based on a multi-degree of freedom mass-spring system.

The methods employed by Huang et al., Pieringer et al. and Ding et al. were used to allow for computation in the time domain. Analytical models of the track as used by De Beer et al. as well as by Thompson and Monk-Steel are not suitable to the step-by-step integration in the time domain and can only be used in frequency domain squeal models.

2.4 PARAMETERS INFLUENCING SQUEAL GENERATION

The following parameters can be identified from literature as being important to squeal, (i) the local kinematic parameters at the wheel-rail contact including the wheelset angle-of-attack and the wheelset lateral displacement, (ii) the contact friction law and (iii) the wheel and rail dynamic parameters. A discussion on the importance of rail dynamics in relation to squeal was concluded as part of Section 2.3. A detailed discussion of the other parameters follows.

2.4.1 Wheelset angle-of-attack

The wheelset angle-of-attack (AoA) is the key kinematic parameter influencing squeal due to unsteady lateral creepage.

For a typical negative friction characteristic, creep saturation is achieved at about 1 % creepage (Kerr et al. 1998, IHHA 2001). Here the lateral creepage is approximately equal to

the AoA in radians. It can thus be expected that squeal will occur if the AoA exceeds 10 mrad as creep saturation is a necessary pre-requisite for squeal to occur due to falling friction. This agrees well with Rudd's (1976) rule of thumb that squeal due to unsteady lateral creepage is expected to occur where the curve radius is about 100 times the bogie wheelbase being equivalent to an AoA of 10 mrad. Other researchers give the threshold value of AoA as 7 - 9 mrad (Remington 1987, De Beer et al. 2003) above which squeal is likely to occur.

To relate the AoA of a rigid frame bogie with a wheelbase W to the curve radius R , Remington (1987) introduced the concept of the W/R ratio as an estimate for the leading wheelset's AoA, i.e.

$$\frac{W}{2R} \leq \alpha \leq \frac{W}{R} \quad (\text{Equation 2})$$

The upper limit W/R is reached on the leading axle when the trailing axle is radial to the track and which is common for tight curves. It can thus be deduced that for a threshold value of AoA of 10 mrad and a bogie wheelbase of 2 m that squeal can be expected to occur in curves with radii smaller than 200 m. For wheelbases typical of railway bogies, Rudd's rule of thumb correlates well with the curve radii in which squeal commonly occurs in practice. Thompson (2009) states: "In practice, squeal mostly does not occur in curves of radius greater than about 500 m, and is only sporadic for curves down to about 200 m radius, whereas for curves of 200 m and below it is common." This statement is confirmed by Vincent et al. (2006): "Normally squeal does not occur for curve radius R higher than 500 m and the risk for squeal increases for radius lower than 300 m."

In Australia extensive work has been carried out to compare the relationship between wheelset AoA and top-of-rail wheel squeal noise (Kerr et al. 1998, Kopke et al. 2004, Anderson et al. 2008, Southern and Alexander 2009, Jiang et al. 2012). The highlights of these investigations are summarised below:

In 1996 Kerr et al. (1998) conducted an in depth investigation into the causes of, and practical control of, wheel squeal in the Sydney metropolitan rail system. Amongst others, the investigation focussed on simultaneously measured acoustic data and wheelset AoA in a 200 m radius curve in Wollstonecraft, Sydney. The study found that 5 % of the axles traversing the test site caused squeal. For this curve the average AoA was 11 mrad for the leading axles and 0.6 mrad for the trailing axles. However no correlation could be found between squeal and irregular AoA or wheelset lateral position.

In 2000 the Australian Rail Track Corporation sponsored a project to compare the AoA of freight wagons with the noise emission in a 220 m curve in the Adelaide Hills region in South Australia (Kopke 2004). The test spanned a period of two weeks and showed that 89 % of the wheels with high wheel noise emission readings due to flanging or squeal had an irregular AoA or inter-axle misalignment. With this said, a number of vehicles that produced a squeal event were tracking normally and there was also a low percentage of wheelsets that were identified as so called “bad actors”, in a tracking sense, that did not produce a high noise emission.

In June 2007 RailCorp (Australia) installed a permanent wayside AoA detection system in the main north railway line in Beecroft, Sydney, on a curve of 284 m radius where noise complaints were arising (Anderson et al. 2008, Southern and Alexander 2009, Jiang et al. 2012). The AoA equipment is occasionally linked to microphones to compare the wheelset tracking to noise emission. The AoA and noise relationship results can be summarised as follows: 95 % of the rolling stock that passes the site has a leading wheelset AoA close to the expected range for the curve (± 10 mrad). The noisiest wheel squeal events occur when axles pass with an AoA exceeding 20 mrad. Generally, the higher the AoA of the wheelset is, the higher the corresponding squeal level. Not all axles with irregular AoA generate squeal and a high number of wheel squeal events are recorded for the bogies and wheelsets showing good tracking.

From the findings of the Australian research, relating the steering of wheelsets under large AoA to the generation of squeal, it can be concluded that wheelsets steering with excessive AoA are in fact generally responsible for the generation of top of rail wheel squeal.

The question however remains why some squealing events originate from wheelsets that don't steer with irregular AoA and why some wheelsets steering with excessive AoA do not produce squeal?

2.4.2 Wheelset lateral displacement

The wheelset lateral displacement influences both the amount of longitudinal creepage present in the wheel-rail contact as well as the contact position on both the wheel and rail.

In distinct studies, researchers have investigated the influence that longitudinal creepage (Monk-Steel et al. 2006) and the wheel tread lateral contact position (Chiello et al. 2006, De Beer et al. 2003) have on squeal due to unsteady lateral creepage.

Monk-Steel et al. (2006) have shown experimentally on a 1:3 scale roller rig that longitudinal creepage increases the threshold AoA for squeal to occur due to unsteady lateral creepage. The relationship under creep saturation is that the level of lateral creepage must exceed that of the longitudinal creepage for squeal to occur. Here it is expected that the saturation of tangential forces by longitudinal creepage may suppress the mechanism responsible for squeal due to unsteady lateral creepage.

Concerning the influence that the lateral contact position on the wheel tread has on squeal, De Beer et al. (2003) have shown that the lateral contact position influences the occurrence of squeal and which resonant frequency becomes dominant. The findings in their model were confirmed by laboratory measurements on a test rig comprising a 1:3 scale model of a wheel in which squeal only occurred for a contact position on the outside of the wheel tread.

Another possible outcome of displacing the wheelset laterally is the possibility of flange contact when the available flangeway clearance is taken up. This condition generally occurs at the leading outer wheel of a bogie during curving, although it can also occur at the trailing outer or trailing inner wheels during curving for certain conditions of cant deficiency and excess respectively. Two theories exist in literature about the relationship between flange contact and squeal. The first theory states that flange contact alone will not produce squeal and that flange contact, with the flange rubbing on the gauge face, reduces the likelihood of stick-slip due to lateral slip and the levels of squeal noise at wheels in flange contact (Remington 1987). The second theory acknowledges that flange contact can produce tonal squeal, although the mechanisms governing squeal in such conditions are not yet known (Curley et al. 2015, Jiang et al. 2015a). It is however known that gauge face lubrication eliminates tonal squeal at sites where squeal originate from the leading outer wheel of a bogie. In a recent study Zenzerovic (2017) showed that modelling two-point wheel-rail contact can actually be important to capture squealing of curve-outer wheels due to mode-coupling instability, although such a model was not validated against experimental data at the time. Here squeal is a result of the dynamic interaction of two contact points and the presence of two closely spaced wheel modes, similar to the model of Squicciarini et al. (2015) that modelled flange-back contact squeal and validated against on-track measurements.

Before Zenzerovic's and Squicciarini et al.'s models, Thompson and Monk-Steel (2003) modelled single point contact in the wheel flange throat and concluded that falling friction can potentially activate squeal in the wheel's radial modes.

Some of the information presented above and related to the wheel lateral position, could help explaining some of the unanswered questions related to the Australian AoA research. For

instance squeal excited in the absence of high AoA could instead have been excited by flange contact. Other instances where no squeal was excited for high values of AoA could be explained by the presence of excessive longitudinal creepage or a wheel tread contact position not favouring the excitation of squeal.

2.4.3 Contact friction law/Friction characteristic

The friction characteristic, which is the functional dependence of the friction force on the relative sliding velocity, is a very important characteristic for any friction driven oscillation. As stated earlier, the classical squeal theory attributes the instability in the lateral creep force to the negative friction characteristic associated with dry steel-on-steel wheel-rail contact. The mode-coupling theory on the other hand predicts instability with a constant friction coefficient beyond creep saturation or even for one specific case shown by Pieringer (2011) for a positive slope of the adhesion curve just before creep saturation occurs.

Because of the almost exclusive belief that railway wheel squeal is dependent on the negative friction characteristic at the wheel-rail interface, modifying the friction-creep characteristic with friction modifiers has been an attractive means to control squeal noise since the pioneering work of Rudd (1976).

Friction modifiers applied at the wheel tread or top-of-rail running surface, aim to provide a positive friction characteristic to suppress the excitation of squeal. In-field investigations with friction modifiers applied to the top-of-rail running surface show varying success, from eliminating squeal, to reducing its duration and strength to having no effect at all (Oertli 2005, Anderson et al. 2008).

Four possible explanations exist for the ineffectiveness of friction modifiers to eliminate squeal in some curves:

(i) The dosage of the top-of-rail friction modifier is not enough. In some field trials, where top-of-rail friction modifiers were applied at quantities known to eliminate squeal in other curves, researchers were able to reduce curve squeal only by increasing this dosage (Oertli 2005).

(ii) In instances where wheelsets steer with excessive angles-of-attack, due to impaired curving ability of the bogie, changes in the top-of-rail friction characteristic provide little or no improvement to the wayside noise levels (Anderson et al. 2008). Such wheelsets normally squeal at acute sound pressure levels (typically 100 to 120 dBA at 15 m). Laboratory tests with friction modifiers (Oertli 2005) have shown that for higher yaw angles, the friction is

similar to that of a clean wheel and that squeal occurs even though friction modifier has been applied.

(iii) Contradictory to common belief, contact between the gauge corner and the wheel flange can under certain conditions lead to squeal. In a French trial in a 150 m radius curve, top-of-rail friction modification did not reduce curve squeal; conversely lubrication applied to the rail gauge face was able to reduce squeal (Oertli 2005). Similar results have been obtained in a 284 m radius curve in Sydney, Australia where gauge face lubrication of the outer rail severely reduced the number and severity of tonal squeal events in the curve (Curley et al. 2015).

(iv) Friction modifiers aim to provide a positive friction characteristic, whilst not impairing the adhesion of rail vehicles during traction or braking. This is achieved by keeping the friction at an intermediate level. In instances where mode-coupling is in fact the responsible mechanism for squeal, it could be that only very low levels of friction will not result in a strong enough frictional coupling between the normal and tangential dynamics of the system to avoid self-excitation. If this is in fact the case, it stands in direct contrast with the adhesion requirements of railway operations.

Both the negative damping and mode-coupling mechanisms are considered to be important for the generation of wheel squeal. This can be said as both negative (De Beer et al. 2003, Monk-Steel et al. 2006, Liu and Meehan 2014) and constant/positive (Koch et al. 2006, Collette 2012) friction characteristics have been observed in twin-disc rolling contact test rig studies that produce squeal.

2.5 FIELD MEASUREMENTS RELATED TO SQUEAL

Very few references in literature describe detailed field experiments aimed at identifying/verifying the mechanisms responsible for squeal.

In part this can be attributed to the fact that until recently the negative dependency of the creep force-creepage characteristic with increasing relative velocity was believed to be the only mechanism that can activate curve squeal. Because the excitation mechanism in the form of negative damping has been well established since Rudd's prediction model (Rudd 1976) and the preceding field work by Von Stappenbeck (1954 as cited in Périard 1998), most research related to squeal here-after took the form of improving theoretical squeal models, laboratory experiments on twin disc roller rigs to perform parametric studies or trials infield to evaluate the effectiveness of various mitigation measures.

With the recent advent of researchers realising that not only the negative dependency of the friction characteristic with increasing creepage, but also mode-coupling can lead to self-excitation, detailed field experiments to identify and verify the mechanisms of squeal were conducted by Vincent et al. (2006) between 2000 and 2001, by Stefanelli et al. (2006) also between 2000 and 2001 and by Jiang et al. (2012) in 2010. The biggest difference between the field experiments above are that Vincent et al. opted for an on-board measurement strategy whilst Stefanelli et al. and Jiang et al. opted for a wayside measurement strategy.

Wayside field experiments related to the unexpected event of squeal occurring in the 1000 m radius Elands Bay curves was also conducted by the author (Fourie 2011) in 2011. The measurement campaign aimed to determine whether the impaired curving ability of self-steering bogies, curving with excessive lateral creep forces, is responsible for the generation of squeal noise and not particularly to investigate the exact underlying mechanisms in terms of negative damping and/or mode-coupling.

From the above field experiments the common themes that could be identified were, (i) to determine the influence of key parameters (identified by the authors) on squeal occurrence, (ii) source identification of the squealing wheel i.e. the exact wheel in the bogie that the squeal event originated from and (iii) identification of the emerging squeal frequencies.

2.5.1 Key parameters accounted for during field measurements

Table 2.1 summarises the key parameters as identified by the authors above and which they used to develop their measurement campaigns.

Table 2-1: Key parameters accounted for during field experiments

Parameter	Vincent et al. (2006)	Stefanelli et al. (2006)	Jiang et al. (2012)	Fourie (2011)
Curve radius	60 m & 75 m	199 m	284 m	1000 m
Sound pressure	X	X	X	X
Squeal frequency	X	X	X	X
Train speed	X	X	X	X
Wheelset angle-of-attack	X	X	X	
Wheelset lateral position	X	X	X	
Wheel modes	X	X		
Modal damping of wheel modes	X	X		
Air temperature		X	X	
Rail temperature		X		
Air humidity		X	X	
Moisture on rails		X		
Vertical and lateral track forces			X	X

2.5.2 Source identification of squealing wheel

Opting for an on-board measuring strategy, Vincent et al. (2006) used four microphones located close to the outer lateral side of the wheel tread of each wheel in the bogie in conjunction with four accelerometers mounted laterally on the mid height of each wheel web. The microphones were used to identify the occurrence and level of squeal noise, whilst the accelerometers were used to quantify the discrimination power of the microphones.

Stefanelli et al. (2006) and Jiang et al. (2012) used similar strategies for wayside source identification. To identify if the squeal noise was emitted from a wheel in contact with the inner or outer rail of the curve, tri-axial accelerometers were installed on the foot of both rails. By comparing the acceleration level difference when the squealing wheel passes, it can be identified if squeal originated from the low rail/inner wheel or high rail/outer wheel interface. Whilst Jiang et al. only distinguished between curve-inner and curve-outer squeal events, Stefanelli et al. identified the exact squealing wheel by considering the time-dependant frequency spectra of the acceleration and acoustic signals attributed to the Doppler Effect. The point of frequency shift identifies the instance in time that the squealing wheel passes the microphone location and can be compared with the signals from a radially inline wheel presence detector. Whilst Fourie (2011) also used the Doppler Effect to identify the squealing axle, he used two free field electret microphones positioned at equivalent distances from the high and low rail and radially in line with a wheel presence detector to identify if it was the inner or outer wheel on the axle that produced the squeal event.

Comparing the maximum sound pressure level from the microphone with the wheel presence detector is not an accurate means of determining the source of squeal due to the sometimes intermittent nature of squeal in a curve as well as the signature of the sound emitted to the wayside due to the directivity of wheel radiation.

The Doppler Effect can be visualised by processing the acoustic signals with a moving window Fast Fourier Transform (FFT) and displaying the data on a colour coded time-frequency diagram known as a spectrogram. Colour is used to display the amplitude of the frequency content for each time step of the calculated FFT (see Figure 2-8).

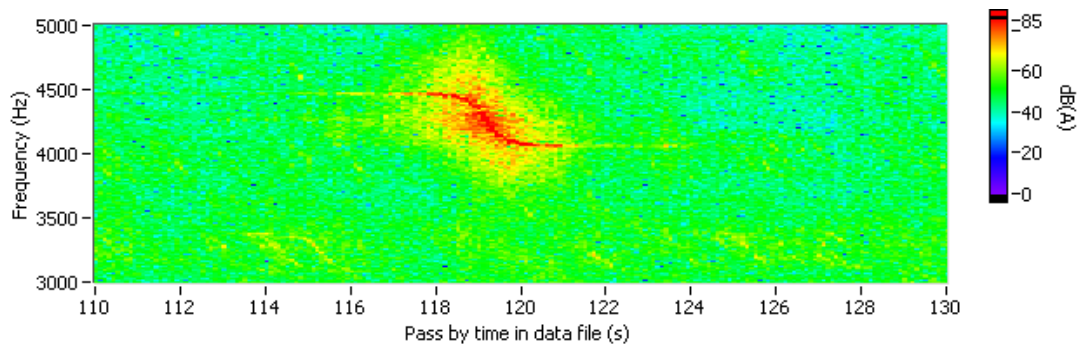


Figure 2-8: Observed frequency shift in acoustic signal due to the Doppler Effect

The source identification technique using the Doppler Effect in the recorded acoustic signals in combination with the signals from the radially aligned wheel presence detectors and as employed in the current study is discussed in detail in Section 3.2.1.

2.5.3 Key findings of field measurement campaigns

Vincent et al. (2006) was able to directly compare the in-field measured squeal frequencies with the modes of vibration of the squealing wheels. The modes of vibration of one of the studied wheels were studied before the on-track tests. Because the studied wheels all had comparable diameters, it was only necessary to study the modal properties of a single wheel. Wheel modes between (2,0) and (9,0) were shown to take part in squeal during the field tests.

This one-to-one comparison of squeal frequencies with wheel modes and natural frequencies is an important feature when studying squeal. Although this was relatively simple for the field measurements conducted by Vincent et al. due to the on-board measuring strategy considering unique wheels, it can be anticipated that this will be a difficult undertaking for a wayside strategy because of the significantly different in-service wheel diameters of passing rolling stock.

Stefanelli et al. (2006) showed that squealing in the 199 m radius test curve occurred in the frequency range between 3 and 5 kHz. For the studied rolling stock, the wheel diameters varied between 820 mm (new) and 760 mm (condemning limit). As an example, Stefanelli et al. (2004) showed how a wheel diameter of 814 mm resulted in squeal at 3 kHz whilst a wheel diameter of 797 mm in squeal at 4 kHz. By comparing the squeal results to eigenfrequencies of the wheel, calculated for diameters between 760 mm and 820 mm, they concluded that different eigenmodes of the wheel are responsible for squeal at 3 kHz and 4 kHz as no eigenmode spans this frequency range for the given wheel diameters. In a parallel study, Glocker et al. (2009) showed that squeal in this curve most likely occurs due to

mode-coupling. They found that three closely spaced wheel modes are necessary for squeal to occur at 4 kHz for a wheel diameter of 800 mm. This is the (5,R) and (4,1) modes being responsible for normal load variation and the (6,0) mode which vibrates in a lateral direction at the wheel rim. In the above field study, data from only four unique train sets was singled out for analysis, resulting in 524 train passages during the measurement period. The train composition of the studied suburban trains consisted of a motor coach, a driving trailer as well as two intermediate coaches (Stefanelli et al. 2006). This implies that only 128 unique wheels formed part of the reported measurements, resulting in 67 072 studied wheel passes past the measurement location. Knowing from Glocker et al. (2009) that only 83 squealing events were recorded in total for these 524 train passages and that 32 of these squealing events can be attributed to four unique wheels (the leading inner wheel of the leading bogie of the driving trailer), it becomes evident that the data set did not contain enough data to perform a detailed analysis concerning the influence of wheel diameter on squeal. This is confirmed by Stefanelli et al. (2004) stating that: “The observation window was too short to observe long term variation due to wear...” In addition, the measurements of Stefanelli et al. (2016) showed that weather had an influence on the occurrence of squealing, however this influence was not quantifiable.

Although Jiang et al.’s measurement set-up included the measurement of meteorological data, wheelset lateral displacement and vertical/lateral rail forces, the influence of these parameters on squeal generation was not studied as part of the documented investigation and would, according to the authors, form part of a continuing investigation. Only the relationship between the wheelset angle-of-attack and curving noise formed part of the documented investigation of which the results are similar to that documented in Section 2.4.1. A surprising finding of this field study was that squeal at the measured curve resulted predominantly from curve-outer wheels.

The key findings of the field measurement campaign conducted by Fourie (2011) were given in Section 1.2. Fourie (2011) used the lateral track force measurements to describe the curving behaviour of passing bogies due to the combination of the lateral forces measured for the four wheels of a bogie and concluded that the squealing bogies all curved with the same unique curving signature. The specific local contact conditions of the squealing wheel could however not be uniquely identified without knowing the lateral displacement of the trailing wheelset with respect to the inner and outer rails of the curve. The curving signature could be interpreted as either the trailing inner or trailing outer wheels making flange contact. If the trailing outer wheel is identified as making flange contact, the trailing inner wheel is subject to predominantly longitudinal creepage given the near radial alignment of the wheelset.

Otherwise, the trailing inner wheel is subject to flange throat/rail gauge corner contact. The current research is a continuation of the previous research by Fourie (2011) and aims to broaden the understanding of the parameters and mechanisms influencing squeal generation in large radius curves.

2.6 GUIDANCE FROM LITERATURE

Researchers studying squeal are in agreement that unsteady lateral creepage is the dominant cause for squeal generation. Squeal due to unsteady lateral creepage occurs at the leading inner wheel of a four wheeled bogie in tight curves ($R < 300$ m).

Both trailing wheels subject to large longitudinal creepage in tight curves have been modelled to be unsteady in their fundamental torsional/circumferential natural vibration mode due to falling friction. Given the low frequency of this mode, it is not relevant to squeal noise and instead considered to be a contributing factor to corrugation formation. Although the modelling approach included evaluating instability due to mode-coupling, including the dynamics of a non-rotating wheel meant that the vertical/longitudinal cross-coupling was included as zero in the model for modes with $n > 0$. This is in contrast with vertical/longitudinal cross-coupling that is non-zero for a rotating wheel subject to moving load excitation. The state of the current knowledge eliminates longitudinal creepage as being relevant to squeal. If experimental evidence shows that squeal in the test curve results from unsteady longitudinal creepage, including the vertical/longitudinal cross-coupling dynamics of a rotating wheel suffering moving load excitation might be important.

In tight curves, the leading outer wheel is in flange contact. Flange contact has been found through experimental observations to bring about a positive effect on squeal control. Generally the leading outer wheel does not squeal and instead produces broadband flange rubbing noise. However, on-track measurements do exist, demonstrating that flange throat contact can activate squeal in certain circumstances. Although not validated against on-track measurements, two models exist for wheel flange throat contact squeal. The first, due to falling friction, predicts squeal in the wheel's radial modes and the second, due to mode-coupling, predicts squeal for the dynamic interaction between two contact points and two closely spaced wheel modes (in this case the (5,0) and (3,1) modes). Similar to the case for longitudinal creepage, the vertical/spin cross-coupling is zero for a non-rotating wheel, but non-zero for a rotating wheel suffering moving load excitation. To the author's knowledge the dynamics of a rotating wheel suffering moving load excitation has not been included in a squeal model in an attempt to model squeal arising from unsteady spin creepage. This might prove important if squeal in the test curve originates due to flange throat contact.

The current research contributes to the development of a future complete squeal model, by identifying the parameters influencing and subsequently modelling squeal occurring at the trailing inner wheel-rail contact of self-steering bogies in large radius curves. Already known a priori is that either longitudinal creepage or wheel flange rubbing provides the source of instability for squeal occurring in the test curve. Once the source of instability has been uniquely classified, this can be used to influence the modelling inputs for the proposed squeal model. Models for curve squeal can be formulated in either the frequency or time domain. Only time-domain models can predict the true squeal frequency and the corresponding squeal amplitude taking into account all system non-linearities. This is however very time consuming. Frequency domain models on the other hand can predict all potential unstable frequencies of a linearised system for a given set of operating conditions and hence are very efficient. In this thesis, curve squeal is investigated in the frequency domain using the Nyquist criterion.

Because it is not known beforehand exactly what parameters need to be modelled to capture curve squealing in a 1000 m curve, it can be seen that the in-field investigation forms the backbone of the current thesis and an important contribution to the literature in the area of squeal field measurements. Questions that guided the field investigation and that influenced the modelled parameters include:

1. What is the direction of the resultant creep force in the wheel-rail contact of the curve-inner trailing wheel? This was studied using rail force and wheelset lateral displacement measurements of the squealing bogies in addition to quantifying rolling radius difference functions for measured wheel and rail profiles. The curving behaviour and resulting creep direction at the wheel-rail contact was confirmed by studying the vehicle dynamics simulation of a bogie with worn wheel and rail profiles.
2. What is the relationship between the squeal frequencies and the wheel diameters for the squealing wheelsets? This was studied by identifying the squeal frequency from the moving time-frequency analyses of the recorded sound pressure and relating this to the wheel diameter of the squealing wheel.
3. If the relationship between the squeal frequency and wheel diameter varies linearly, this data can be used to relate the squeal frequency to the modal behaviour of a single wheel of known diameter. This will eliminate the need to study the modal behaviour of different wheels having different diameters to identify if the same modes are responsible for squeal. Identifying a relationship between the wheel diameter and

squeal frequency is an important contribution of the current study and has not been shown in the literature before.

4. What is the modal behaviour of the measured wheel that can be linked with squeal occurring due to the resultant creep force acting in the quantified direction?

3 EXPERIMENTAL CHARACTERISATION OF RAILWAY WHEEL SQUEAL OCCURRING IN LARGE RADIUS CURVES

This chapter presents an in-field study of the key parameters that influence self-excitation of railway wheels in large radius curves. The main parameters that are investigated are the kinematic parameters influencing the generation of squeal in the 1000 m radius curve.

The field measurements for the current research use a modified measurement setup compared to that of Fourie (2011). The modification consists primarily of the inclusion of laser triangulation sensors to measure the lateral wheelset displacement within the available flangeway. The complete measurement setup and the evaluation of such field measurements are explored in detail in this chapter.

The modified measurement campaign also identified the wheel diameter and wheel type of the squealing wheels. The objective of the field measurements was to qualify the source of squeal, the squeal frequencies and creepages in the wheel-rail contact of the squealing wheel as well as to establish a correlation between wheel types, wheel diameter and squeal frequency. Wheels from three different manufacturers are used on the Sishen-Saldanha railway line.

The effect of top-of-rail friction modification on squeal occurrence was also evaluated.

3.1 FIELD MEASUREMENTS

3.1.1 Measurement setup

A measurement methodology was developed to identify the frequency of squeal, the source of squeal i.e. the exact wheel in a bogie that the squeal originated from, the steady state curving attitude of the bogie as well as the creepages present in the wheel-rail contact of the squealing wheel.

The measurement setup consisted of two free field microphones positioned 7.5 m from the track centre on either side of the track and radially aligned with a set of strain gauge bridges configured to measure the lateral and vertical forces on the low and high rails of the curve. This set-up allowed squealing wheels to be identified from the magnitude difference of the sound pressures recorded by the inner and outer microphones in combination with comparing the point of frequency shift of the squeal event due to the Doppler effect with the simultaneously sampled force signals of the radially aligned strain gauge bridges. The web chevron and base chevron strain gauge configurations (TTCI 2010) were used respectively for

the measurement of vertical and lateral rail forces. More details of these strain gauge configurations can be found in Appendix A. In addition two laser triangulation sensors were used to measure the lateral displacement of the wheelset within the available flangeway.

The vertical force signals provided impulse signals that could be used to determine the wagon speed and the speed profile for each recorded train. Only trains with a constant or increasing speed profile past the measurement location were considered for the subsequent analysis. Trains with mechanical brakes being applied were not considered as squeal due to braking could distort the sound signal.

Figure 3-1 shows a schematic of the test setup. All data was recorded using a sampling rate of 50 kHz.

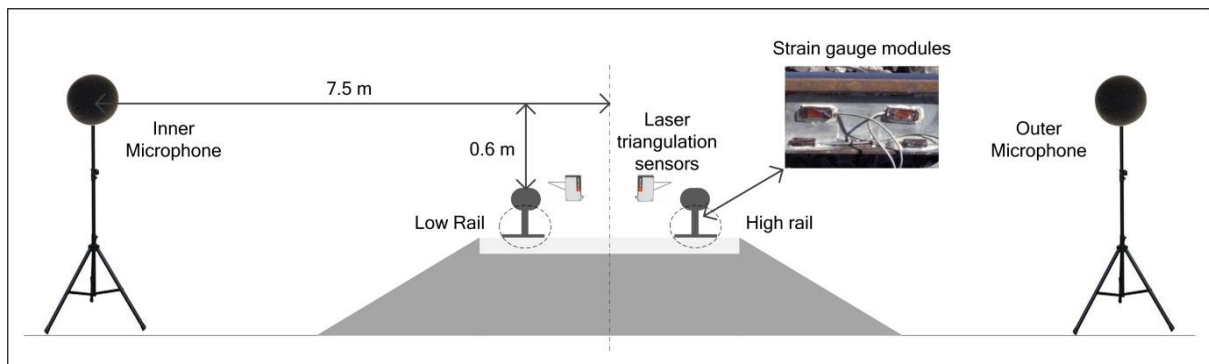


Figure 3-1: Test setup in test curve

Vehicle identification numbers and orientations of the recorded trains were obtained after the measurement campaign via Transnet's train condition monitoring database. This allowed the squealing to be attributed to a specific wheel of a specific wagon. Knowing the exact wheel which emitted the squeal event allowed for obtaining the wheel diameters of the squealing wheels, which were also available in the train condition monitoring database. The vehicle numbers and orientations were used to manually identify the wheel type of squealing wheels from a slow speed video recording of trains leaving and arriving the Saldanha yard. At the time of the slow speed video recording, lateral wheel-rail forces and wheelset lateral displacement measurements were also recorded to verify the tracking condition of some squealing bogies on tangent track. This was used to identify any tracking impairment that will influence the curving behaviour of the squealing bogies in the test curve.

The on-track measurement campaign in the test curve was conducted 18 to 23 October 2012 whilst the wheel type identification was performed 18 to 21 November 2012.

3.1.2 The Sishen-Saldanha railway line

The Sishen-Saldanha heavy haul iron ore export line is an 861 km single line with 19 equally spaced crossing loops to allow trains travelling in different directions to pass.

The iron ore trains are 342 wagons long using Radio Distributed Power (RDP) technology. These trains consist of three 114 wagon rakes divided by four locomotive consists. The locomotives are generally a mix of electric and diesel-electric, although some trains use only five class 15E electric locomotives as shown in Figure 3-2. Such trains are 3.78 km long. Figure 3-3 shows an aerial image of a 342 wagon train passing Elands Bay.

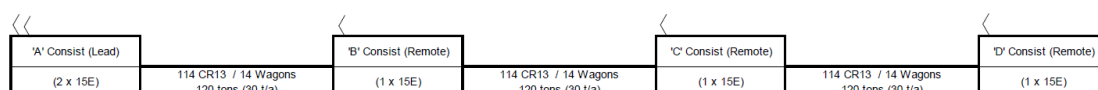


Figure 3-2: Iron ore train compilation



Figure 3-3: Aerial image of Elands Bay including 342 wagon train

The CR13/14 type wagons are loaded to 30 tons/axle, giving a total train mass of 41 400 tons.

A total of 10 loaded and 12 empty iron ore trains were measured during the October 2012 field measurement campaign.

53 Low frequency audible squeal events were recorded in the frequency range between 3816 Hz and 6448 Hz.

Lateral forces of a total of 5 loaded and 2 empty iron ore trains were measured on 20 and 21 November 2012 to verify the tracking condition of squealing bogies on tangent track and at low speed.

3.2 EVALUATION OF FIELD MEASUREMENTS

3.2.1 Source of squeal

The combined study of the time-dependent frequency spectra, the sound pressure levels as well as the signals from the radially aligned strain gauge bridges enabled the identification of the source of squealing. The time dependent linear frequency analysis revealed how the frequency of a passing train changes over time, whilst equivalent continuous sound pressure levels in 1/8 second intervals revealed the time sound pressure level history of the passing train with a high resolution and an accurate representation of the instantaneous sound pressure.

The time-dependent frequency spectra of the recorded sound pressure showed characteristics due to the Doppler effect when squealing wheels passed the microphone location (see Figure 3-4(a)). This implies an increase or decrease of the frequency observed by the stationary device depending on the direction of relative movement of the source.

By comparing the point of frequency shift of the squeal event due to the Doppler Effect with the simultaneously sampled force signals of the radially aligned strain gauge bridges, the source of the squeal could be identified along the length of the train. The peaks of the measured forces on the rail indicate the exact time that a wheel passed the measurement location. A similar technique (using the Doppler effect) was employed by Stefanelli et al. (2006) to detect the squealing source along the length of the train.

The point of frequency shift is determined as follows.

As a first step, the true squeal frequency f_b (line B in Figure 3-4(a)) is approximated from the observed frequencies before f_a and after f_c the passage of the source (lines A and C respectively in Figure 3-4(a)) by solving Equations 3 and 4 simultaneously.

$$f_a = \left(\frac{v}{v-v_s} \right) f_b \quad \text{(Equation 3)}$$

$$f_c = \left(\frac{v}{v+v_s} \right) f_b \quad \text{(Equation 4)}$$

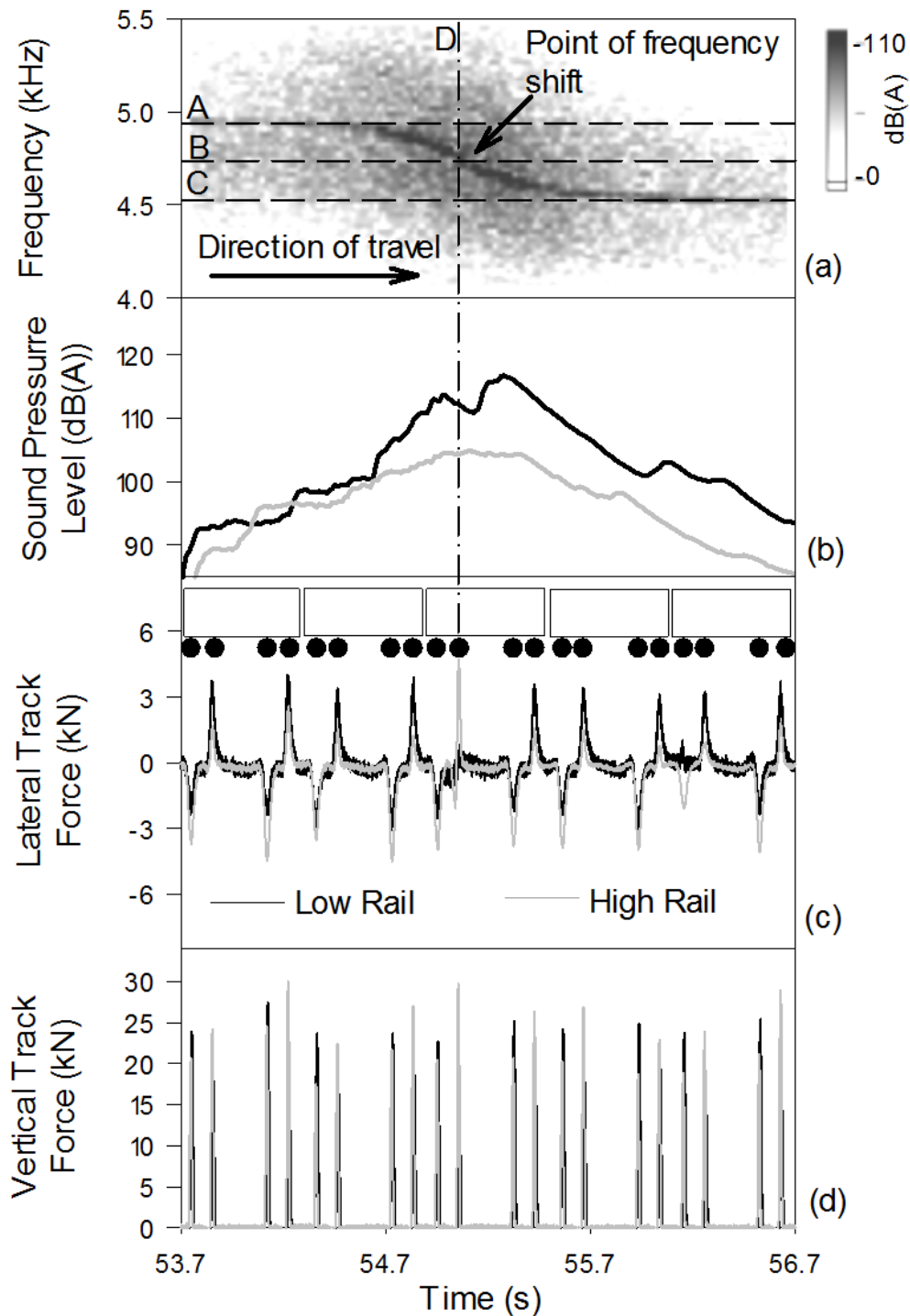


Figure 3-4: Identification of squealing wheel from simultaneously measured sound pressure and lateral forces: (a) Time-dependent frequency spectra showing Doppler effect. (b) Sound pressure level recorded by inner and outer microphones. (c) Lateral force signals from strain gauge bridges. (d) Vertical force signals from strain gauge bridges.

In Equations 3 and 4, v is the speed of sound in air (343 m/s at 20°C) and v_s the source speed.

This time dependent linear frequency analysis is a compromise between resolution in the frequency domain and resolution in the time domain. For this analysis a window length of 16384 samples was chosen giving a frequency resolution of 2.44 Hz and a time resolution of 409.6 ms. This enables the required frequency resolution to accurately determine the squeal frequencies.

Solving Equations 3 and 4 simultaneously also yields an estimate of the wagon/source speed. To gain additional confidence in the estimated real squeal frequency, the estimated speed was compared to the true speed of the wagon (see Figure 3-5). A diagonal line indicating a 1:1 relationship between the true and estimated speed is also shown in Figure 3-5. On average the estimated speed of the wagon deviated 0.5 km/h from true speed of the wagon for the recorded speed range between 56.3 km/h and 66.0 km/h. This implies that on average the error of the speed estimated from the Doppler curve is less than 1 %.

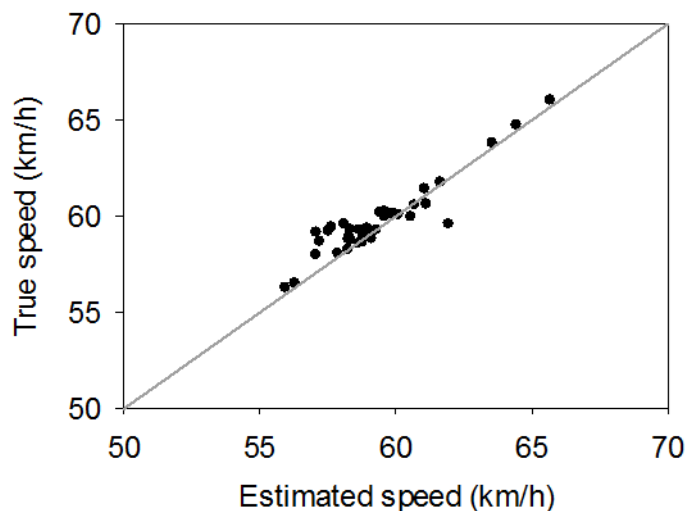


Figure 3-5: Estimated wagon speed vs. true wagon speed

Secondly, the instantaneous time that the squealing wheel passes the microphone location (line D in Figure 3 4(a)), also known as the point of frequency shift, is determined by the point where the squeal frequency line crosses the Doppler curve. For this time-frequency analysis a window length of 1024 samples was chosen, giving a frequency resolution of 39.06 Hz and a time resolution of 26 ms. In addition an overlap of 67% was chosen in the analysis to further increase the time resolution to 8.67 ms. For a maximum expected speed of 70 km/h in the test curve, a time resolution of 8.67 ms translates into a moving source

resolution of 0.169 m compared to a bogie wheelbase of 1.83 m. In addition the location of the microphone compared to the vertical force impulse signals leads to a constant time delay of the recorded sound pressure of 20.4 ms compared to the moving source. Because this constant time delay only shifts the moving source resolution to 0.566 m, compared to a bogie wheelbase of 1.83 m, it was not necessary to subtract this constant time-delay from the sound pressure signal to enable a better resolution for source identification of the squealing wheelset.

For both the first and second stages of the point of frequency shift analysis, it is important to select the amplitude range for colour coding the amplitude of the frequency content such that the Doppler curve can be clearly distinguished from the surrounding frequency content in the time-frequency plot.

Comparing the sound pressure level difference between the inner and outer microphones allows identification of the side of the train that the squeal event originated from. It is evident from Figure 3-4(b) that the point of frequency shift doesn't coincide with the maximum sound pressure level due to squeal. This can most likely be attributed to the directivity of wheel radiation. The measured sound pressure generally has a minimum on or close to the axis of the wheel due to cancellation between the contributions from different parts of the mode shape (Thompson 2009).

Combining the point of frequency shift analysis with the sound pressure level difference analysis yields the exact wheel in a bogie that the noise event originated from. It can be seen from Figure 3-4 that this squeal event originated from the second axle of the third wagon and from the wheel in contact with the low rail.

Similar to Fourie (2011), results from the current measurement campaign also proved that squeal in the large radius test curves can be uniquely attributed to the trailing inner wheel of a bogie in contact with the low rail.

To gain confidence in the source identification technique described above, the position of the closest wheelset to the squealing wheelset is shown in Figure 3-6.

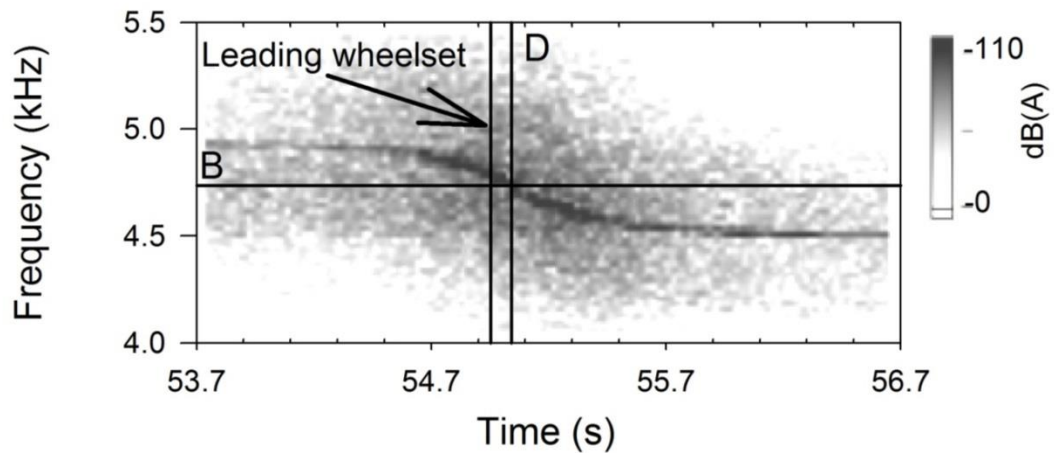


Figure 3-6: Position of leading wheelset with respect to Doppler curve

This technique for identifying the frequency shift from the Doppler effect in time-frequency curves is limited to squeal events that occur sufficiently far from one another in the time or frequency domains so that the Doppler curves do not interfere with one another. For squeal events that occurred close to one another in the time domain with closely matched squeal frequencies this technique shows limited success. 51 of the 53 squeal events for the 342 wagon long trains had sufficient spacing in the time domain ensuring the success of the described technique.

If the squeal events occur close to one another in the time domain, but sufficiently far apart in the frequency domain, then band pass sound pressure filtering must be used to distinguish if the squeal events originated from the inner or outer wheels.

3.2.2 Bogie curving characteristic

The measurement of lateral track forces on curved track, combined with information on the condition of rolling stock, can provide valuable information about the curve negotiation characteristics of bogies. The lateral force curving signature not only reveals the levels of wheel-rail forces required for bogie curving, but also whether the bogie is curving by means of creep forces generated at the wheel-rail interface only or if contact is necessitated between the wheel flange throat and rail gauge corner to help steer the bogie around the curve. Wheel flange throat/rail gauge corner contact can be confirmed by additional measurement of the wheelset lateral displacement within the available flangeway.

Lateral force curving signatures for a bogie under an empty wagon and representative of curving by means of creep (frictional) forces (C) only, with the leading outer wheel in flange

contact as well as both the leading and trailing outer wheels making simultaneous flange contact, are presented in Figure 3-7. Flange contact results in flange and spin creep forces and are denoted by the letter F in Figure 3-7. These three curving characteristics can be used to describe the curving behaviour of most bogies under the empty wagons.

The black dots in Figure 3-7 represent the lateral wheelset displacement measurements. Lateral wheelset displacement from the track centre towards the high rail is given a positive convention, whilst displacement towards the low rail is given a negative convention. The available flangeway clearance is also indicated.

Curving solely by means of creep forces (see Figure 3-7(a)) occurs with a positive AoA of the leading wheelset and a negative AoA of the trailing wheelset of a two axle bogie. Using the convention of a positive lateral force to the outside of the curve for both the high and low rails, curving by means of only creep forces will result in lateral track forces acting towards the inside of the curve for the leading wheelset and lateral track forces acting towards the outside of the curve for the trailing wheelset. Both wheelsets displace an equal distance towards the outer rail due to the steering mechanism of the wheelsets in a curve.

The convention for AoA and lateral force are graphically depicted in Figure 3-8 and Figure 3-9 respectively.

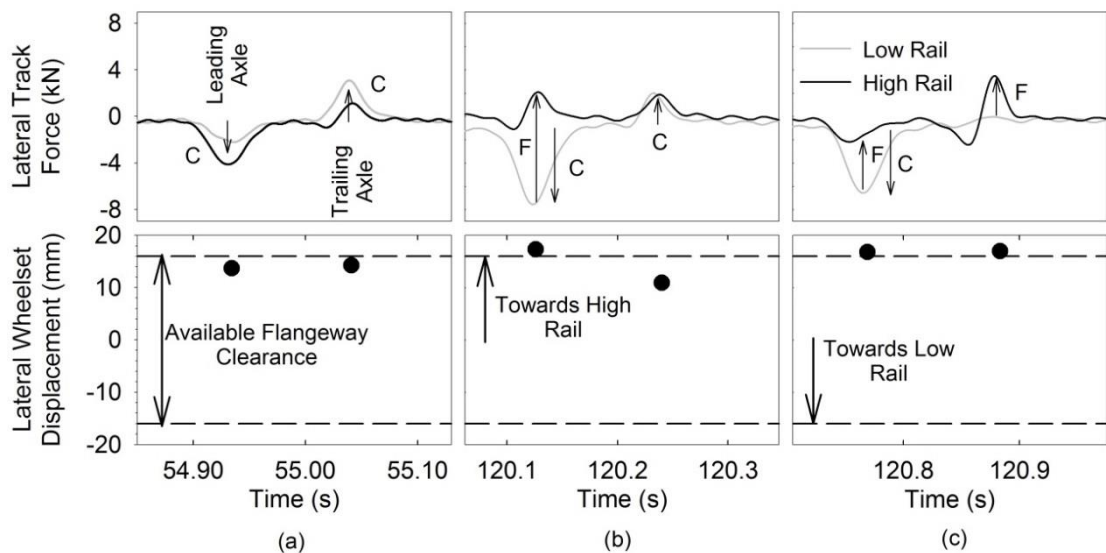


Figure 3-7: Lateral force curving signatures: (a) Curving solely utilising creep forces. (b) Flange contact of leading outer wheel. (c) Flange contact of leading and trailing outer wheels.

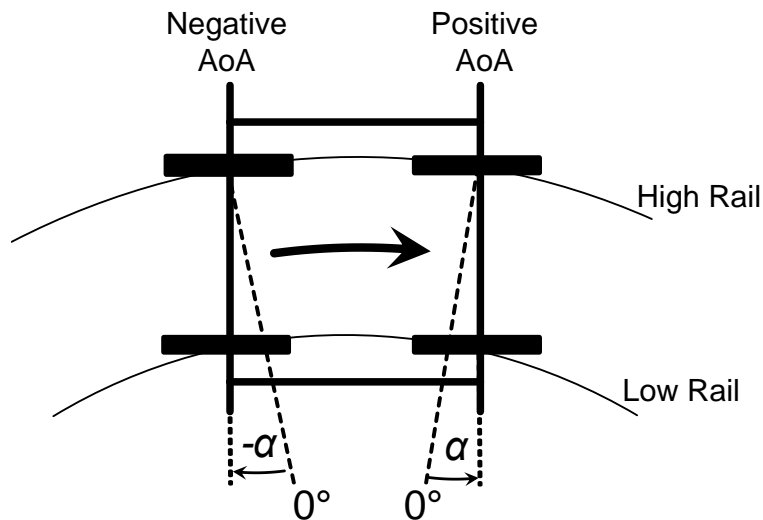


Figure 3-8: Angle-of-Attack notation



Figure 3-9: Force convention for lateral track force measurements in test curve

Once a bogie has lost its ability to steer using only creep forces, the flange or flange throat of the leading outer wheel comes into contact with the gauge corner of the high rail to steer the bogie. Subsequently, flange contact and high levels of spin creepage result in a lateral force opposing the lateral force component due to lateral creep. The resultant lateral force of the leading wheelset thus becomes less negative or even positive on the high rail while the lateral forces on the low rail remain largely unchanged (see Figure 3-7(b)). Flange and spin creep forces (F) act in a direction opposite to the lateral creep forces (C).

Under certain conditions, the flange of both the leading outer and trailing outer wheels of a bogie can be in flange contact as shown in Figure 3-7(c). This implies that both wheelsets of the bogie are displaced towards the high rail taking up all the available flangeway. This curving signature was recorded for a squealing bogie, the squealing wheel being the inner

trailer of the bogie. From the close to zero lateral force acting on the trailing inner wheel of the bogie curving signature in Figure 3-7(c), it can be deduced that the trailing wheelset is curving radially aligned with the centre of the curve. This implies that the trailing wheelset is curving with a near zero AoA and that the trailing inner squealing wheel is subject to little to no lateral creepage. The lateral force curving signatures for six other squealing bogies are presented in Figure 3-10. The seven presented curving signatures of squealing bogies show similar characteristics. Some of these characteristics are unique to the squealing bogies, whilst others are shared with the larger population of recorded bogie curving signatures under empty wagons.

Firstly, all squealing bogies recorded large wheelset lateral displacements of both the leading and trailing wheelsets. Figure 3-11 shows that a large lateral displacement of the trailing wheelset is not a unique feature of the squealing wheelsets in the test curve. Figure 3-11 presents the lateral displacement of the bogie trailing wheelsets for one of the 342-wagon empty trains recorded during the measurement campaign. Eight inner-trailer wheels were identified as squealing during the passage of the train and are indicated with the black dots and black star in Figure 3-11. The black star corresponds to the trailing wheelset that was identified as the squealing wheelset of the bogie corresponding to the curving signature shown in Figure 3-7(c).

Secondly, all the inner-trailer wheels (squealing wheels) that are shown in Figure 3-11 and Figure 3-7(c), recorded very small lateral forces. These forces at the inner-trailer of the squealing bogies are set up by lateral creepage, indicating that the squealing wheels are subject to little to no lateral creepage.

Lastly, the lateral forces recorded for the outer-trailing wheels combined with the large lateral displacement of the trailing wheelsets, give the unique curving condition of the inner-trailers that most likely leads to squeal. The lateral forces recorded for the outer-trailers all show the influence of a large eccentric (offset compared to shear centre of the installed rail) vertical load on the measured lateral load. A large eccentric vertical load normally goes hand-in-hand with the outer wheel making conformal contact with a large wheel radius at the gauge corner of the rail. This leads to a large rolling radius difference between the outer and inner wheels and large longitudinal creepage. The possibility of the squealing wheels curving with large longitudinal creepage in this wheel-rail contact is explored in Section 3.2.3.

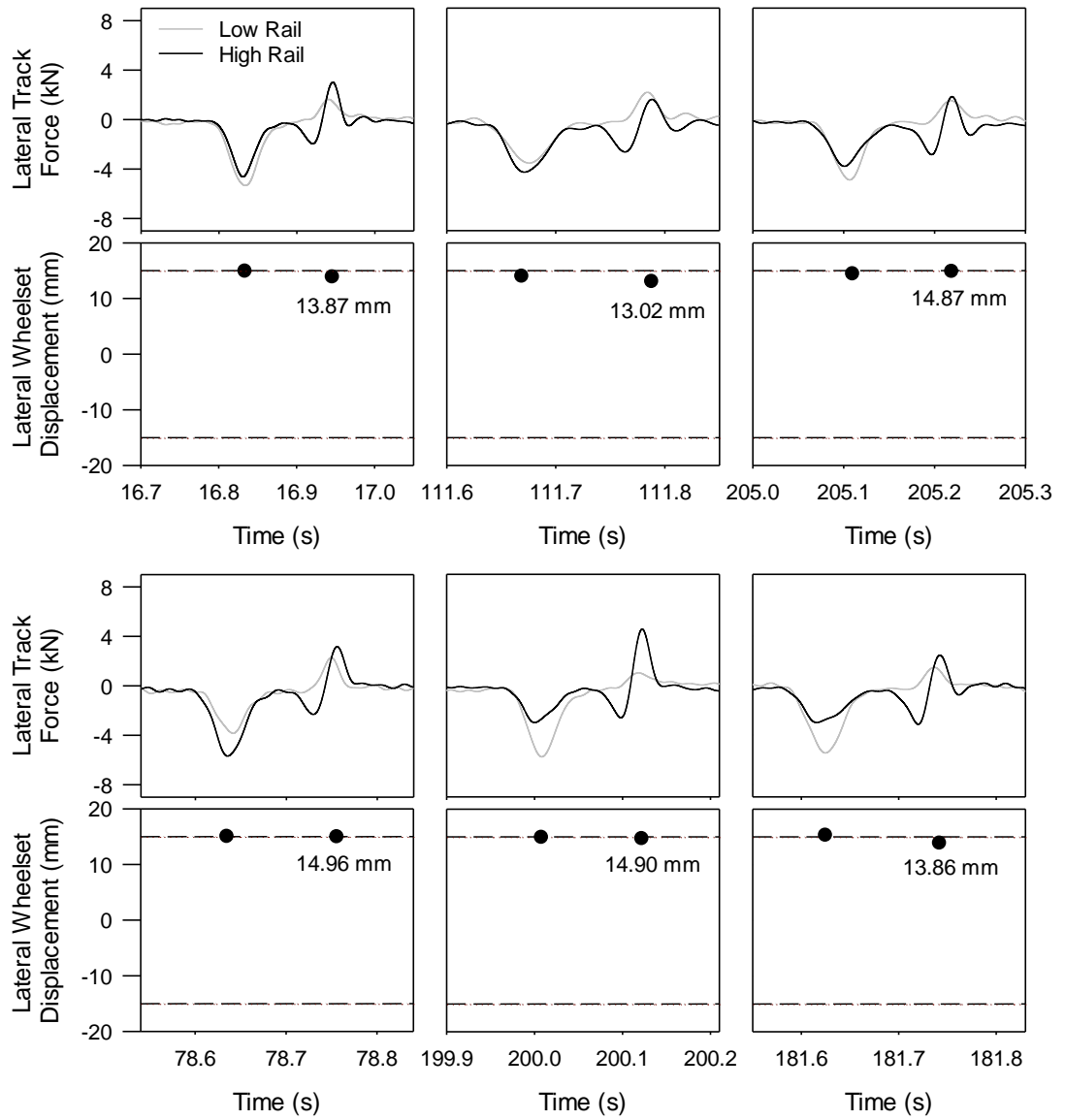


Figure 3-10: Example curving signatures of 6 randomly chosen inner trailer squeal events

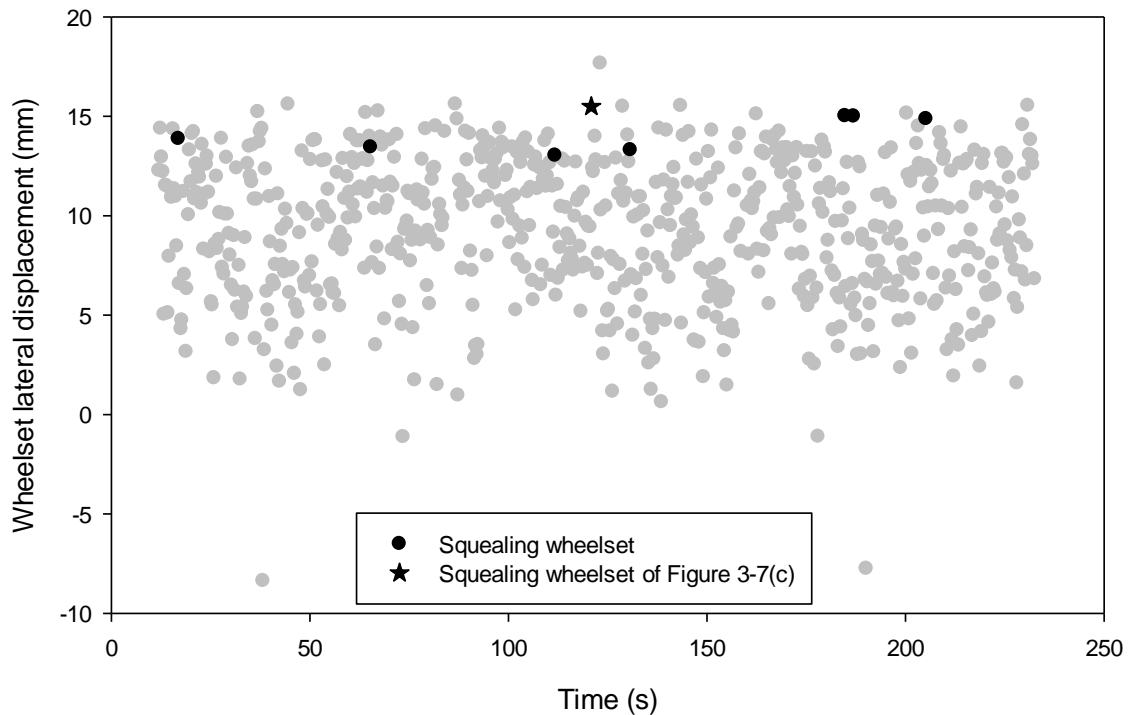
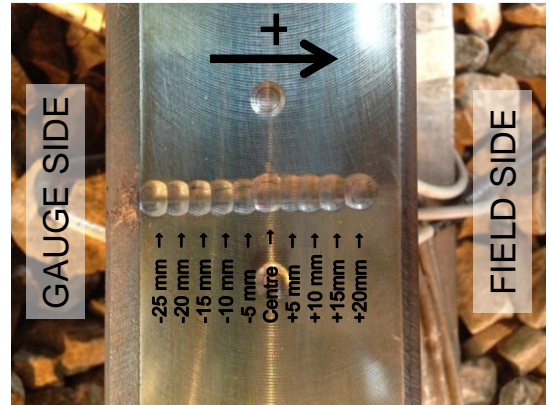
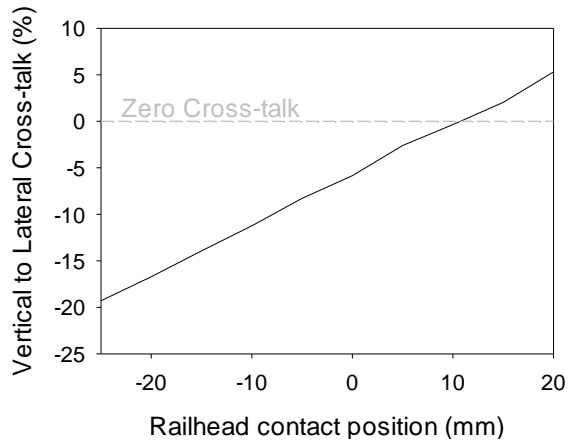


Figure 3-11: Lateral displacement of bogie trailing wheels

The influence of an eccentric vertical load on the lateral load can be explained at the hand of Figure 3-12 and Figure 3-13. Figure 3-12 shows the results of a laboratory test that was conducted to quantify the vertical force cross-talk on the lateral force measuring circuit for different contact positions on the railhead. Figure 3-13 shows an example of the recorded lateral force for an outer-trailing squealing wheel with the magnitude and direction of the acting forces. Here the lateral force is the resultant of the lateral creep force due to lateral creepage, the lateral force due to spin creepage, the lateral force due to the large contact angle as well as the influence of an eccentric vertical load on the recorded lateral force. All the lateral force components act towards the field side of the outer rail, whilst the vertical-lateral cross-talk acts in an opposite sense. This reduces the measured lateral force compared to the actual lateral force and results in a W-shape of the recorded lateral force for large eccentricities.



(a)

(b)

Figure 3-12: Influence of vertical load on measured lateral load: (a) Percentage cross-talk. (b) Contact position and positive convention of lateral force. (Redrawn from Reitman (2013))

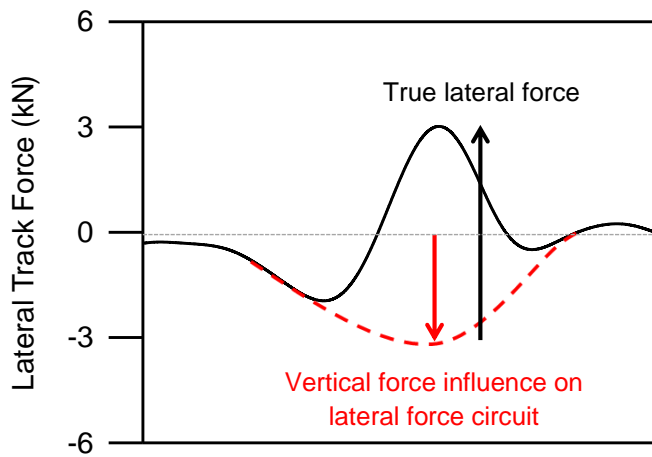


Figure 3-13: Vertical force influence on lateral force circuit

3.2.3 Longitudinal creepage present in wheel-rail contact of squealing wheel

Figure 3-14 shows a histogram of the lateral wheelset displacement recorded for the 53 squealing wheelsets recorded during the October 2012 measurement campaign in the test curve. It can be seen from Figure 3-14 that squeal occurred for a narrow band of wheelset lateral displacements (Mean 14.43 mm; Standard deviation 1.13 mm; Minimum 12.22 mm; Maximum 17.88 mm). Table 3-1 shows how the lateral wheelset displacement of squealing wheels compares to that of the entire population of trailing wheelsets under empty wagons recorded during the field tests. The squeal event recorded at 17.88 mm can be treated as an outlier in the data set. Ignoring this outlier it can be seen that the probability of squeal increases for increasing wheelset lateral displacements between 12 and 16 mm.

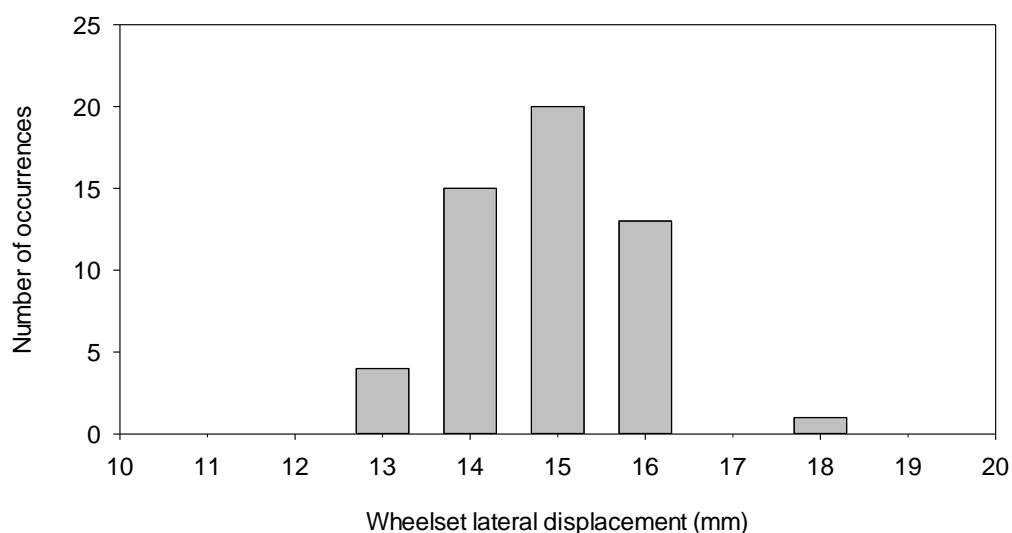


Figure 3-14: Histogram of lateral displacement of squealing wheelsets

Table 3-1: Percentage squeal events per trailing wheelset lateral displacement category

Lateral displacement (mm)	\leq	18	17	16	15	14	13	12
	$>$	17	16	15	14	13	12	-15
Squeal events		1	0	13	20	15	4	0
Percentage squeal of bin population	%	14.29	0.00	21.31	11.43	4.81	1.01	0.00

The magnitude of the quasi static longitudinal creepage λ_1 acting on the trailing inner squealing wheels can be estimated using Equation 5 and knowing the rolling radius difference Δr vs. lateral displacement y functions of the squealing wheelsets.

$$\lambda_1 = (\Delta r - \Delta r_{1000m})/r_0 \quad (\text{Equation 5})$$

Δr_{1000m} is the rolling radius difference required to achieve pure rolling of a wheelset in the 1000 m radius curve. Δr_{1000m} is 0.53 mm. r_0 is the wheel radius at the taping line of the wheel. Δr to achieve pure rolling, was calculated using Equation 6 with a wheel radius r_0 of 458 mm and a wheelset taping-to-taping line distance, l , of 1152 mm.

$$\Delta r_{1000m} = r_0 l / 1000000 \quad (\text{Equation 6})$$

The rolling radius difference functions for eight squealing wagons identified during November 2011 were calculated from wheel and rail measurements recorded during December 2011. In addition, the rolling radius difference functions for two squealing wheelsets identified during February 2011 in test curve is available from Fourie (2011). Wheel profile measurements were not conducted as part of the November 2012 measurement campaign. Although this does not yield a one-to-one comparison between wheelset lateral displacement and rolling radius difference for the squealing wheelsets recorded during the current measurement campaign, it does enable a qualitative comparison between wheelset lateral displacement and longitudinal creepage.

The rolling radius difference vs. lateral displacement (Δr vs. y) functions of the squealing axle's wheel profiles and the matching test curve high and low rail profiles were determined using the kinematic simulation software RsGeo (Kik 2010). The wheel and rail cross sectional profiles were measured using MiniProf wheel and rail profile tracers.

Figure 3-15 shows the Δr vs. y functions for ten squealing wheelsets on the test curve rails. The squealing wheelsets are identified by the respective wagon number. Also shown in the figure is the Δr vs. y function for a wheelset having the design No 21 Transnet Freight Rail (TFR No 21) wheel profiles making contact with the measured rail profiles. A positive lateral displacement implies a lateral displacement away from the track centre towards the high rail in the curve.

Figure 3-15 shows that the rolling radius difference functions of the ten squealing wheelsets can be grouped into two groups. The first group (60 250 577, 60 248 556, 60 259 469,

60 247 185 and 60 221 054 (Feb 2011)) shows rolling radius differences exceeding 1 % longitudinal creepage (5.11 mm rolling radius difference) for lateral displacement values between 10.00 mm and 12.73 mm. The second group (60 204 087, 60 249 242, 60 253 266 and 60 257 881, 60 249 587 (Feb 2011)) shows rolling radius differences exceeding 1 % longitudinal creepage for lateral displacements values between 13.46 mm and 14.46 mm. Squeal is very likely to occur for creepage exceeding 1 % (Jiang et al. 2016).

During the November 2011 squeal measurement campaign, 20 squeal events were recorded during the five day measurement campaign. Of the 23 squeal events, 13 (65.00 %) could be attributed to new built wagons being in-service for between 2 and 17 months. All these wagons were running with new built bogies and had not been maintained at the time of recording the wheel measurements. Five (25.00 %) squeal events were associated with wagons being in service for between 67 and 126 months, however each of these wagons received repaired bogies during their previous maintenance intervention. The last two (10.00 %) wagons that squealed were in service for 37 and 39 months respectively after being built and were still running with the bogies they were first introduced with into service. From the above statistics it can be realised that squeal is strongly related to new or repaired bogies. A total of 1616 new built wagons (3232 new built bogies) were running on the ore line at the time of the November 2011 measurement campaign that had never been into the workshop for maintenance. Only 14 of these new built bogies produced squeal and needed further investigation.

The first group of wheelsets was found to either have the incorrect wheel profile (60 250 577, 60 248 556, 60 259 469 and 60 247 185) or in one instance the wheelset back-to-back distance was 997 mm instead on the design of 987 mm (60 249 881). The incorrect wheel profile found on the squealing wheelsets is the Transnet Freight Rail No 23 wheel profile (TFR No 23), which is used on the heavy haul coal export line and for which new built wagons was being manufactured at the same wagon building plant. The TFR No 23 wheel profile makes one point contact with the ore line target rail profile in the rail gauge corner/wheel flange throat contact area, explaining the possibility of high rolling radius differences. In all the cases where squeal was linked to the TFR No 23 wheel profile, the leading wheelset of the squealing bogie was profiled to the TFR No 21 wheel profile causing a mismatch between the leading and trailing wheelset's wheel profiles.

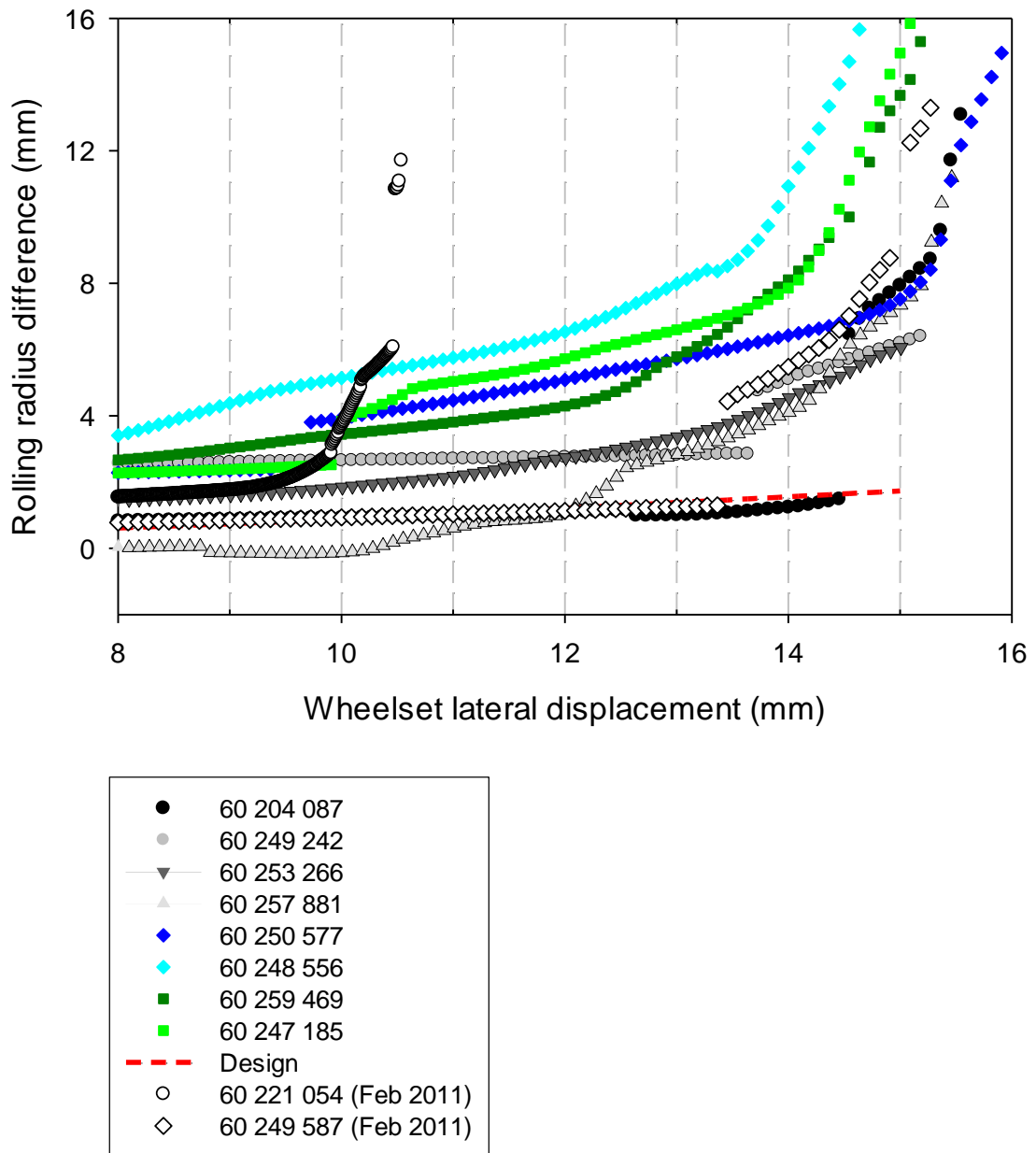


Figure 3-15: Δr vs. y functions of squealing wheelsets ($y \geq 8$ mm)

For the second group of wheelsets, the TFR No 21 wheel profile had worn conformal with the ore line target rail profile, which otherwise makes two point contact with an unworn TFR No 21 wheel profile in the rail gauge corner/wheel flange throat contact area. The contact distribution of the target wheel-rail pair (TFR No 21 on ore line rail profile), simulated with RsGeo, is shown in Figure 3-16. This contact distribution together with 67 % of tangent track on the line and the use of Scheffel self-steering freight bogies (Scheffel 1974 and 1978) result in concentrated hollow wheel wear in a very narrow band on the wheel tread. This leads to the formation of false flanges at both the gauge and field side of the wheel profile. A typical

hollow worn shape of the No 21 wheel profile on the ore line is shown in Figure 3-17. When the gauge side false flange is worn away, the wheel has worn conformal to the average rail profile found on the line. A conformally worn No 21 wheel profile was present on all outer wheel profiles measured for the squealing No 21 wheelsets. An example of a conformally worn outer wheel profile of a squealing wheelset is shown in Figure 3-18. By comparing this conformally worn profile with a No 23 wheel profile (Figure 3-19), it becomes evident that these two profiles are very well matched in the flange throat region of the wheel profile. A conformally worn wheel profile is characteristic of a skew running bogie on the ore line.

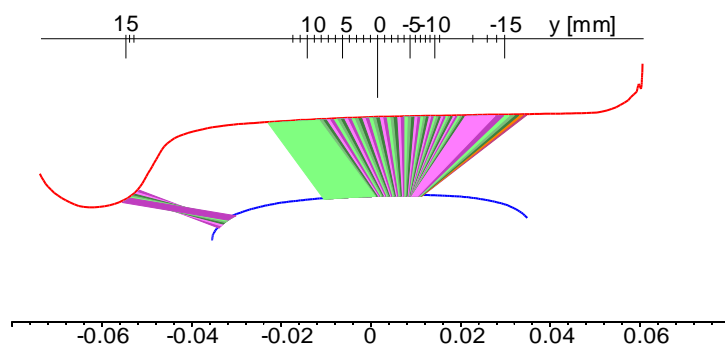


Figure 3-16: Contact distribution of target wheel-rail pair

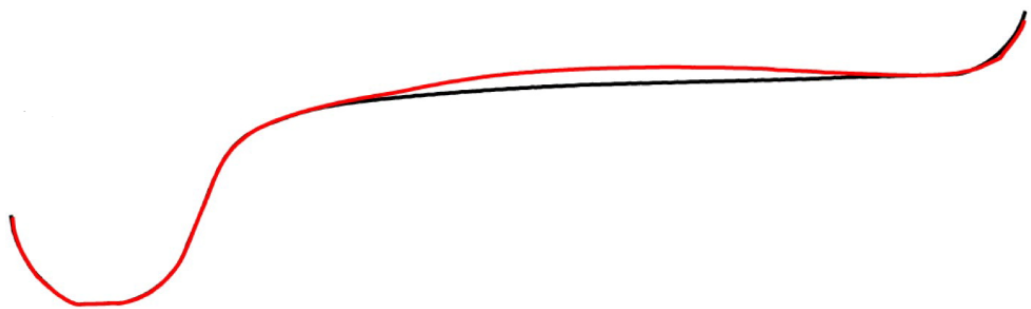


Figure 3-17: Typical hollow worn shape of No 21 wheel profile on ore line

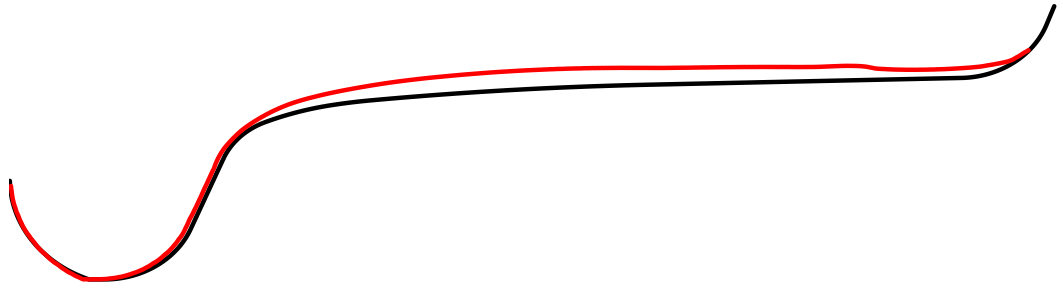


Figure 3-18: Typical outer wheel profile of squealing wheelset

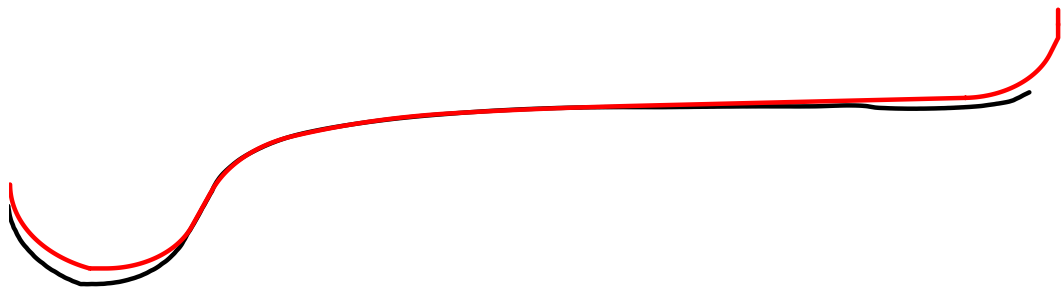


Figure 3-19: Squeal outer (black) vs. No 23 wheel profile (red)

From Figure 3-7(c), the leading inner wheel could also have high levels of longitudinal creepage. In addition, the leading inner wheel also exhibits a high lateral force which implies lateral creepage. The leading inner wheel has not been identified as squealing in the test curves. To better understand this phenomenon, the rolling radius difference function of the leading and trailing (squealing) wheelsets on the measured rail profiles for four different squealing bogies are shown in Figure 3-20. Also shown in Figure 3-20 is the design rolling radius difference function for the ore line. Figure 3-20(a), (b) and (c) show rolling radius difference functions where the wheel profile of the trailing outer wheel has worn conformal to the test curve high rail profile, whilst the wheel profile of the leading outer wheel has not worn conformal to the test curve high rail profile. Figure 3-20(b) show rolling radius difference functions where the leading wheelset has worn TFR No 21 profiles and the trailing wheelset worn TFR No 23 wheel profiles.

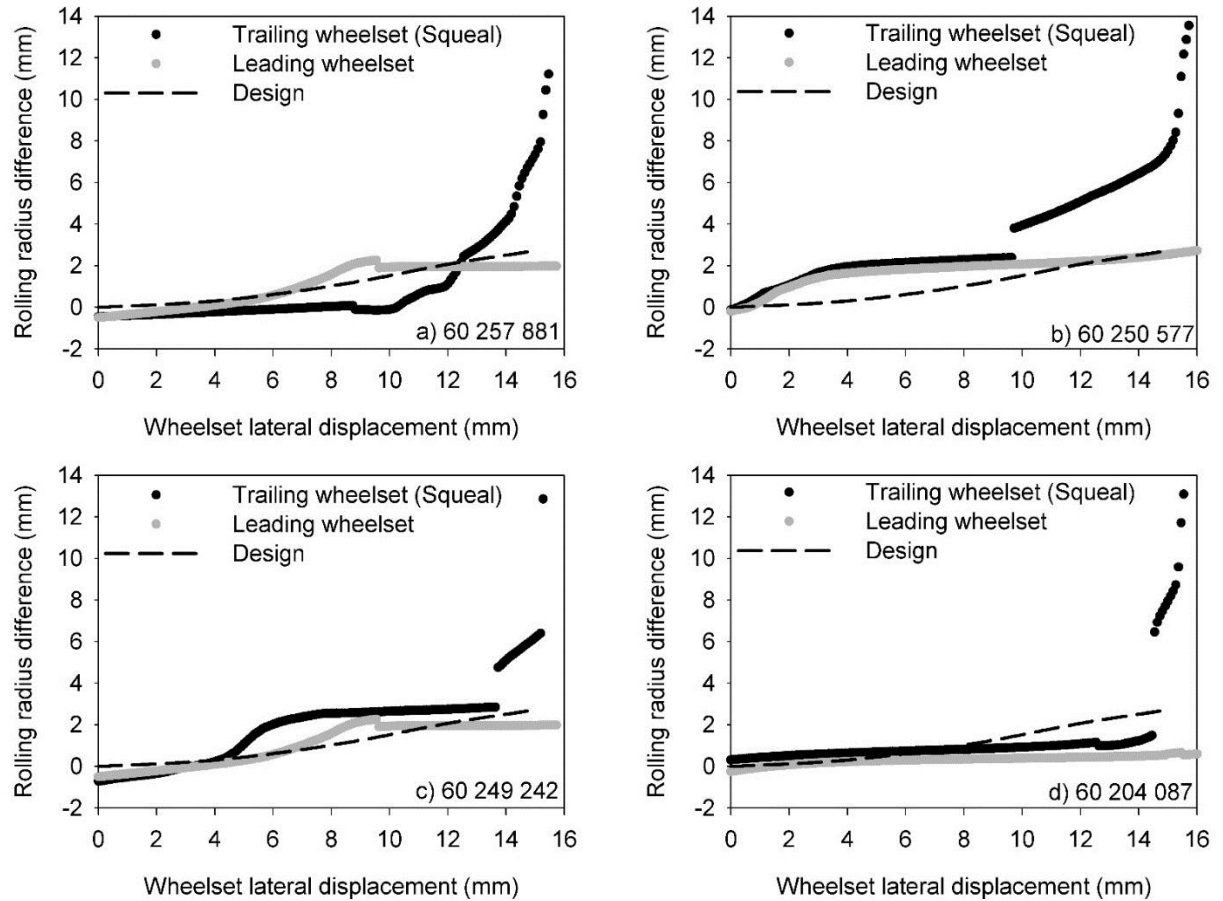


Figure 3-20: Rolling radius difference functions of four different squealing bogies

From Figure 3-20 it can be seen that for the four cases shown, the trailing wheelset (squealing wheelset) has much larger rolling radius differences compared to the leading wheelset for large lateral displacements. This lower rolling radius difference on the leading wheelset for large lateral displacements potentially explains why squeal due to unsteady longitudinal contact is not excited at the leading inner wheel of the bogie.

The large rolling radius differences at large lateral displacements on the trailing wheelset can be attributed to wheel and rail profiles that have worn conformal.

3.3 TRACKING CONDITION OF SQUEALING BOGIES

To understand why the squealing wheelsets curve with such large rolling radius differences in the test curve, ideally it is necessary to simulate the curving behaviour of such bogies taking into consideration the worn wheel and rail profiles in addition to any geometric deviations present in the bogie. This will likely give the required insight as to what is causing the bogie to track skew and the squealing wheel to wear conformal with a typical rail profile found on the line.

Performed curving simulations of squealing bogies are presented in Chapter 4. The importance of this section is to discuss the tracking condition of squealing bogies on tangent track and how this influences the curving behaviour in the test curve.

The presence of geometric deviations influencing the tracking condition of bogies can be judged by the measurement of wheel-rail forces and wheelset lateral displacement on tangent track and at slow speed. The bogie tracking signature for a healthy bogie on tangent track is shown in Figure 3-21. The lateral force signature in Figure 3-21(a) shows a small lateral force towards the gauge side of both the left and right rails due to the vertical-to-lateral cross-talk of the lateral force measurement circuit as discussed in Section 3.2.2. A positive lateral force has the convention of acting towards the left of the measurement site facing the direction of movement of empty ore trains. The wheelset lateral displacement in Figure 3-21(b) shows that both wheelsets are running close to the centre of the track with a small (1.23 mm) wheelset tracking error (TE). The wheelset TE is defined in Figure 3-22.

Lateral force and wheelset displacement measurements on tangent track were conducted on 20 and 21 November 2012. Of the two empty trains that were recorded during 20 and 21 November 2012, eight wagons could be identified that squealed in the 1000 m left hand test curve during the October 2012 measurement campaign. Of these eight wagons, only six had the same running orientation as a month earlier and was chosen for analysis. The other two wagons that were running with a reverse orientation can be attributed to the regular turning around of wagons in service to combat asymmetrical wheel wear.

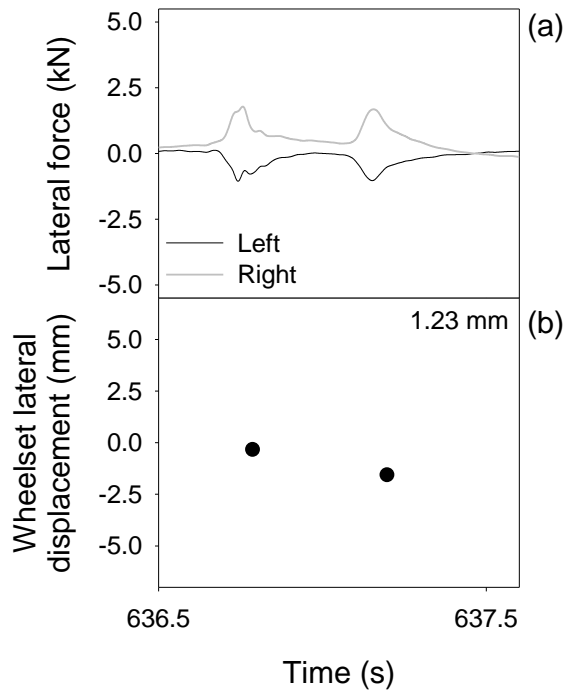


Figure 3-21: Lateral force signature for a healthy bogie on tangent track

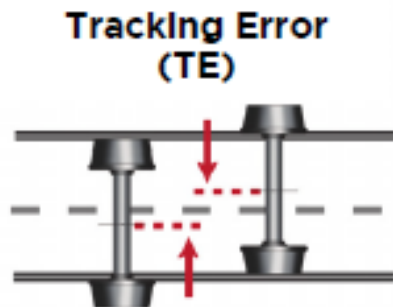


Figure 3-22: Bogie tracking error

The lateral force signatures of the six squealing bogies recorded on tangent track and running in the same orientation as in the test curve is shown Figure 3-23. Compared to the lateral force signature in Figure 3-21, all the squealing bogies were curving with creep forces at tangent track. This is an indication that the squealing bogies all have some sort of geometrical error causing the bogies to track skew on tangent track. Most noticeably the bogies were curving with negative creep forces at the leading wheelset and positive creep forces at the trailing wheelset (Figure 3-23(a), (b), (d) and (e)). In three of four cases above, the bogie had a tracking error of about + 4 mm. A positive tracking error implies that the leading wheelset

was displaced towards the left of the track compared to the trailing wheelset and in the direction of train movement.

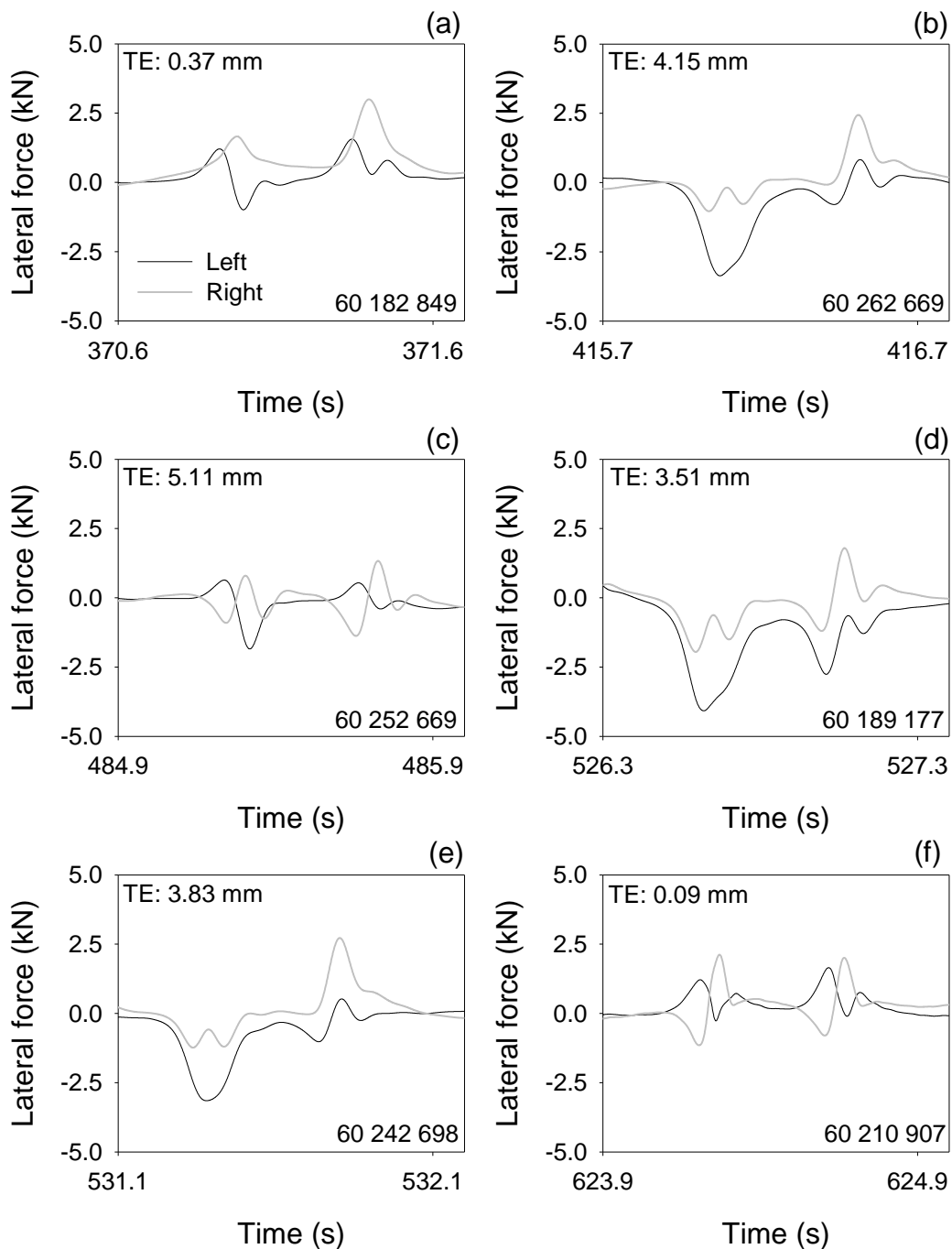


Figure 3-23: Lateral force tracking signatures of six squealing bogies on tangent track

The influence of a + 4 mm tracking error on the rolling radius difference functions of the leading and trailing wheelsets with No 21 wheel profiles on the design ore line rail profiles are shown in Figure 3-24. Figure 3-24 shows that the 4 mm tracking error significantly influences the symmetry of the rolling radius difference functions. Such a bogie will not be able to run on tangent track without generating longitudinal creep forces. To combat these longitudinal creep forces the bogie will generate creep forces on tangent track (lateral and longitudinal) as shown in Figure 3-25. Here the forces acting on the wheels are shown in contrast to the rail force measurements (action-reaction forces). The wheelset tracking error results in a yaw misalignment of the self-steering bogie to compensate for the longitudinal creep forces caused by the inter-axle misalignment.

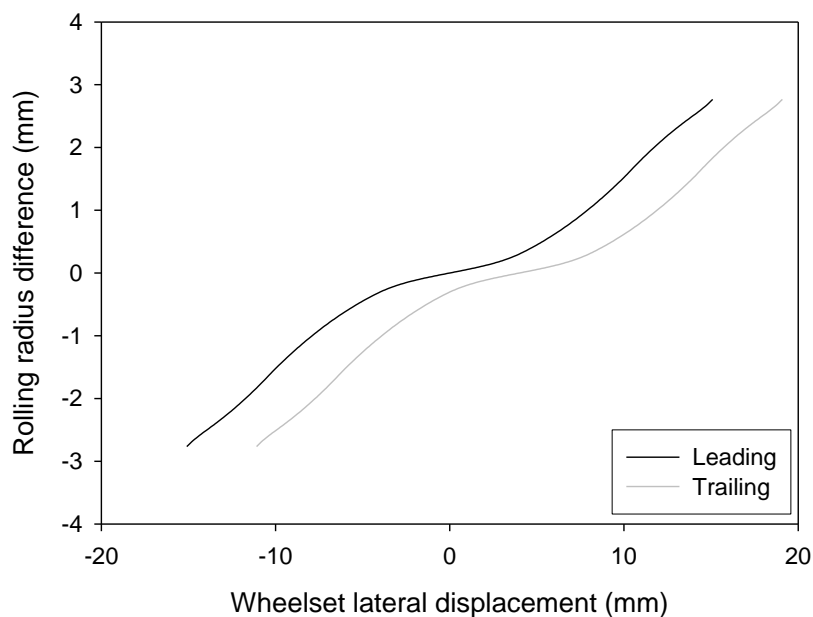


Figure 3-24: Rolling radius difference function mismatch due to + 4 mm TE

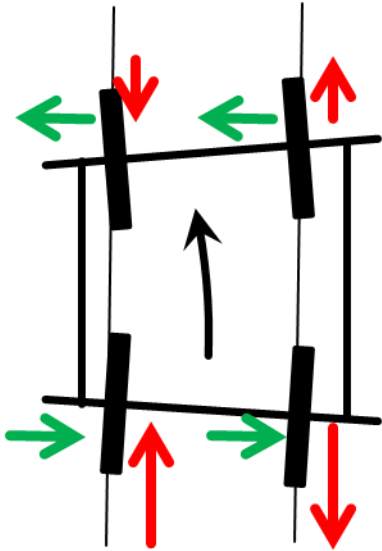


Figure 3-25: Prevalent curving signature of squealing bogies on tangent track

A yaw-misalignment of the wheelsets as shown in Figure 3-25 is beneficial to bogie curving in a left hand curve (see Figure 3-26(a)) and detrimental to curving in a right hand curve. Similarly, if the leading wheelset is displaced to the right with respect to the trailing wheelset (negative tracking error), bogie curving is impaired in a left hand curve (see Figure 3-26(b)) and assisted in a right hand curve. Figure 3-26 only shows a left hand curve to correspond to the left hand test curve.

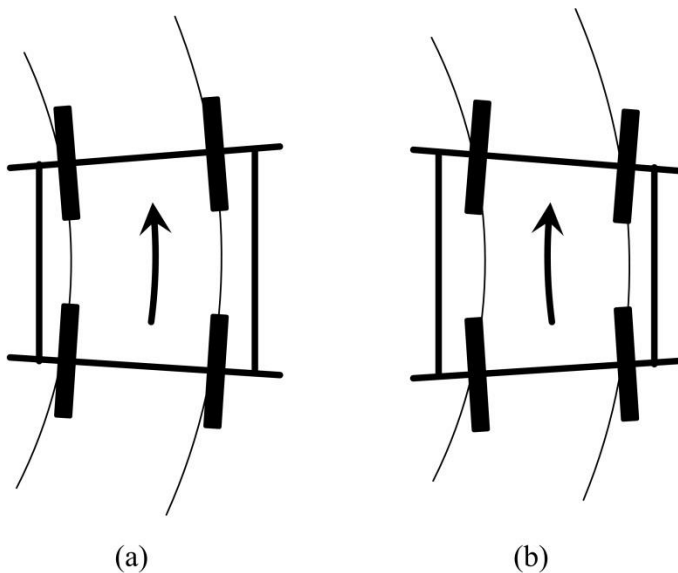


Figure 3-26: Wheelset curving positions in a left hand curve (a) Self-steering (b) Over-steering

Judging from the tracking signature of the squealing bogies on tangent track (Figure 3-25), it can be anticipated that the non-symmetric rolling radius difference functions for a positive tracking error should assist bogie curving in the left hand test curve. Because this is not the case, the question can be asked why the squealing bogies did not curve with lateral track forces indicative of self-steering in the test curve but instead with large lateral creep forces at the leading wheelset and large lateral wheelset displacements of both the leading and trailing wheelsets. The answer to this question is contained in the measured rolling radius difference functions of the squealing bogies' wheelsets originally profiled to the No 21 wheel profile. The rolling radius difference functions for the squealing bogie's wheelsets on the test curve's rail profiles shown in Figure 3-20 was calculated with the assumption that the leading and trailing wheelsets are symmetric with a zero tracking error. Figure 3-20(a) is reproduced as Figure 3-27 for convenience. It can be seen from Figure 3-27 that for wheelset lateral displacements exceeding about 12 mm, the rolling radius difference of the trailing wheelset is exceeding that of the leading wheelset, whereas for smaller lateral displacements the rolling radius difference of the leading wheelset is below that of the trailing wheelset. This implies that the bogie will behave different due to this rolling radius difference mismatch at different lateral displacements, i.e. the bogie can run on tangent track as shown in Figure 3-25 and then over-steers in a left hand curve for bigger lateral displacements when the bogie displaces towards the outer rail in the curve.

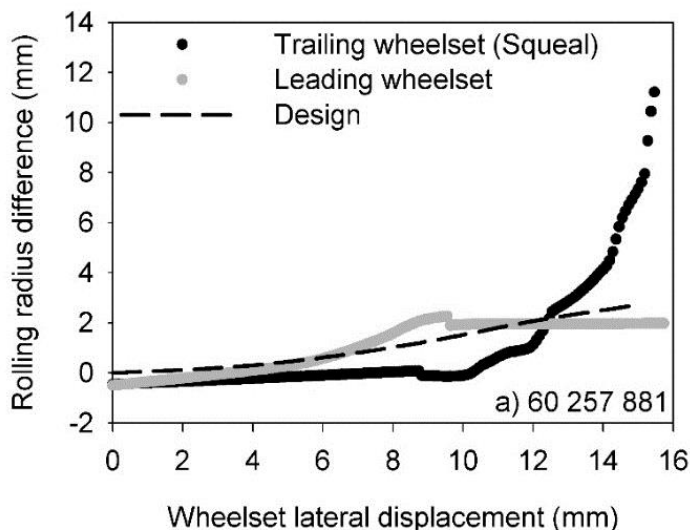


Figure 3-27: Rolling radius difference functions of trailing bogie of wagon 60 257 881

The criteria causing the over-steering of squealing bogies in the test curve and the subsequent high longitudinal creep forces can be summarised as follows:

The tracking error will exacerbate the flange throat wear on two of the diagonally opposite wheels of the bogie, whilst limiting the flange throat wear on the other two wheels. Because the design wheel and rail profile pair are non-conformal in the rail gauge corner/wheel flange throat contact area, the flange throat area of the wearing wheels will wear conformal to the dominant worn rail profile found on the ore line, whilst the other wheels will have a limited probability of wearing conformal. This is because the lateral displacement of the bogie is limited by the two wearing wheels, in essence shielding the other two wheels from wear except if the bogie takes on a severely rotated attitude. If the leading outer wheel has a non-conformal wheel profile and the trailing outer wheel a conformally worn wheel, the likelihood of the bogie curving with an over-steering curving attitude and large creepages at the trailing inner wheel increases and so the probability of squeal as well.

3.4 SQUEAL FREQUENCY VERSUS WHEEL DIAMETER

A plot of the identified squeal frequencies and wheel diameters for the three different wheel types is presented in Figure 3-28.

An estimation of the frequency before and after the passage of the source based on time-frequency plots similar to Figure 3-4(a) leads to an approximate squeal frequency, solving Equations 3 and 4 simultaneously. Wheel diameters were assessed statistically as the median of measurements stretching over a two month period, allowing for outliers due to measurement anomalies to be excluded from the data set.

The wheel diameters are 916 mm initially and are progressively machined down to maintain an acceptable wheel profile. The minimum allowed wheel diameter is 870 mm. The different wheel types are denoted as Types A, B and C.

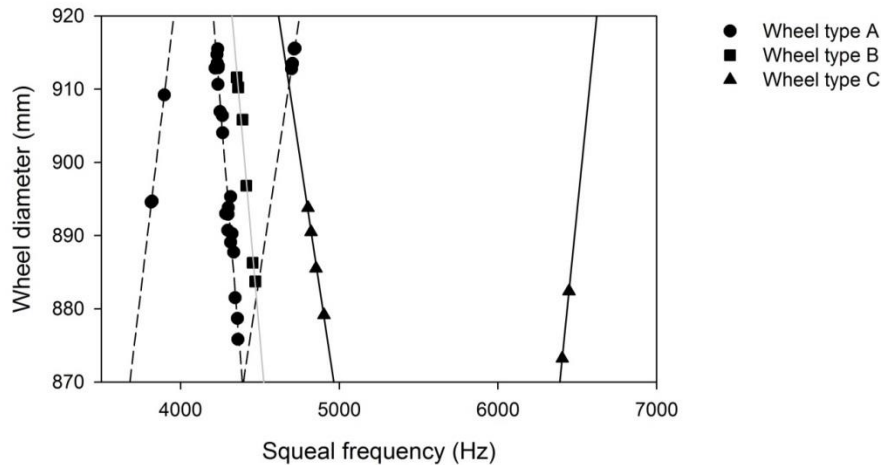


Figure 3-28: Squeal frequency vs. wheel diameter for three wheel types used on line

Figure 3-28 shows how the measured squeal frequencies of the different wheel types change over the lifespan of the wheel. It is evident from Figure 3-28 that for wheel Type A, three unstable modes can be identified from the measurement results. These are possibly related to three distinct eigenmodes of the wheel. The existence of three unstable modes for wheel Type A becomes evident from the linear variation of the measured squeal frequencies against wheel diameter for three distinct linear varying sets of data points associated with wheel Type A. This has been highlighted in Figure 3-28 with three dashed black linear regression lines. For wheel Type B, only one unstable mode can be identified as shown by the solid grey linear regression line. For wheel Type C, two unstable modes can be identified as highlighted by the solid black regression lines.

The results also prove that the wheels retain the ability to squeal over their entire lifespan. The reason that squeal for wheel Type C was only observed at smaller wheel diameters can be attributed to this wheel type currently being phased out from the ore line i.e. no new Type C wheels are being introduced and the existing wheels are allowed to be progressively machined down to 870 mm diameter.

It can also be observed from Figure 3-28 that the eigenfrequencies of some wheel modes increases with decreasing wheel diameter, whilst the eigenfrequencies of other wheel modes decreases with decreasing wheel diameter. Here it should be remembered that decreasing the wheel diameter will not only result in a reduction of mass, but also in changes to the stiffness matrix of the wheel. If the reduction in wheel diameter has a greater influence on the mass of the wheel compared to the local stiffness changes, the eigenfrequency will increase with decreasing wheel diameter and vice versa.

A correlation between the squeal frequencies and the wheel modes responsible for squeal are given in Section 5.2.

3.5 TOP-OF-RAIL FRICTION MODIFICATION

Top-of-rail friction modification is one of the known mitigation measures to combat curve squeal, although its success is site dependent. To verify if top-of-rail friction modification can be used as a measure to combat squeal in the test curve, field tests were conducted from 15 to 18 August 2013.

During the field test a hand-pushed tribometer was used to evaluate the effect of the top-of-rail friction coefficient on the emitted squeal noise. The dry top-of-rail coefficient of friction was 0.64. During dry top-of-rail conditions all empty trains had at least one inner squeal event occurring with very high amplitude. With the adequate spread of friction modifier in the curve, the coefficient of friction reduced to 0.43 and no squeal events emanated from the empty trains. At a coefficient of friction of 0.52 some weak instances of audible squeal was again observed from the empty trains. The reported coefficient of friction is the average coefficient of friction measured over a length of rail of 150 m and consisted between 50 and 70 coefficient of friction measurements.

The top-of-rail friction modifier was applied by hand using a paint brush on both the inner and outer rails of the curve over a length of 200 sleeper spacings in both directions from the microphone location. Starting at the microphone location the top-of-rail friction modifier was painted on the top of the inner and outer rail every 6th sleeper spacing.

The coefficient of friction of 0.43 was measured after the first loaded 342 wagon train passed over the test section. The subsequent passing of trains removed more friction modifier from the railhead allowing a relationship to be obtained between the coefficient of friction and the presence of squeal.

3.6 FLANGE THROAT SQUEAL

Recording sound pressure levels of passing trains in the test curve using a sampling frequency of 50 kHz, provides a usable frequency range of 25 kHz. This allowed squeal to be classified as low frequency audible, high frequency audible and ultrasonic squeal. Low frequency audible squeal occurs below 10 kHz where human hearing is most sensitive and where abatement of the unacceptable sound level is important. High frequency squeal occurs between 10 and 20 kHz. Here human hearing has diminished sensitivity. Frequencies above 20 kHz are classified as ultrasonic and are inaudible to humans. Whilst only low frequency

audible squeal is important from a noise abatement perspective, it is equally important to understand the physics behind high frequency squeal and why it occurs at such frequencies.

Figure 3-29 shows the time-dependent linear frequency spectra of the sound pressure levels recorded for the passing of a typical empty ore train. Figure 3-29 does not show the entire length of the train. It only shows about 40 wagons of the 342 wagon consist. The low frequency audible squeal occurring between 4 and 5 kHz occurs at the trailing inner wheel contact due to unsteady longitudinal creepage as discussed earlier. In addition to the low frequency audible squeal events, a significant number of high frequency audible and ultrasonic squeal events can be identified from Figure 3-29. Using the source identification technique described in Section 3.2.1, the squeal events occurring above 10 kHz could be attributed to the leading outer wheel in flange contact.

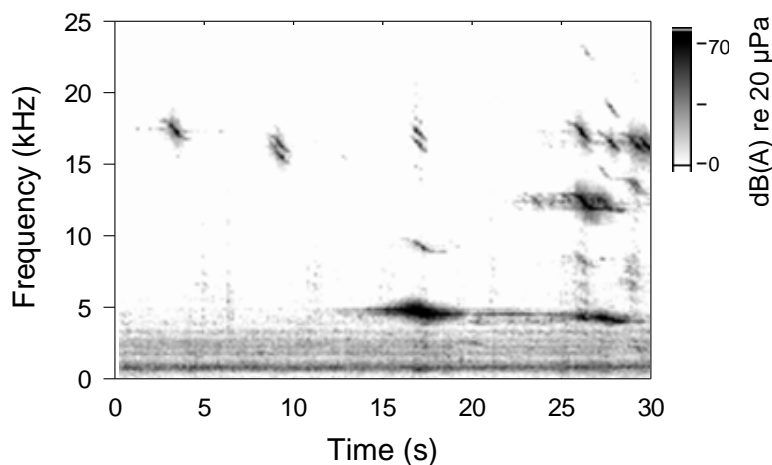


Figure 3-29: Time/frequency analysis showing squeal for an empty ore train

In contrast to the passing of empty ore trains, the passing of loaded ore trains was characterised by high amplitude broadband flanging noise. Flanging noise occurring during the passage of empty ore trains occurred intermittently and never at high sound pressure levels. See for example the time period between 5 and 7 seconds in Figure 3-29. An example of flanging noise during the passage of a loaded ore train is shown in Figure 3-30. Figure 3-30 is representative of the passing of approximately 40 loaded ore wagons. In addition to the broadband flanging noise, one high frequency audible squeal event at low amplitude can be identified occurring at roughly 17 kHz and 28 seconds.

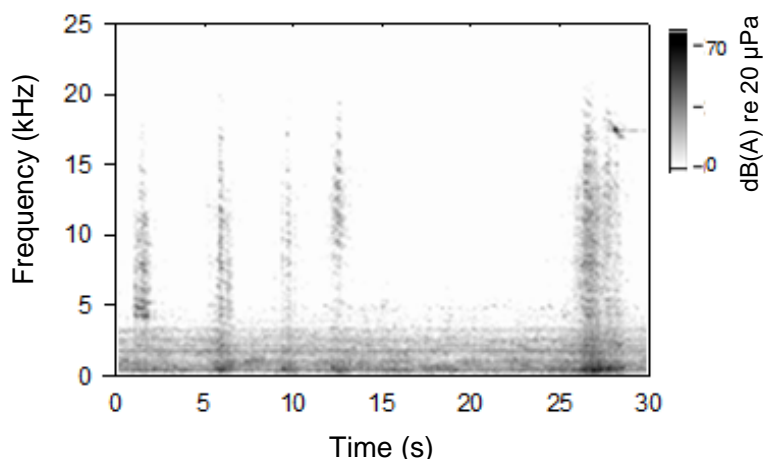


Figure 3-30: Time/frequency analysis of a portion of a passing loaded ore train

A joint time-frequency analysis of the wayside sound pressure measurements showed that reduced squeal amplitudes from empty trains can be associated with increased flange rubbing on the squealing wheel. This was observed by comparing the flanging frequencies in the time-dependent linear frequency spectra representing high, medium and low amplitude squeal events occurring at similar frequencies. High, medium and low amplitude squeal amplitudes represent squeal occurring at A-weighted sound pressure levels greater than 110 dB (re 20 μ Pa), between 100 and 110 dB (re 20 μ Pa), and below 100 dB (re 20 μ Pa). This result is similar to that in Remington (1987), showing that flange contact/rubbing brings about a reduction in squeal noise amplitude.

3.6.1 Flanging/squeal noise and bogie curving

The lateral force curving signature of an empty wagon curving using creep forces alone and emitting rolling noise is shown in Figure 3-31. Although one expects the lateral creep forces acting on the high and the low rail to be similar for the same wheelset, Figure 3-31 shows a difference of about 1 kN (100 kg) between the high and the low rail for an empty wagon. This is due to some cross-talk (due to torsion) between the vertical wheel/rail force and the lateral stress arising from torsion measured on the foot of the rail. The measured lateral forces on the high and the low rail thus both have a small measuring error towards the inside of the track for most wheel-rail contact conditions. Depending on their direction, the measured lateral creep forces will thus either increase or decrease due to the small measurement error. The magnitude of this influence increases as contact is made further towards the field or gauge corner side of the rail. This measurement error does, however, not distort the lateral force curving signatures that are discussed in this thesis.

Once a bogie has lost its ability to steer around a curve using only frictional (creep) forces, the flange face or flange throat of the leading outer wheel comes into contact with the gauge face or gauge corner of the high rail to steer the bogie. Subsequently, flange contact and high levels of spin creepage, that are associated with wheel-rail contact occurring at high contact angles between the rail gauge corner and the wheel flange throat, result in a lateral force opposing the lateral force component due to lateral creep. The resultant lateral force of the leading wheelset thus becomes less negative or even positive on the high leg while the lateral forces on the low leg remain largely unchanged. Figure 3-32 and Figure 3-33 show respectively the curving signatures for a bogie under an empty wagon and making contact between the rail gauge corner and wheel flange throat as well as for a bogie additionally making contact between the rail's gauge face and the flange face. Flange and spin creep forces (F) act in a direction opposite to the lateral creep forces (C).

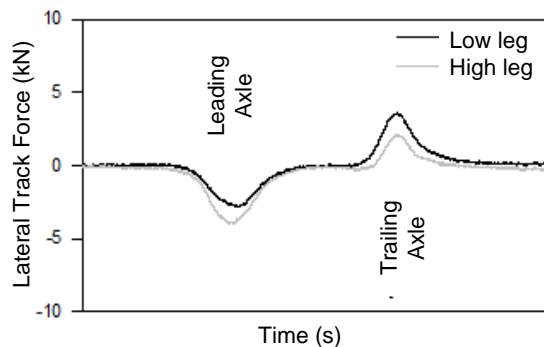


Figure 3-31: Lateral force curving signature for bogie curving solely using creep forces (empty wagon)

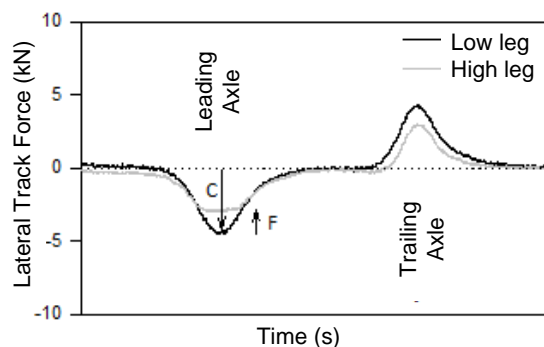


Figure 3-32: Lateral force curving signature with flange root contact of the leading outer wheel (empty wagon)

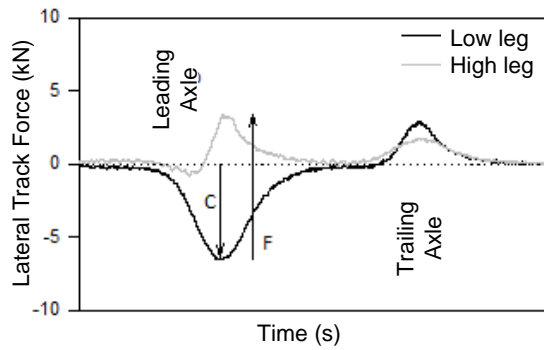


Figure 3-33: Lateral force curving signature with flange contact of the leading outer wheel (empty wagon)

Figure 3-34 shows the typical bogie curving signature for a flanging bogie under a loaded ore wagon. Comparing Figure 3-32 and Figure 3-33 with Figure 3-34, it is clear that the magnitude of the flange contact force for a loaded wagon is significantly larger compared to the flanging force occurring for empty wagons. This can be attributed to the axle load difference; being 50 kN/axle for an empty wagon and 300 kN/axle for a loaded wagon.

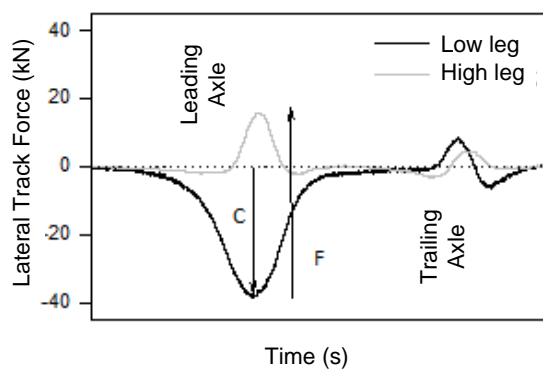


Figure 3-34: Bogie curving signature for loaded wagon flange contact event

For the bogie curving attitudes and load scenarios depicted in Figure 3-32 to Figure 3-34, the leading outer wheel was emanating (i) high frequency high amplitude squeal with no flanging noise (Figure 3-32), (ii) high frequency low amplitude squeal with a moderate amount of flanging (Figure 3-33) and (iii) high amplitude flanging noise with no squeal (Figure 3-34).

It thus becomes clear that as the flange contact force increases, the wheel moves away from emitting a tonal high amplitude squealing noise to emitting broadband flanging noise. Flange rubbing can thus be seen to introduce positive damping to wheel-rail contact, reducing the amplitude of flange throat contact squeal or preventing its excitation.

3.7 DISCUSSION

3.7.1 Inner wheel squeal

Low frequency squeal in the test curve occurs exclusively for empty wagons due to high levels of longitudinal creepage. The high levels of longitudinal creepage result from the contact conditions of some worn wheels on worn rail profiles, resulting in large rolling radius differences between the inner and outer wheels in the curve. The large rolling radius differences at the curve-inner squealing wheel is set-up by a mismatch between the worn rolling radius difference functions of the leading and trailing wheelsets, which in return is caused by initial geometrical deviations of the squealing bogie.

Similar to Fourie (2011), results from the current measurement campaign proved that low frequency squeal in the large radius test curve can be uniquely attributed to the trailing inner wheel of a bogie in contact with the low rail. All of the three wheel types used on the line are prone to inner wheel squeal and maintain this ability over the lifespan of the wheel. For wheel Type A three different unstable frequencies were identified, for wheel Type B only one, whilst for wheel Type C two unstable frequencies were identified.

The trial with top-of-rail friction modification has proven to be successful in mitigating squeal in the test curves.

3.7.2 Outer wheel squeal

Experimental results presented for a 1000 m radius curve have shown that the likelihood of flange contact squeal diminishes with increased rolling stock axle loading. This is because increased flange rubbing with high flange forces, as is likely to occur for higher axle loads, introduce positive damping to the wheel-rail contact. This positive damping reduces the amplitude of high frequency flange contact squeal or eliminates it completely. Instead flange rubbing with high flange forces causes broadband flange rubbing noise. Here it is important to distinguish between contact occurring solely between the rail gauge corner and wheel flange throat or additionally between the rail gauge and wheel flange faces.

4 CURVING BEHAVIOUR OF “SQUEALING” BOGIES

To confirm the experimental deduction that the large rolling radius differences at the curve-inner squealing wheel is set-up by a mismatch between the worn rolling radius difference functions of the leading and trailing wheelsets, which in return is caused by initial geometrical deviations of the squealing bogie, ideally it is necessary to simulate the curving behaviour of such bogies taking into consideration the worn wheel and rail profiles in addition to any geometric deviations present in the bogie and causing the bogie to track skew.

Simulating bogie geometric deviations with a symmetrical bogie model requires special modelling approaches, such as imposing a torque on the bogie's wheelsets to simulate different side frame lengths (Hettasch et al. 2017). This is because Multibody dynamic simulation software is configured to deal with perfect geometries or symmetric geometries such as equal wheel diameters, equal side frame lengths and zero tracking error. Alternatively it is necessary to build an unsymmetric bogie model by defining unsymmetric markers for each separate geometric entity without making use of symmetry in the model. Because a validated vehicle model of a CR-13 type iron ore wagon body with two Scheffel MkV self-steering freight bogies (Scheffel 1974 and 1978) is available at the author's research institution, the researcher opted not to build an unsymmetric bogie model taking into consideration a wheelset tracking error. Instead the researcher opted to simulate the curving behaviour and creepages occurring during squeal by considering the unique situation that a bogie with a TFR No 21 leading wheelset and a TFR No 23 trailing wheelset produced squeal in the test curve. This situation is likely to produce squeal even in the absence of bogie geometric deviations as the rolling radius difference functions contain the required features to produce squeal as discussed in Section 3.3. Worn wheel profiles of wagon 60 250 577 of which the rolling radius difference functions on the test curve rail profiles are shown in Figure 3-20(b) were used in the simulations. Comparing the rolling radius difference functions between the squealing bogies of wagons 60 257 881 (see Figure 3-20(a); both leading and trailing wheelsets with worn TFR No. 21 profiles) and 60 250 577 (leading TFR No. 21 (worn) and trailing TFR No. 23(worn)) it can be seen that the deviation of the rolling radius difference functions between the leading and trailing wheelsets of the squealing bogie appears similar at large lateral wheelset displacements. It is however noteworthy to mention that simulating the curving behaviour of wagon 60 257 881 with worn wheel profiles only, did not predict over-steering in the test curve and high longitudinal creepages at the trailing wheelset's wheel-rail contacts. For wagon 60 257 881 it can be anticipated that the geometrical error present will result in the bogie reaching equilibrium curving for larger wheelset lateral displacements and higher longitudinal creepages.

4.1 VEHICLE DYNAMICS SIMULATIONS

Full details of the vehicle dynamics model as well as its accuracy and validity can be found in Spangenberg (2016) and Spangenberg et al. (2016). Vehicle dynamics modelling and simulations were carried out in VI-Rail (VI-grade GmbH 2014). Some of the model highlights are repeated here for convenience.

The bogie model shown in Figure 4-1 includes non-linear friction elements to model the side bearers, the friction wedges and the centre bowl interface. The properties of these frictional elements were determined from test data. The connections between the various rigid bodies are graphically depicted in Figure 4-2.

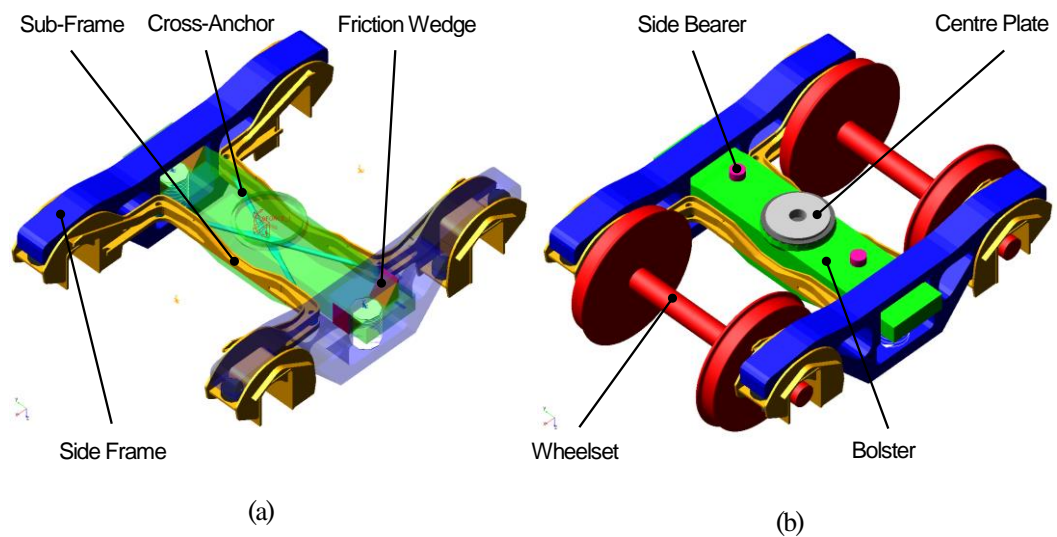


Figure 4-1: Model of MkV bogie illustrating (a) the hidden components and (b) the assembled bogie (Spangenberg 2016)

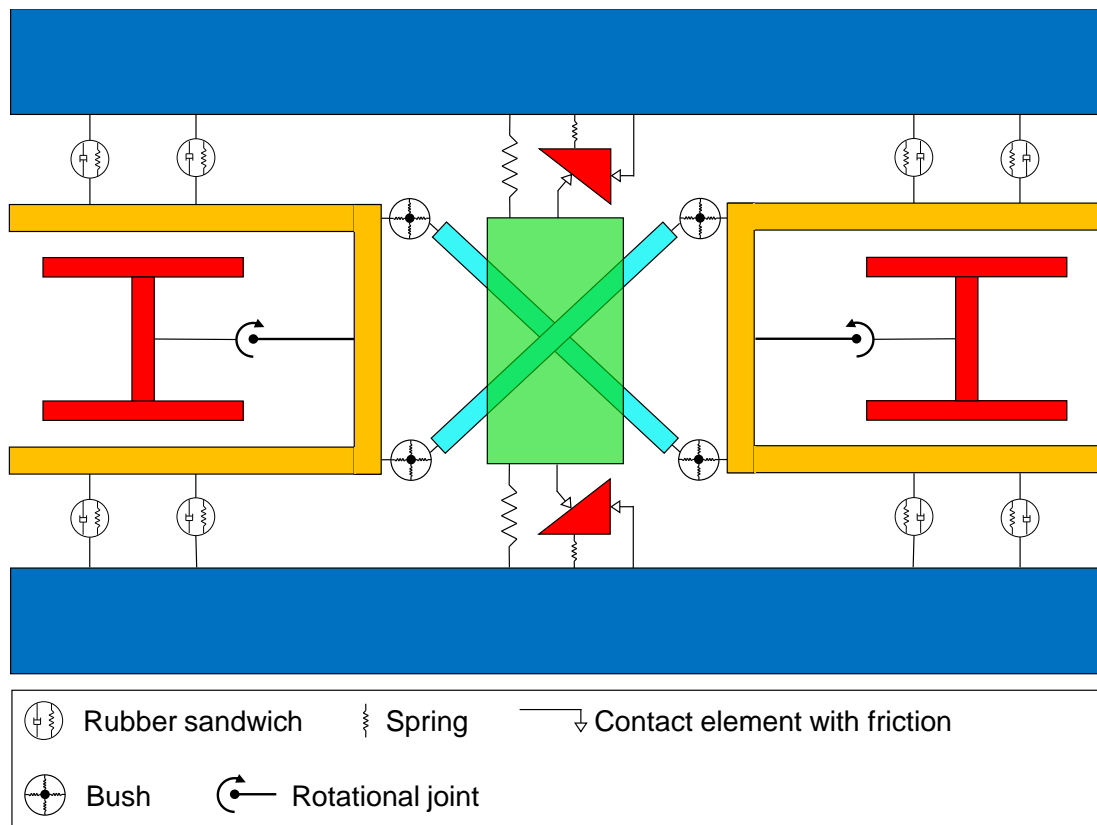


Figure 4-2: Graphical depiction of the connections between bodies of the MkV bogie model (Spangenberg 2016)

The primary suspension connecting the sub-frame and the side frame was established with the six degree-of-freedom (DOF) rubber sandwich element contained in Vi-Rail of which the stiffness (linear) and damping (non-linear) properties were determined experimentally. The secondary suspension located between the bolster and side frame was modelled with a six DOF linear spring. The connection between the cross-anchors and sub-frames were modelled as linear bushing elements with proportional damping. To model the connection between the axle boxes and the sub-frame as stiff in the horizontal plane rather than rigid, a rotational joint was implemented between the sub-frame and the wheelset to allow for rotation of the wheelset in the horizontal plane.

The fully assembled wagon is shown in Figure 4-3. The bogie and body are connected via the centre plate element locating the bogie relative to the body and allowing rotations of the bogies relative to the wagon body. In addition the side bearers allow frictional contact between the bolster and the wagon body once a defined gap is closed. The WRGEN wheel-rail contact element is used to model the interaction between the wheel and the rail. This contact model allows the use of general or measured wheel and rail profiles and calculates the

actual contact kinematics at each simulation step. This model allows the solution of multiple contact points, evaluating the local contact parameters based on the geometry and material properties. The FASTSIM algorithm (Kalker, 1982) was used in conjunction with this contact element to solve the wheel-rail contact problem.

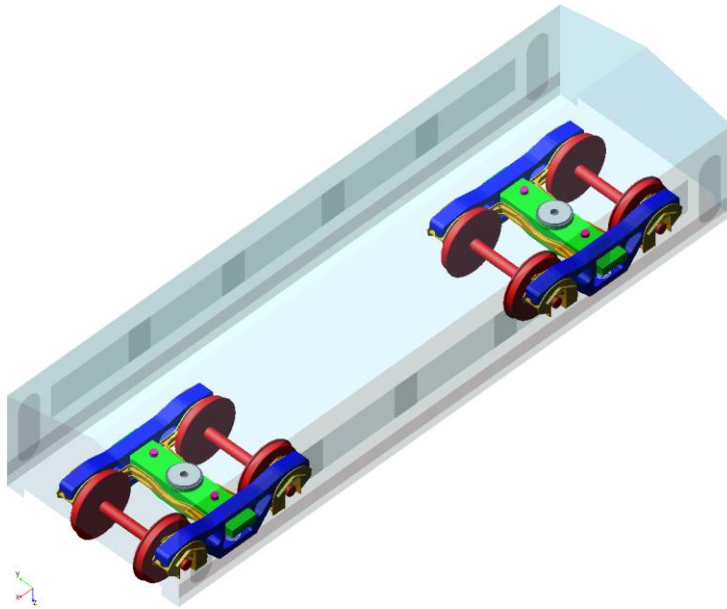


Figure 4-3: Assembled CR-13 wagon with two MkV self-steering bogies (Spangenberg 2016)

In the current study curving simulations were performed in a 1000 m radius curve with the measured worn wheel profiles of squealing wagons and the rail profiles measured in the test curve.

The simulation results for wagon 60 250 577 with worn wheel profiles are presented in this chapter. The scenarios considered are shown in Table 4-1.

Table 4-1: Simulation configuration for scenarios considered

Scenario	Coefficient of friction	Travel direction*	Tare/Loaded
1	0.6	Forward	Tare
2	0.4	Forward	Tare
3	0.6	Forward	Loaded
4	0.6	Reverse	Tare

* Forward is defined as the direction of travel producing squeal during the field tests.

Scenario 1 is the as-is squeal scenario of the wagon and is included to verify that the trailing inner wheel of the bogie indeed curves with large longitudinal creepage at the trailing inner wheel-rail contact, as suggested by the experimental results in Chapter 3. Scenario 2 is included to compare the curving ability of the squealing bogie when the wheel-rail coefficient of friction is 0.6 and 0.4 respectively. This comparison is included to verify that it is indeed the reduction in the coefficient of friction that is responsible for squeal mitigation and not a possible change in curving behaviour of the bogie. Scenario 3 is included to verify that similar to the experimental results, the worn wheel profiles do not influence the curving ability of the bogie in the loaded condition. Scenario 4 is included to understand how the curving behaviour of the squealing bogie changes when its orientation is reversed, i.e. when the conformally worn wheelset is leading.

In addition to the Scenarios 1 to 4, Scenario 0 is included in all figures reporting the curving performance of Wagon 60 250 577 as the curving performance for the case of an empty wagon with the design wheel and rail profile combination.

4.1.1 Bogie curving performance

When a rigid frame bogie with two parallel axles negotiates a curve, the sum of the absolute values of the AoA of the leading and trailing axles is equal to the bogie wheelbase divided by the curve radius (Remington 1987). For a rigid frame bogie with a wheelbase of 1.83 m (wheelbase of MkV bogie) in a 1000 m curve, this sum equals 1.83 mrad. For a MkV self-steering bogie the compliance of the two wheelsets rotating into radial curving positions in a 1000 m radius curve can be judged as a deviation from 1.83 mrad. If this value is smaller than 1.83 mrad, the wheelsets have rotated in the same sense as the curve radial direction. This is beneficial to bogie curving as shown in Figure 3-26(a). If this sum is larger than 1.83 mrad, the longitudinal creep forces acting at the suspension elements have rotated the two wheelsets away from the curve radial direction resulting in an over-steering bogie. See Figure 3-26(b).

The curving performance of the squealing bogie of Wagon 60 250 577 for the four scenarios in Table 4-1 is summarised in Figure 4-4 as the sum of absolute values of the AoA of the leading and trailing wheelsets. It can be seen from the results that the curving performance of the squealing bogie is significantly impaired for Scenarios 1 and 2, whilst for both the loaded scenario and travelling in the reverse direction, the wheel profiles of the bogie allow it to make use of the bogie's self-steering capabilities.

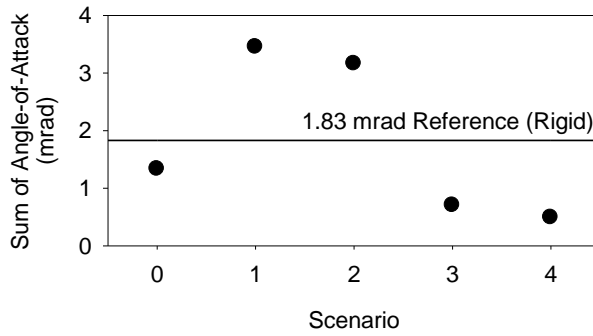


Figure 4-4: Bogie curving performance for different scenarios

In addition to the sum of AoA results, the simulation results for the four scenarios in Table 4-1 are summarised in Figure 4-5 and Figure 4-6 as the wheelset lateral displacement and AoA of the squealing bogie respectively. In Figure 4-7 the longitudinal and lateral creepage at the squealing wheel-rail contact are shown.

The wheelset lateral displacement and longitudinal creepage results are included to confirm the experimental findings in Chapter 3 in that the key kinematic parameter influencing squeal in the large radius test curve is the lateral displacement of the wheelset leading to high levels of longitudinal creepage. The AoA and lateral creepage results are included to verify the experimental deduction in Chapter 3 that the squealing wheelsets curve with small AoAs and that lateral creepage is not important for the generation of squeal in the test curve.

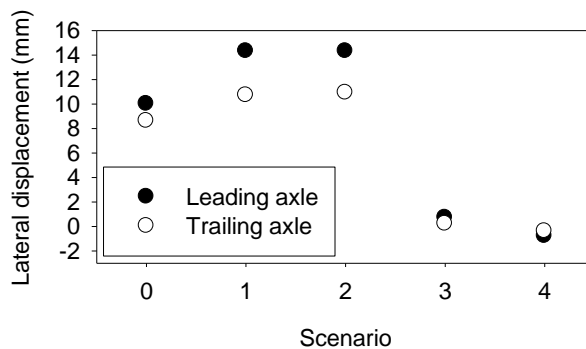


Figure 4-5: Wheelset lateral displacement results

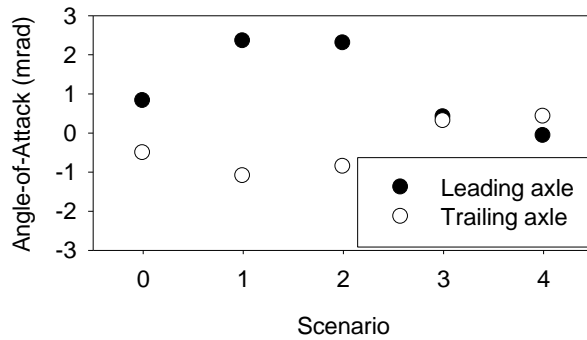


Figure 4-6: Angle-of-Attack results

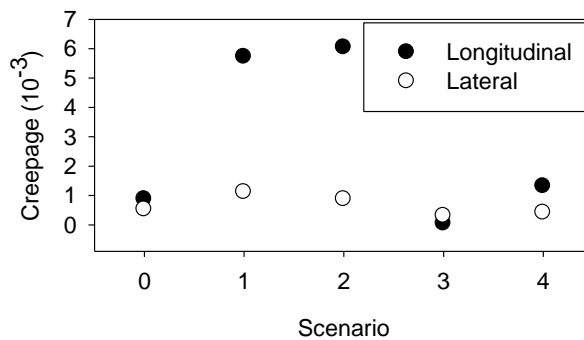


Figure 4-7: Creepages at squealing wheel-rail contact

4.2 OPERATING POINT OF SQUEALING WHEEL ON ADHESION CURVE

The operating point of the squealing wheel on the adhesion curve is crucial to the instability. It is known in advance that creep saturation with a negative slope of the adhesion curve is a pre-requisite for squeal to occur due to falling friction. This is because a negative gradient of the adhesion curve indicates negative damping. On the other hand a positive gradient of the adhesion curve corresponds to positive damping. If the positive frictional damping is small enough and doesn't exceed the positive energy generation associated with mode-coupling instability, instability can occur for the small positive gradients of the adhesion curve leading up to the adhesion optimum in addition to the falling part of the adhesion curve.

In practice the exact shape of the creep force-creepage relationship is seldom known, making it difficult to identify the exact operating point on the adhesion curve.

In an attempt to model curve squeal, authors assume different creep force-creepage models. As an example Périard (1998), Huang et al. (2008) and Squicciarini et al. (2015) implemented

a falling friction law in FASTSIM. FASTSIM is the name given by Kalker (1982) for his simplified steady-state non-linear rolling contact theory. FASTSIM originated from Kalker's efforts to reduce the computational cost associated with his "exact" rolling contact theory CONTACT (1990). CONTACT is currently the only rolling contact theory that is fully non-linear and transient. Pieringer (2011) implemented Kalker's theory CONTACT in her time-domain squeal model with a constant friction coefficient in addition to considering the roughness of the wheel and rail running surfaces. In their work De Beer et al. (2000, 2003) implemented Vermeulen and Johnson's (1964) approximate non-linear rolling contact theory with Kraft's (1967) model for falling friction. Kraft's model for falling friction was also used by Fingberg (1990). On the other hand Huang et al. introduced a falling friction coefficient based on previous experimental roller-rig findings which were also used by Ding et al. (2016). Zenzerovic (2017) aims at making Pieringer's (2011) squeal model faster by including a point contact model for the tangential contact defined beforehand using CONTACT.

Kalker's non-linear rolling contact theories CONTACT and FASTSIM describe the case for clean and smooth surfaces. In reality the surfaces are neither smooth nor clean and surface roughness as well as contamination at the wheel-rail interface have a significant impact on the initial slope of the creep force-creepage relationships that have been measured (Meymand et al. 2016). To accommodate the effects of contamination and surface roughness a coefficient called "percent" Kalker is often used (see e.g. Magel and Liu (2009)). Polach (2005) introduced two reduction factors, one for the adhesion area (k_A) and the other for the slip area (k_S) to accommodate both the initial gradient and the gradient of the creep force-creepage function for large creep near creep saturation. The gradient of the creep force-creepage function for low creepages corresponds to the reduction of Kalker's coefficient by

$$k = \frac{k_A + k_S}{2} \quad k_A, k_S \leq 1 \quad (\text{Equation 7})$$

In addition, Polach's model also considers falling friction that is typically measured for large creepage values by using a variable coefficient of friction expressed by

$$\mu = \mu_0[(1 - A)e^{-Bv} + A] \quad (\text{Equation 8})$$

where A is the ratio of limit friction coefficient μ_∞ at infinite slip velocity to maximum friction coefficient μ_0 , v the creep velocity and B is the coefficient of exponential friction decrease.

In Polach's model, the adhesion coefficient for pure longitudinal creepage μ_1 is given by

$$\mu_1 = \frac{2\mu}{\pi} \left(\frac{k_A \varepsilon_1}{1+(k_A \varepsilon_1)^2} + \arctan(k_S \varepsilon_1) \right) \quad (\text{Equation 9})$$

where ε_1 is the gradient of the tangential stress in the contact longitudinal direction given by

$$\varepsilon_1 = \frac{1}{4} \frac{G\pi ab C_{11}}{Q\mu} \lambda_1 \quad (\text{Equation 10})$$

G is the shear modulus, a and b the contact area half axes of the assumed elliptical contact area in the longitudinal and transverse directions, Q the wheel load, λ_1 the longitudinal creepage and C_{11} the creepage coefficient from Kalker's linear theory (Kalker 1990).

To define a creep force-creepage relationship for the current study, Polach's model using Equations 9 and 10 was used. To use Polach's model the following parameters need to be defined: the reduction variables k_A and k_S , the contact variables a , b , Q and C_{11} as well as the friction model μ .

Typically the reduction factor k for dry rails as evaluated from measurements is 0.6 to 0.85 (Polach 2005). Choosing the value of k as 0.85, due to the very little environmental contamination expected, and choosing a reduction factor for the area of adhesion k_A as 1.00, k_S is calculated using Equation 7 as 0.70. Very little environmental contamination is expected based on the very high top-of-rail coefficient of friction of 0.64 measured in the test curve for dry wheel-rail contact conditions.

Typical contact parameters for the wheel-rail contact area of a squealing wheel are available from the vehicle dynamics simulations and summarised in Table 4-2.

Table 4-2: Contact parameters from vehicle dynamics simulation

Contact parameter	Value	Unit
a	4.5	mm
b	2.5	mm
Q	20	kN
C_{11}	5.31	-

Not knowing the parameters A and B from experimental measurements to define a falling friction model according to Equation 8, Kraft's (1967) model for falling friction (as was used in previous squeal models) is used. Kraft's formula for the friction coefficient was derived theoretically and then adapted to fit experimental measurements under longitudinal creepage and can be written as

$$\mu = \mu_0 [1 - 0.5e^{-0.138/|v|} - 0.5e^{-6.9/|v|}] \quad (\text{Equation 11})$$

where v is the sliding velocity which can be expressed as $v = \lambda V_0$. Here λ is the creepage and V_0 the rolling velocity. For the present study, μ_0 is chosen as 0.64 as measured for dry wheel-rail contact conditions using a hand pushed tribometer in the test curve.

The creep force-creepage relationship assumed in the current study and calculated for a speed of 60 km/h (typical of the speed in the 1000 m test curve for the squealing iron ore wagons) with the above defined parameters is shown in Figure 4-8. The adhesion optimum occurs at 0.62 % longitudinal creepage, beyond which the friction curve has a negative slope.

The longitudinal creepage of 0.57 % predicted by the vehicle dynamics simulations for the investigated squealing case, most likely places the squealing wheel at a point on the adhesion curve with a positive friction slope before the point of creep saturation is reached. This is the first clue that the instability in the test curve might be caused by mode-coupling instability. Instability due to falling friction can only be excited beyond creep saturation if the creep force-creepage relationship has a falling slope. On the other hand Pieringer (2011) shows that for a specific squeal case excited due to mode-coupling, instability occurs below the adhesion limit. Here the positive frictional damping is not of magnitude to overcome the positive energy generation associated with mode-coupling instability.

Although 0.57 % longitudinal creepage most likely places the squealing wheel at a point on the simulated adhesion curve before creep saturation is reached, a conclusion cannot be given with certainty as to which side of the saturation point the squealing wheel is operating. This uncertainty stems from the fact that it is difficult to accurately calculate/assume the adhesion curve for a particular wheel-rail contact situation. For this reason both situations are possible, i.e. the squealing wheel operating below and beyond the point of creep saturation, and will be assessed in the thesis going forward.

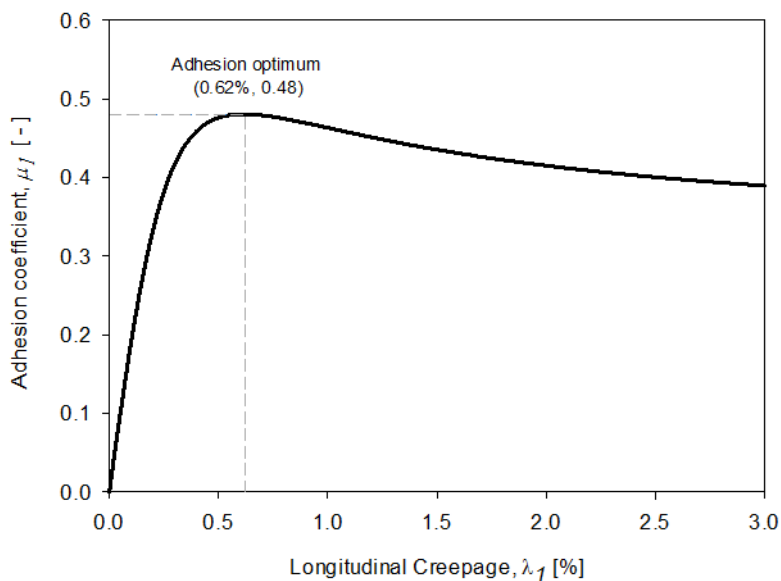


Figure 4-8: Adhesion curve assumed for current study

4.3 DISCUSSION

Vehicle dynamics simulations confirm the experimental result that the key kinematic parameter influencing squeal in the large radius test curve is lateral displacement of the wheelset leading to high levels of longitudinal creepage at the wheel-rail contact of the squealing wheel. The simulations also confirm that the squealing wheels are subjected to predominantly longitudinal creepage with little lateral creepage.

The operating point of the squealing wheel on the adhesion curve gives the first clue that instability in the test curve might result from mode-coupling instability. This deduction will be confirmed by the curve squeal model in Chapter 6.

5 WHEEL EIGENMODES INVOLVED IN SQUEAL

Chapters 3 and 4 provided a description of the key kinematic and vehicle dynamics parameters influencing the generation of squeal in the test curve.

To complete the experimental characterisation of squeal, the current chapter is concerned with identifying the wheel eigenmodes involved in squeal and establishing a relationship between the kinematic parameters found to be important to squeal and such eigenmodes.

The study of the wheel eigenmodes involved in squeal were conducted via modal analysis of wheel Types A and B of known diameter (916 mm) and mounted under an empty ore wagon. In addition the damping ratios of wheel modes with $n \geq 2$ were also determined for the freely suspended wheelset for wheel Type A.

In addition finite element modal analysis was used to visualise the wheel modes identified as being involved in squeal. This also confirmed that such eigenmodes have significant out-of-plane vibration that can be linked to the high noise levels associated with squeal.

5.1 EXPERIMENTAL MODAL ANALYSIS

Due to the regular sinusoidal pattern in the circumferential direction of the mode shapes of the wheel, a detailed modal analysis was not used to identify the modes of vibration of the wheel responsible for squeal. Instead a simplified approach was followed to study the mode shapes of the mounted wheel.

Firstly, a modal analysis was conducted to identify the sinusoidal pattern of each mode in the circumferential direction around the wheel tread. The measurement grid encompassed nine measurement points spaced at unequal distances around a quarter of the wheel (see Figure 5-1).

The angular positions of grid points A to G and O were chosen to correspond with nodal diameters of the sine modes with 1 to 8 nodal diameters and aligned to have one of their nodal points at the wheel-rail contact point. Excitation was provided at grid point H, which was selected to not coincide with a nodal diameter of one of the 1 to 8 nodal diameter sine modes. The wheel was excited in the radial, axial and circumferential directions at the excitation point. Excitation in the radial direction was applied on the wheel tread, excitation in the axial direction on the field side of the wheel rim and excitation in the circumferential direction was applied via a small steel block rigidly mounted on the wheel tread.

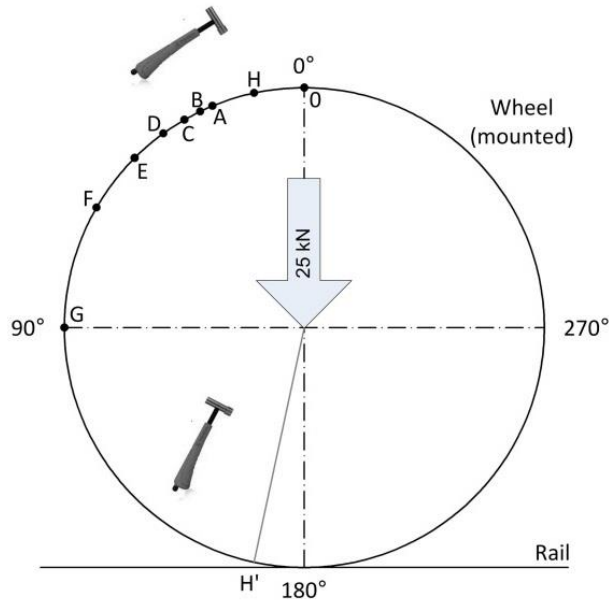


Figure 5-1: Measurement grid on wheel

For the modal analysis an instrumented hammer was used to provide the excitation and the response was measured using a single tri-axial accelerometer. A roving accelerometer approach was used to capture the wheel mode shape components in the radial, axial and circumferential directions at each measurement point. An average of three impacts was used for each measurement. The response, radial and circumferential excitation points on the wheel tread were chosen 105 mm from the back of the flange to correspond with the average of the contact positions identified for the inner squealing wheels via the results of the RsGeo simulations. The receptance for each input/output location was recorded and later used to extract the modal parameters of each mode using the least squares exponential curve fitting algorithm available in the Labview environment.

The eigenvectors representative of the different modes were normalised to unit modal mass.

An example of the results for sinusoidal pattern recognition is presented in Figure 5-2. The results are plotted for the unwrapped rim between 0° and 90° . Because the wheel-rail contact point fixes the location of the nodal diameters, the cosine modes could also be identified from the modal analysis.

Figure 5-2 shows the radial, circumferential and axial mode shape components for the six-nodal-diameter radial doublet modes occurring at 3942 Hz and 3970 Hz respectively.

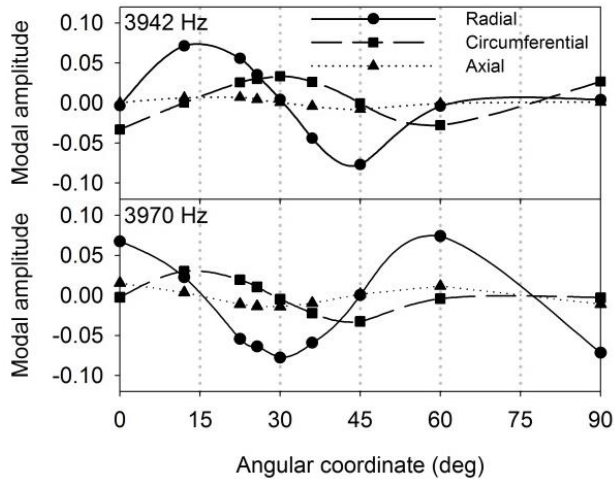


Figure 5-2: Mass normalised sinusoidal mode shape components at wheel tread

It is evident from the mode shape components that the modes have large modal amplitudes in the radial and circumferential directions at the wheel tread.

Secondly, a modal analysis was carried out on a single cross section of the wheel. The grid points were spaced 25 mm apart and were located at the wheel cross section indicated by H' in Figure 5-1. By studying the response of a single cross section the number of nodal circles can be determined.

5.2 EIGENMODES INVOLVED IN SQUEAL

Figure 5-3 shows a comparison between the measured squeal frequencies and the eigenfrequencies of the wheel eigenmodes most likely to be involved in squeal for wheel Types A and B at the test curve. Because the relationship between the squeal frequency and wheel diameter varies linearly, this data can be used to relate the squeal frequency to the modal behaviour of a single wheel of known diameter and that did not produce squeal in the test curve. Using the linear regression lines shown in Figure 5-3 the squeal frequency can be estimated for a 916 mm diameter wheel. This eliminates the need to study the modal behaviour of unique squealing wheels having different diameters to identify if the same modes are responsible for squeal.

Figure 5-4 shows the measured vertical and longitudinal point receptances of the measured wheel (wheel Type A freely suspended) in relation to the squeal frequencies estimated for a 916 mm diameter wheel. Figure 5-5 shows the measured vertical and longitudinal point receptances of the measured wheel (wheel Type B freely suspended) in relation to the squeal frequencies estimated for a 916 mm diameter wheel. The estimated squeal frequencies are

shown in the figures using a vertical dotted line. The peaks in the vertical and longitudinal contact point receptances at the unstable frequencies belong to the two separate doublet modes of the shown unstable modes.

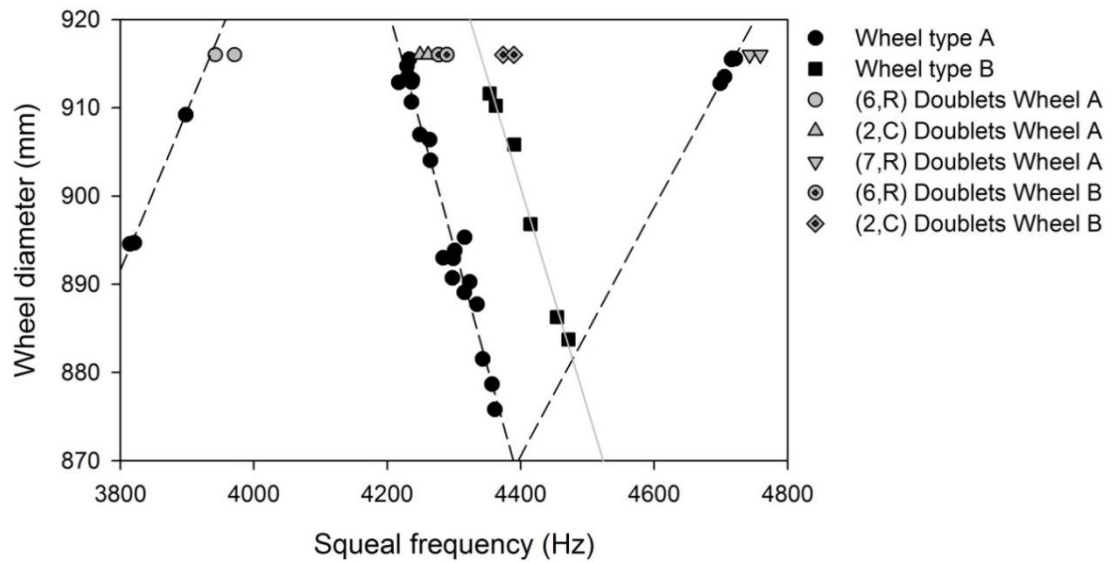


Figure 5-3: Comparison between wheel eigenfrequencies and squeal frequencies

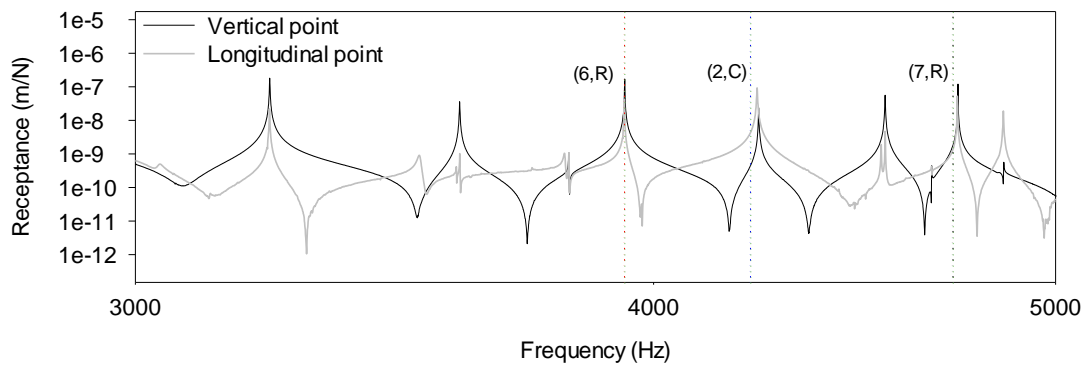


Figure 5-4: Magnitude of wheel receptances (vertical point and longitudinal point) on wheel tread measured for a 916 mm diameter wheel in relation to squeal frequencies for wheel type A

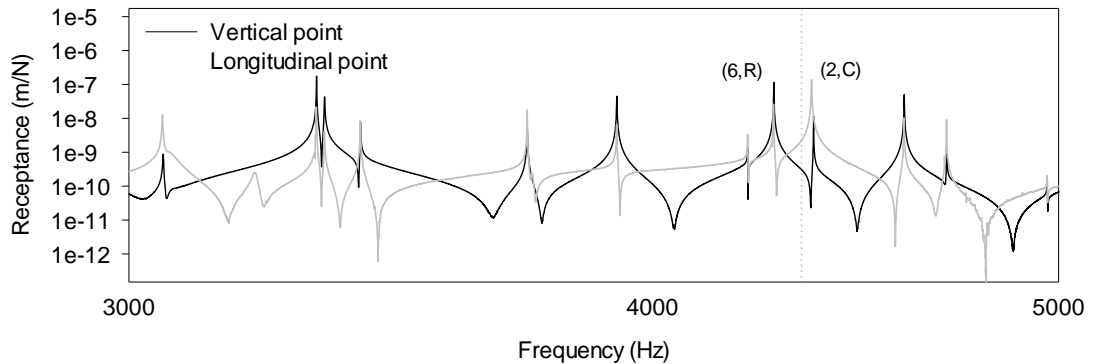


Figure 5-5: Magnitude of wheel receptances (vertical point and longitudinal point) on wheel tread measured for a 916 mm diameter wheel in relation to squeal frequencies for wheel type B

Table 5-1 compares the estimated squeal frequency of wheel Types A and B for a 916 mm diameter wheel with both the eigenfrequencies of the mounted and freely suspended wheelset.

It is evident from Figure 5-3 and Table 5-1 that the squeal frequencies associated with wheel Type A closely match the eigenfrequencies of (i) the six-nodal-diameter radial doublet modes, (ii) the two-nodal-diameter circumferential doublet modes and (iii) the seven-nodal-diameter radial doublet modes. Also evident from Table 5-1 for wheel Type A is that the three squeal frequencies occur at a lower frequency compared to the eigenfrequencies measured for both the mounted and suspended wheelset. Whilst the doublet modes for the suspended wheelset occur at the same frequency, the wheel-rail contact conditions causes the symmetry of the wheel to be broken and causes the doublet modes to occur at different frequencies.

Table 5-1: Estimated squeal frequency versus measured eigenfrequencies

	Mode	Mounted wheelset	Suspended wheelset	Squeal frequency
Wheel A	(6,R)	3942 & 3970 Hz	3937 Hz	3935 Hz
	(2,C)	4249 & 4261 Hz	4240 Hz	4220 Hz
	(7,R)	4743 & 4760 Hz	4736 Hz	4722 Hz
Wheel B	(6,R)	4277 & 4289 Hz	4276 Hz	4340 Hz
	(2,C)	4374 & 4390 Hz	4365 Hz	

In contrast to this, the squeal frequency associated with wheel Type B occurs approximately halfway between the sets of eigenfrequencies representing the six-nodal-diameter radial doublet modes (4277 Hz and 4289 Hz for a 916 mm diameter wheel) and the two-nodal-diameter circumferential doublet modes (4374 Hz and 4390 Hz for a 916 mm diameter wheel) of the mounted wheelset.

This behaviour where the unstable frequency of a self-excited system occurs not at an eigenfrequency of the system, but between eigenfrequencies of the system is characteristic of mode-coupling instability where the eigenfrequencies of two structural modes of an undamped system come, as a function of the control parameter, closer and closer together until they coalesce and a pair of a stable and unstable mode results (Hoffmann 2002). Thus, this type of behaviour might indicate mode-coupling between the (6,R) and (2,C) modes. However, the frequency difference between the (2,C) doublets (for both the mounted and suspended wheelset) and the squeal frequency is comparable between wheel Type A and B suggesting that only the (2,C) doublets could be important to squeal for wheel Type B. The frequency difference between the measured eigenfrequencies and the squeal frequency is shown in Table 5-2 and Table 5-3 for the mounted and suspended wheelsets respectively.

Table 5-2: Estimated squeal frequency versus eigenfrequencies of mounted wheelset

	Mode	Mounted wheelset	Squeal frequency	Difference
Wheel A	(6,R) cosine	3970 Hz	3935 Hz	35 Hz
	(6,R) sine*	3942 Hz		7 Hz
	(2,C) cosine*	4261 Hz	4220 Hz	41 Hz
	(2,C) sine	4249 Hz		29 Hz
	(7,R) cosine	4760 Hz	4722 Hz	38 Hz
	(7,R) sine*	4743 Hz		21 Hz
Wheel B	(6,R) cosine	4289 Hz	4340 Hz	-51 Hz
	(6,R) sine*	4277 Hz		-63 Hz
	(2,C) cosine*	4390 Hz		50 Hz
	(2,C) sine	4374 Hz		34 Hz

Table 5-3: Estimated squeal frequency versus eigenfrequencies of suspended wheelset

	Mode	Mounted wheelset	Squeal frequency	Difference
Wheel A	(6,R) cosine	3937 Hz	3935 Hz	2 Hz
	(6,R) sine			
	(2,C) cosine	4240 Hz	4220 Hz	20 Hz
	(2,C) sine			
	(7,R) cosine	4736 Hz	4722 Hz	14 Hz
	(7,R) sine			
Wheel B	(6,R) cosine	4276 Hz	4340 Hz	-64 Hz
	(6,R) sine			
	(2,C) cosine	4365 Hz		25 Hz
	(2,C) sine			

5.2.1 Mode shape components of eigenmodes relevant to squeal

Figures 5-6(a) to (d) present the radial and circumferential mode shape components of the mode shapes identified to be relevant to squeal and having an anti-node at the wheel-rail contact point. The mode shape components in Figure 5-6 were obtained by fitting a sine curve to the estimated mode shape components shown in Figure 5-2 and extended for the full circumference of the wheel. The mode shapes are plotted for an unwrapped rim between 90° and 270° with the contact point occurring at 180° and additionally indicated with an arrow in the figures.

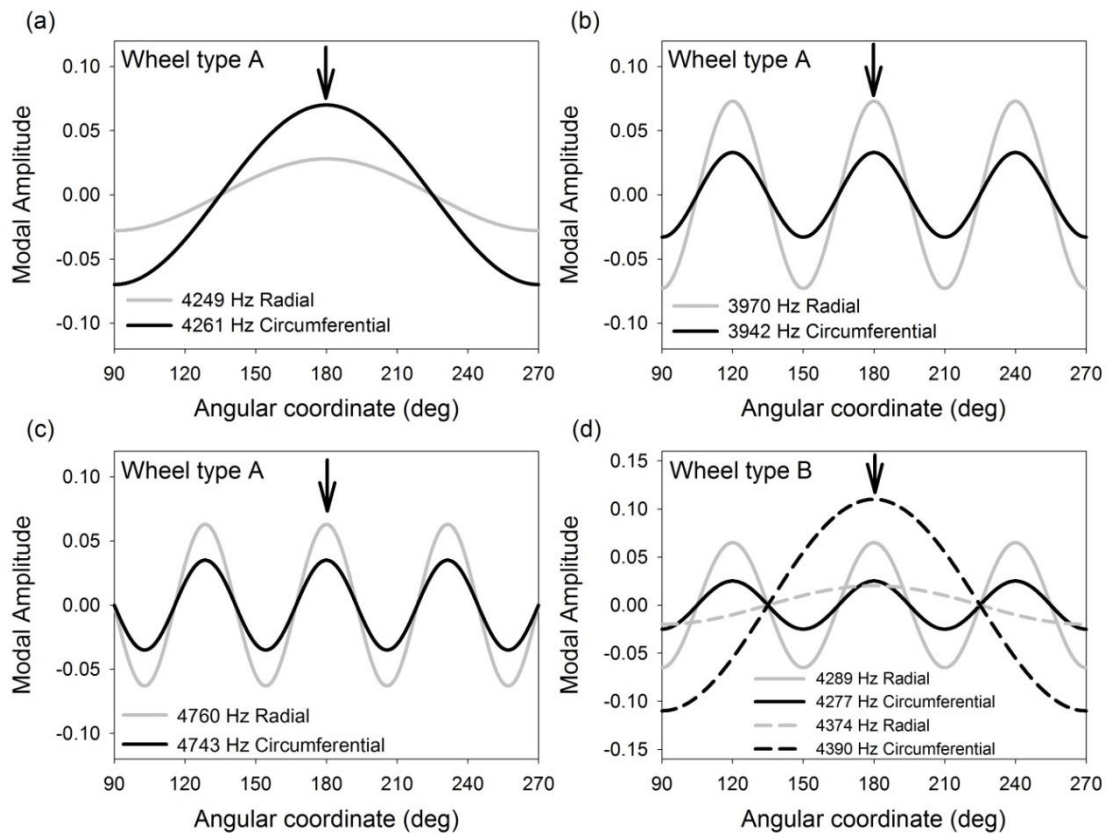


Figure 5-6: Radial and circumferential mode shape components of eigenmodes most likely to be relevant to squeal

It is difficult to overlook the fact that two modes are present for each squeal frequency, one with a large mode shape component in the contact radial direction and the other with a large mode shape component in the contact longitudinal direction. For wheel Type A the modes are the independent doublet modes occurring at almost identical frequencies. For wheel Type B the modes are the cosine modes of the (6,R) and (2,C) doublet modes respectively, but could also be the (2,C) doublet modes. All of the above doublet modes will experience strong frictional coupling in addition to strong structural coupling. The structural coupling is a consequence of the moving load nature of the rotating wheel, causing the otherwise independent sine and cosine doublets to become two complex modes with vertical/longitudinal cross-coupling with respect to the contact. This vertical/longitudinal cross-coupling that is non-zero for a wheel being exposed to moving load excitation might prove important for squeal due to unsteady longitudinal creepage.

If mode-coupling instability was to be applied to curve squeal excited as a result of the presence of large longitudinal creepage at the wheel-rail interface, it would suggest that the

self-excited oscillations are to be caused by the proportionality between the longitudinal creep force and the normal force during sliding as well as structural coupling between the vertical and longitudinal degrees of freedom of the wheel-rail system with respect to the contact. Both of the above criteria are met by the doublet modes of the rotating wheel subject to moving load excitation, where the one doublet has a large mode shape component in the radial direction at the wheel-rail contact and the other a large mode shape component in the longitudinal contact direction.

If the friction force causes the vertical and longitudinal oscillations to become out-of-phase, the longitudinal friction force, which depends on the vertical displacement, becomes out-of-phase with longitudinal motion and could potentially feed energy into the vibrating system due to positive work. This hypothesis for squeal occurring due to longitudinal creepage will be evaluated in Chapter 6.

5.3 FINITE ELEMENT MODAL ANALYSIS

Similar to a loudspeaker membrane, the wheel web forms a disk that radiates noise very efficiently when vibrating in a form normal to its plane. Wheel modes having significant out-of-plane vibration generate the main part of curve squealing. To ascertain that the identified radial and circumferential modes would indeed be capable of the high noise levels associated with squeal occurring in the test curve, it is necessary to verify that these mode shapes have significant out-of-plane wheel web displacement.

The mode shapes of the five eigenfrequencies identified from the previous analysis to be relevant to squeal, were calculated (for wheel Types A and B) using commercial finite element software. The wheel diameter considered in the FE model is 916 mm. The wheel was modelled using three-dimensional 8-node solid elements. This was achieved by constructing a 2D mesh of a single cross section of the wheel which was then revolved 100 times around the circumference using an angular spacing of 3.6° to create 3D brick elements. Only a single wheel of the railway wheelset was modelled, with the axle omitted and the wheel rigidly constrained at the center of the hub. The omission of the axle results in negligible errors for mode shapes with two or more nodal diameters (Thompson 2009). In total the model consisted of 98 041 nodes and 287 049 degrees of freedom and was evaluated between 0 and 6 kHz. The wheel material properties used in the model are a Modulus of Elasticity of 210 GPa, a Poisson's ratio of 0.3 and a density of 7850 kg/m^3 .

Example mode shapes calculated with the 3D model of wheel type A are shown in Figure 5-7(a) to (c). The finite elements of the mode shapes in the contact plane (on the right side of

each mode in Figure 5-7) have been coloured dark grey from the wheel hub to the wheel tread to assist with visualising the behaviour of the mode shape in the wheel-rail contact.

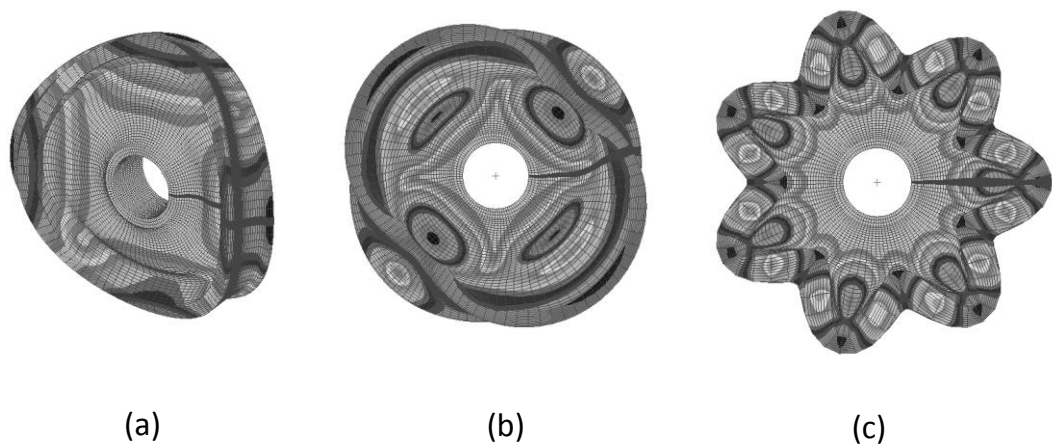


Figure 5-7: Example mode shapes of the 3D wheel model of wheel type A: (a) (2,0) cosine doublet (b) (2,C) cosine doublet (c) (7,R) cosine doublet

The deformation of the cross-section for wheel Types A and B for the modes identified to be relevant to squeal is presented in Figure 5-8. The undeformed shape is shown by the dashed lines in the figure. It is evident from the deformed cross-sections that the radial and circumferential modes for both wheel Types A and B contain considerable coupled axial motion of the web. This confirms that the identified mode shapes are capable of emitting high sound pressures.

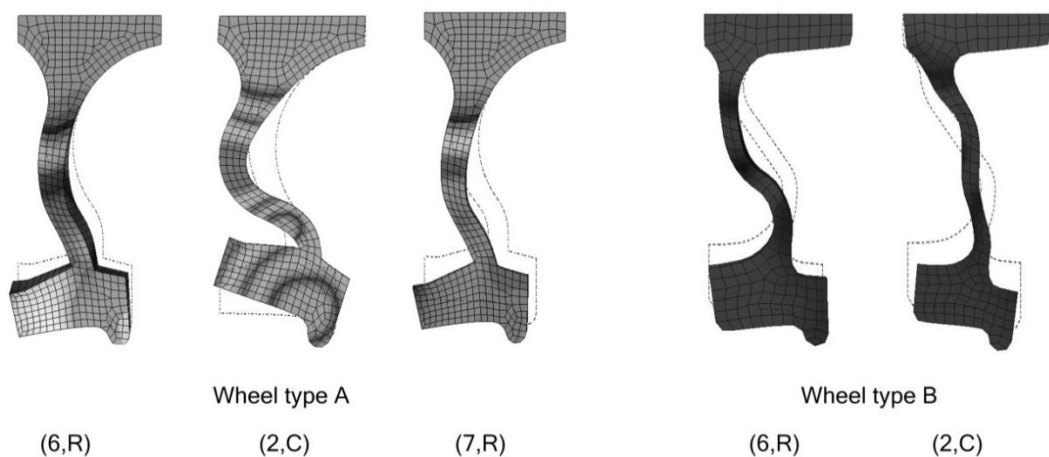


Figure 5-8: Modes of vibration of wheel Types A and B identified to be relevant to squeal

5.4 DISCUSSION

This chapter gives the second clue that mode-coupling might be responsible for squeal resulting from unsteady longitudinal creepage in the test curve. If mode-coupling instability was to be applied to curve squeal excited as a result of the presence of large longitudinal creepage at the wheel-rail interface, it would suggest that the self-excited oscillations are to be caused by the proportionality between the longitudinal creep force and the normal force during sliding as well as the coupling between the radial and circumferential degrees of freedom of the wheel-rail system with respect to the contact. In line with the above statement, modal analysis of a mounted wheel revealed that for each unstable frequency, two eigenmodes are likely to be important: one which has a large mode shape component at the wheel-rail contact in the circumferential direction and another which has a large mode shape component at the wheel-rail contact in the radial direction. This proves the existence of strong frictional coupling between the radial and circumferential degrees of freedom in the wheel-rail contact in the presence of high levels of longitudinal creepage at the unstable frequencies. Strong structural coupling between the above pair of modes (with respect to the wheel-rail contact point) exists due to the rotating wheel suffering moving load excitation. The moving load nature of the wheel causes the otherwise independent sine and cosine doublets to become two complex modes with vertical/longitudinal cross-coupling with respect to the contact. It is postulated that the vertical/longitudinal cross-coupling that is non-zero for a wheel being exposed to moving load excitation might prove important for squeal due to unsteady longitudinal creepage.

Based on the above evidence, a frictional self-excitation mechanism based on mode-coupling is favoured as being responsible for squeal excited in the large radius test curves. A model based on this mechanism will be developed in Chapter 6. The descriptive phase of the research provides the necessary data to validate a model based on mode-coupling instability.

6 FREQUENCY DOMAIN MODEL FOR RAILWAY WHEEL SQUEAL RESULTING FROM UNSTEADY LONGITUDINAL CREEPAGE

Contrary to the widely accepted belief that longitudinal creepage is not considered relevant to squeal, the author demonstrated in the Chapters 3 to 5 the importance of longitudinal creepage as a source of instability for squeal. The in-field study identified lateral displacement of the wheelset leading to high levels of longitudinal creepage at the wheel-rail contact of the squealing wheel as the key kinematic parameter influencing squeal in the 1000 m radius test curve. Vehicle dynamics simulations have shown that the combination of worn wheel and rail profiles cause affected Scheffel self-steering bogies underneath empty freight wagons to over-steer in the test curves. Over-steering causes both wheelsets of the bogie to displace laterally towards the outside of the curve causing high levels of longitudinal creepage. The simulations also showed that the squealing wheels are subject to predominantly longitudinal creepage with little lateral creepage. Over-steering occurs because of a tracking error between the wheelsets in the bogie causing the two sets of diagonally opposite wheels to wear differently. The tracking error exacerbates the flange throat wear on one pair of diagonally opposite wheels, whilst it reduces the probability of flange throat wear on the other pair of diagonally opposite wheels. Because the current ore line wheel-rail profile pair is designed to make two-point contact in the rail gauge corner/wheel flange throat contact area the one pair of diagonally wheels that protrudes the most into the flangeway will wear conformal. This causes the large rolling radius difference between the leading and trailing wheelset that results in an over-steering bogie and large longitudinal creepage at the trailing wheelset.

The current chapter presents a frequency domain model for the excitation of squeal due to longitudinal creepage with increasing, constant and falling friction. In this model the time varying part of the longitudinal creep force is modelled as a feedback loop and tested for stability with the Nyquist criterion.

6.1 FREQUENCY DOMAIN MODEL USING THE NYQUIST CRITERION

The self-excited vibration between the wheel-rail contact forces and their responses can be described as a feedback loop. Combining the equations for contact dynamics, wheel dynamics and rail dynamics, produces a loop gain for the tangential contact force. If the loop gain encircles the point (+1,0) on the Nyquist plane, the system is unstable. By plotting the real part of the open loop transfer function against frequency, the frequencies associated with these unstable points can be defined as potential unstable frequencies.

Such a frequency domain model to describe squeal due to unstable lateral creepage using a feedback loop was developed by De Beer et al. (2000, 2003). Whilst De Beer et al. include the variation of the normal contact force in their frequency domain squeal model, the motivation behind it was not to study mode-coupling instability. Instead the variation in the normal force was included to account for the influence that the lateral contact position on the wheel tread has on squeal noise due to lateral creepage with a falling friction characteristic.

Thompson and Monk-Steel (2003) extended the model developed by De Beer et al. to include longitudinal and spin creepage in addition to lateral creepage and normal load variations.

The feedback loop of De Beer's basic frequency domain model, which is based on unstable lateral creepage, is shown in Figure 6-1. f_2 is the potentially unstable lateral creep force, v_2 is the time varying lateral creep velocity and V_0 the rotational speed of the wheelset. The upper path represents the excitation due to falling friction and the middle path containing the term H_2 represents the influence of variations in the normal force on the lateral force. The term G in the upper path contains the mobilities of the wheel-rail system and H_2 contains terms for the contact mechanics including the slope of the adhesion curve.

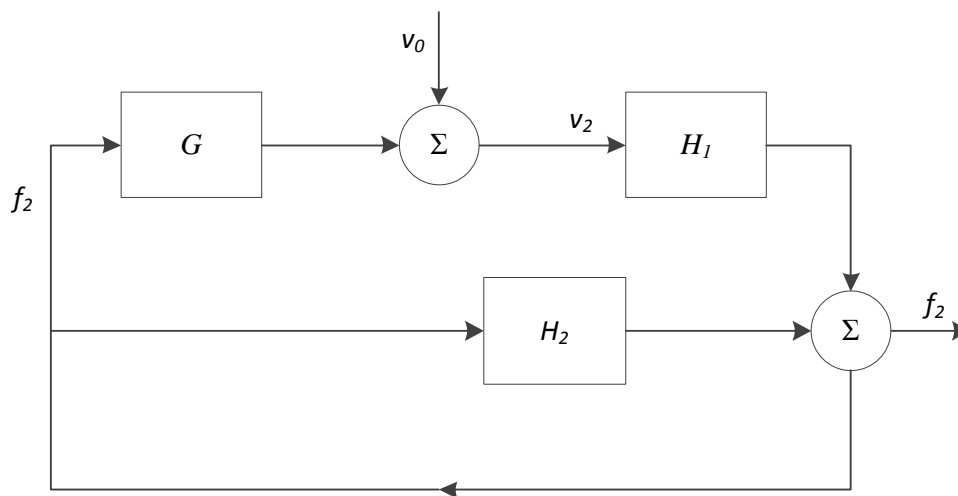


Figure 6-1: Feedback loop for squeal model (redrawn from Thompson 2009)

6.1.1 Unsteady longitudinal creepage

From Thompson and Monk-Steel (2003), for a case where only longitudinal creepage is important in producing squeal the loop gain, $H(\omega)$, for the potentially unstable longitudinal creep force f_1 is given by

$$H(\omega) = - \left(Y_{11} - \frac{Y_{13}Y_{31}}{Y_{33}} \right) \left(\frac{F_0}{V} \frac{\partial \mu_1}{\partial \lambda_1} \right) - \left(\mu_1 + \frac{F_0}{V_0} \frac{\partial \mu_1}{\partial f_3} \right) \frac{Y_{31}}{Y_{33}} \quad (\text{Equation 12})$$

where the indices 1 and 3 describe the longitudinal and normal directions with respect to the contact patch and described in Figure 6-2. $Y_{ij} = Y_{w,ij} + Y_{r,ij} + Y_{c,ij}$ is the sum of the wheel ($Y_{w,ij}$), track ($Y_{r,ij}$) and contact spring ($Y_{c,ij}$) mobilities. Mobility refers to the ratio of the output velocity to a harmonically varying unit input force at a given frequency. F_0 is the quasi-static vertical contact force and V_0 the rolling velocity of the wheel. μ_1 is the adhesion coefficient in the longitudinal direction, $\partial \mu_1 / \partial \lambda_1$ is the gradient of the creep force-creepage function for longitudinal creepage whilst $\partial \mu_1 / \partial f_3$ is the dependence of the adhesion coefficient on the normal force. The term $\partial \mu_1 / \partial f_3$ is only relevant in the unsaturated regime where there is still an adhesion zone in the contact. This term reduces to zero for creep saturation. The term $\partial \mu_1 / \partial f_3$ is ignored in the current model and Equation 12 simplifies to

$$H(\omega) = - \left(Y_{11} - \frac{Y_{13}Y_{31}}{Y_{33}} \right) \left(\frac{F_0}{V_0} \frac{\partial \mu_1}{\partial \lambda_1} \right) - (\mu_1) \frac{Y_{31}}{Y_{33}} \quad (\text{Equation 13})$$

The first term of Equation 13, $-\left(Y_{11} - \frac{Y_{13}Y_{31}}{Y_{33}} \right) \left(\frac{F_0}{V_0} \frac{\partial \mu_1}{\partial \lambda_1} \right)$, represents the excitation due to falling friction, whereas the second term, $-(\mu_1) \frac{Y_{31}}{Y_{33}}$, represents the influence of variations in the normal force on the longitudinal force. For a positive relationship of the creep force-creepage relationship, the first term can also represent positive frictional damping.

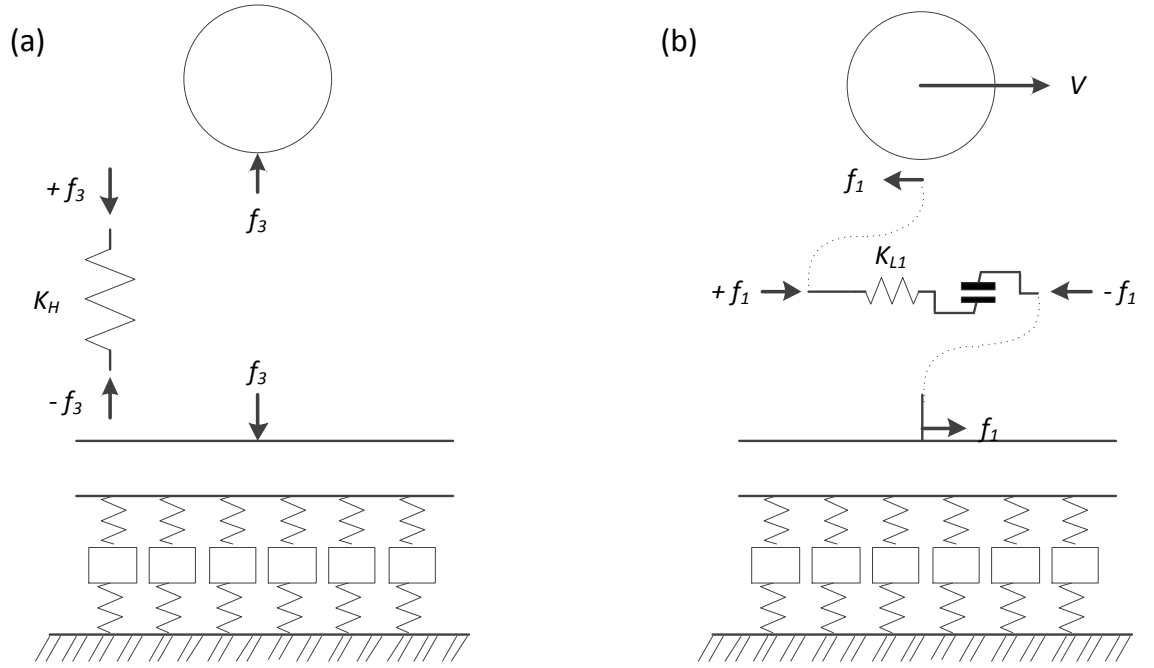


Figure 6-2: Sign conventions at wheel-rail interface: (a) Normal/Vertical direction, (b) Longitudinal direction

6.2 WHEEL MODEL

Modal parameters of the stationary wheel are calculated from a finite element (FE) model of wheel types A and B of diameter 916 mm. The details of the finite element model of the wheel can be found in Section 5.3. The equivalent modal parameters of the rotating wheel (which is excited and observed in a fixed contact point) are expressed as a function of the rotational speed and the original stationary status modal parameters using Equations 14 to 18.

From Thompson (1993), the vertical and longitudinal point mobility of the rotating wheel subject to moving load excitation as seen at the contact patch can be calculated using Equations 14 and 15 respectively

$$Y_{w,33}(\omega) = i\omega \sum_{m,n} \left\{ \frac{\psi_{mn3}\psi_{mn3}}{2m_{mn}} \left(\frac{1}{d_+(\omega)} + \frac{1}{d_-(\omega)} \right) \right\} \quad \text{(Equation 14)}$$

$$Y_{w,11}(\omega) = i\omega \sum_{m,n} \left\{ \frac{\psi_{mn1}\psi_{mn1}}{2m_{mn}} \left(\frac{1}{d_+(\omega)} + \frac{1}{d_-(\omega)} \right) \right\} \quad \text{(Equation 15)}$$

and the vertical/longitudinal and longitudinal/vertical cross mobilities using Equations 16 and 17

$$Y_{w,31}(\omega) = i\omega \sum_{m,n} \left\{ \frac{\psi_{mn1}\psi_{mn3}}{2m_{mn}} \left(\frac{-i}{d_+(\omega)} + \frac{i}{d_-(\omega)} \right) \right\} \quad \text{(Equation 16)}$$

$$Y_{w,13}(\omega) = i\omega \sum_{m,n} \left\{ \frac{\psi_{mn1}\psi_{mn3}}{2m_{mn}} \left(\frac{i}{d_+(\omega)} + \frac{-i}{d_-(\omega)} \right) \right\} \quad (\text{Equation 17})$$

Here ψ is the mode shape amplitude of mode (m,n) , m_{mn} is the modal mass of the corresponding mode and d_{\pm} is given by :

$$d_{\pm} = \omega_{mn}^2 - (\omega \pm n\Omega)^2 + 2i\zeta_{mn}(\omega \pm n\Omega)\omega_{mn} \quad (\text{Equation 18})$$

where ω_{mn} is the natural frequency and ζ_{mn} is the modal damping ratio.

The terms $Y_{w,31}$ and $Y_{w,31}$ are skew-symmetric i.e. $Y_{w,31} = -Y_{w,13}$.

The eigenfrequencies of all modes with two and more nodal diameters were assigned the experimentally measured damping ratios of a freely suspended wheelset as shown in Table 6-1. Eigenmodes with zero and one nodal diameter were assigned a modal damping ratio, ζ , using the approximate values proposed by Thompson (2009):

$$\zeta = \begin{cases} 10^{-2} & \text{for } n = 1 \\ 10^{-3} & \text{for } n = 0 \end{cases} \quad (\text{Equation 19})$$

In addition the (1,R) mode was assigned a damping ratio of 1 since this mode appears too strongly in the frequency response function (FRF) when the influence of the axle is disregarded (Thompson 2009). The (0,C) mode that was previously found by Huang et al. (2008) as the unstable mode in the presence of falling friction was included in the model by using the mode shape amplitude and damping ratio determined from a single degree of freedom curve fit of the (0,C) mode in the experimentally obtained point circumferential receptance. In addition the (0,0) mode was assigned a frequency of 231 Hz to correspond with the first peak in the point radial FRF.

The vertical and longitudinal contact point mobilities and the vertical/longitudinal cross contact point mobility for a point on the wheel tread 105 mm from the back of flange were calculated using modal summation including the effects of wheel rotation. See Figure 6-3. This was done using a frequency resolution of 0.1 Hz and a vehicle speed of 60 km/h. The mobilities were calculated using the eigenmodes and eigenfrequencies calculated from the FE model.

With eight being the largest number of nodal diameters for any mode in the frequency range between 0 and 6 kHz, a circumferential division of 100 elements exceeds the minimum recommended number of elements of six per structural wavelength (Thompson 2009) in the circumferential wheel direction. Instead the current model attains 12.5 elements per structural wavelength for the frequency range of interest.

Table 6-1: Eigenfrequencies (measured and calculated) and damping ratios for wheel Type A

Mode (n,0)		2,0	3,0	4,0	5,0	6,0	7,0	8,0
Measured frequency	Hz	387.0	972.5	1759.4	2649.0	3591.8	4547.5	5482.9
Frequency FEA model	Hz	383.6	954.8	1728.0	2602.4	3527.2	4469.4	5404.0
Damping ratio ($\times 10^{-4}$)	-	2.6	0.9	2.2	0.9	0.6	0.6	0.9
Mode (n,0)		2,R	3,R	4,R	5,R	6,R	7,R	8,R
Measured frequency	Hz	1671.1	2113.9	2624.7	3232.4	3936.5	4736.0	5639.4
Frequency FEA model	Hz	1707.9	2129.1	2630.9	3224.6	3912.0	4689.8	5553.0
Damping ratio ($\times 10^{-4}$)	-	2.3	0.9	0.9	0.8	0.8	0.6	0.6
Mode (n,1)		2,1	3,1	4,1	5,1	6,1		
Measured frequency	Hz	2223.7	2984.7	3816.0	4666.9	5396.3		
Frequency FEA model	Hz	2297.0	2946.1	3690.6	4468.5	5263.0		
Damping ratio ($\times 10^{-4}$)	-	3.4	1.6	0.8	1.4	2.2		
Mode (n,2)		2,2	3,2	4,2				
Measured frequency	Hz	4856.3	5416.3	6032.7				
Frequency FEA model	Hz	4882.2	4947.3	5473.8				
Damping ratio ($\times 10^{-4}$)	-	1.7	6.0	0.7				
Mode (n,C)		0,C	2,C					
Measured frequency	Hz	111.3	4240.4					
Frequency FEA model	Hz	730.4	4189.6					
Damping ratio ($\times 10^{-4}$)	-	15.2	1.2					

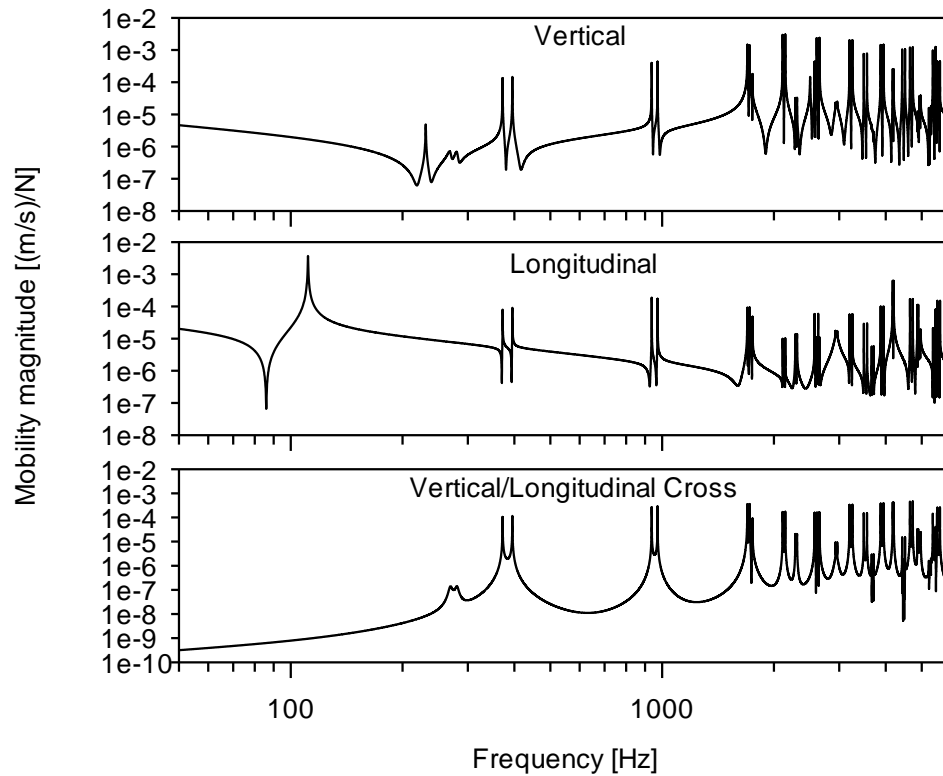


Figure 6-3: Contact point mobilities of wheel including the effects of wheel rotation (moving load)

6.3 RAIL MODEL

The vertical dynamics of the track is represented by a Timoshenko beam resting on a continuous two-layer elastic foundation (Thompson 2009). Damping of the rail, rail pads and ballast were modelled using hysteretic damping based on a constant loss factor.

The Timoshenko beam model assumed the cross sectional properties of an UIC60 rail. The vertical rail pad stiffness per unit length was set to 150 MN/m^2 , corresponding to the dynamic stiffness of a Hytrel rail pad under a 25 kN preload (Maree 1993), whilst the vertical ballast stiffness per unit length was chosen as 100 MN/m^2 (Thompson 2009). The damping loss factors of the rail pad, ballast and the rail were 0.2, 1.0 and 0.02 respectively (Thompson 2009). The damping loss factor of the rail was chosen as 0.02 to model the increase in damping of the rail pad at higher frequencies and associated with large motion of the rail foot (Thompson 2009). The sleepers were assigned a mass per unit length of 230 kg/m. The rail material data used in the model was a Modulus of Elasticity of 210 GPa, a Shear Modulus of 79 GPa and a density of 7850 kg/m^3 .

The longitudinal dynamics of the track is modelled as a uniform infinite bar resting on a continuous support (Grassie et al. 1982). The longitudinal rail pad stiffness per unit length was chosen as 75 MN/m^2 (Thompson 2009), corresponding to a soft rail pad and assuming that the lateral and longitudinal stiffness of the rail pad will be equal, whilst the longitudinal ballast stiffness per unit length was chosen as 50 MN/m^2 (Grassie et al. 1982). Damping of the rail pads and ballast were assigned a viscous damping coefficient per unit length of 60 kNs/m^2 and 80 kNs/m^2 respectively. The uniform infinite bar also assumed the cross sectional properties of an UIC60 rail and the rail material data as listed above for the vertical dynamics model.

The vertical/longitudinal cross-coupling dynamics of the rail in the wheel-rail contact point is not considered in the current study.

6.4 CONTACT SPRING

In the contact zone, only the vertical and longitudinal-tangential contact springs are considered. The equivalent Hertzian contact spring stiffness, K_H , was calculated for the known lateral contact displacements of a number of known squealing wheel profiles in combination with the measured rail profiles of the test curve using the kinematic simulation software RsGeo.

In the test curve, squeal only occurred for wheels under empty iron ore wagons, having a design wheel load of 25 kN . A distribution graph of the vertical load reacted by the trailing inner wheels in contact with the low rail for 2394 empty ore wagons in the 1000 m radius test curve is shown in Figure 6-4. Here the minimum recorded wheel load at the trailing inner wheel contact of the measured bogies was 11.92 kN and the maximum 29.74 kN . These measurements were recorded during the field tests presented in Chapter 3. Trailing inner wheels that squealed recorded wheel loads between 13 kN and 24 kN . Using the simulation software RsGeo, this yielded a range for the normal contact spring stiffness considered in the model between $6 \times 10^8 \text{ N/m}$ (13 kN) and $8 \times 10^8 \text{ N/m}$ (24 kN).

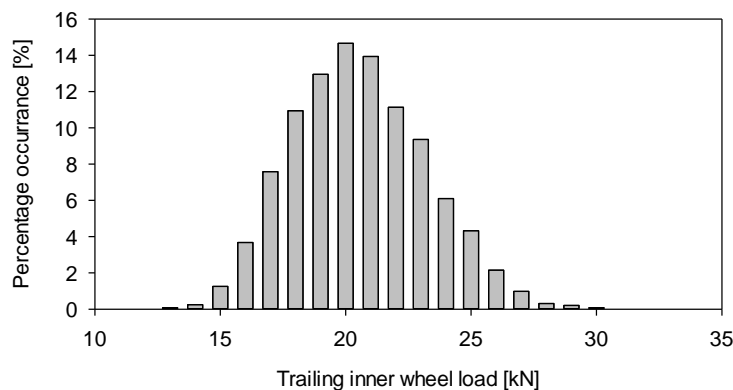


Figure 6-4: Trailing inner wheel, wheel load distribution

The contact between two elastic bodies has stiffness in the longitudinal-tangential direction, K_{L1} , given by (Thompson 2009)

$$K_{L1} = K_H \left[1 + \frac{\nu}{1-\nu} \left(\frac{1}{4} + \frac{1}{\pi} \tan^{-1} \frac{a}{b} \right) \right] \quad (\text{Equation 20})$$

where ν is the Poisson's ratio and a and b the contact area half axes of the assumed elliptical contact area in the longitudinal and transverse directions.

For the contact parameters defined in Table 4-2 and a Poisson's ratio of 0.3

$$K_{L1} = 1.25K_H \quad (\text{Equation 21})$$

The vertical/longitudinal cross-coupling dynamics of the contact area is not considered in the current model.

6.5 RESULTS

This section provides the results of the model in terms of the potential unstable frequencies predicted by the model for a contact position 105 mm from the back of flange. It also contains the validation of the model against on-track measurements.

6.5.1 On-track measured squeal frequencies

Figure 6-5 shows the spread of measured squeal frequencies against wheel diameter for the modelled wheel type as measured in the 1000 m radius test curve. The squeal frequencies have previously been related to the (2,C), (6,R) and (7,R) modes of the wheel. It is evident from Figure 6-5 that squeal for the modelled wheel is predominantly associated with the (2,C) mode, with very few occurrences due to the (6,R) and (7,R) modes.

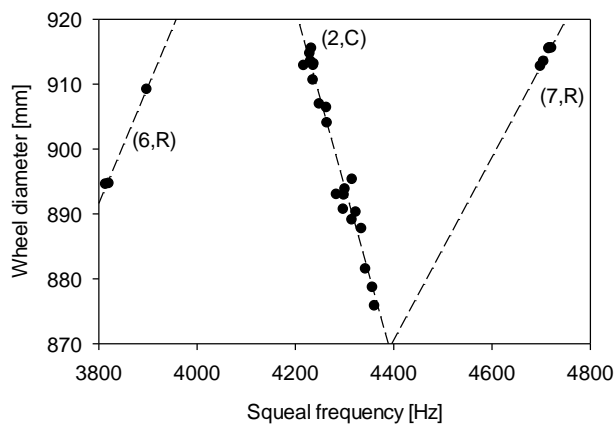


Figure 6-5: Measured squeal frequencies for modelled wheel

6.5.2 Model results: $k_H = 8 \times 10^8$ N/m

Figure 6-6 shows a stability chart for the modelled wheel for a position 105 mm from the back of the flange. For this stability chart the Hertzian contact spring stiffness was selected as 8×10^8 N/m, corresponding to the upper range of wheel loads recorded for the squealing wheels, i.e. 24 kN.

The stability chart shows the assumed adhesion curve, in addition to the loop gain exceeding one (indicating instability) for all the potential unstable frequencies found in the model as a function of longitudinal creepage. It is evident from the stability chart that two regions can be identified where different wheel modes have the largest loop gain for the range of longitudinal creepage associated with that region on the stability chart.

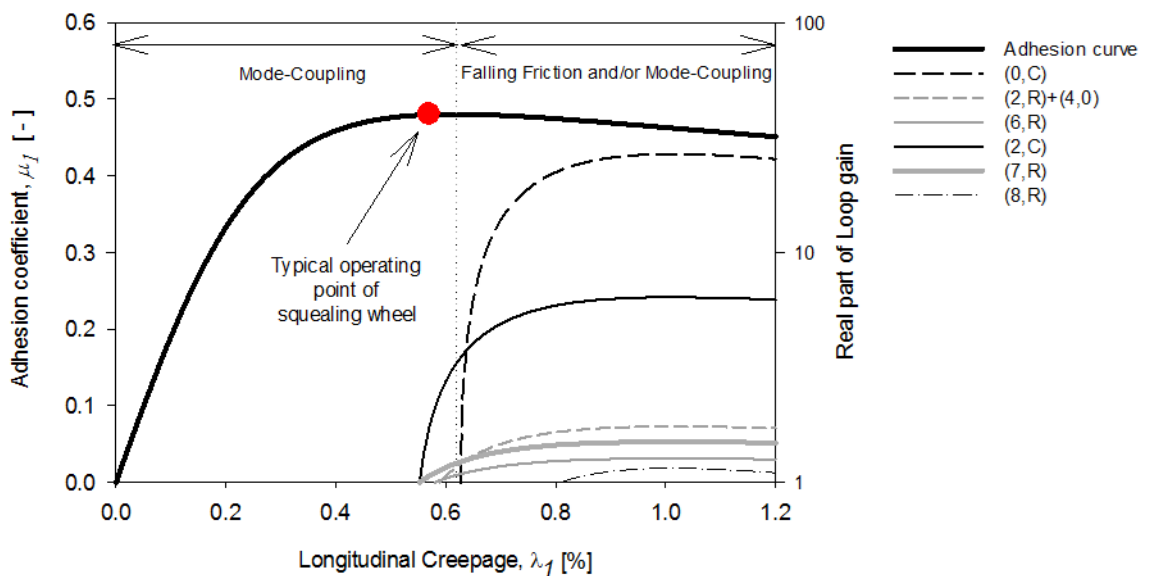


Figure 6-6: Stability chart for a contact position 105 mm from back of flange ($k_H = 8 \times 10^8$ N/m)

For the region with longitudinal creepage between 0.55 % and 0.64 %, the (2,C) doublet mode pair has the largest loop gain and will be unstable, whereas for creepage values exceeding 0.64 % the (0,C) cosine mode has the largest loop gain and will be unstable.

From the stability chart it is evident that the instability associated with the (2,C) doublets occur for the region on the adhesion curve in close proximity to the adhesion optimum, and occurs due to mode-coupling. Below the adhesion optimum, the gradient of the adhesion curve is positive and provides positive damping to unstable modes. Modes excited due to falling friction

alone will be inherently stable for values of longitudinal creepage below the adhesion optimum, whilst modes excited due to mode-coupling will still be unstable for small positive gradients of the adhesion curve, i.e. small positive damping values. Beyond the adhesion optimum modes can be unstable as a consequence of falling friction alone (e.g. (0,C) mode) or as a combination of mode-coupling and falling friction (e.g. (2,C) doublets).

Figure 6-7 shows the gradient of the adhesion curve as a function of longitudinal creepage and also shows the two regions of instability where mode-coupling and falling friction are responsible for the instability. Instability of the (2,C) doublets simulated for wheels curving with longitudinal creepage close to the adhesion optimum, correlates with the wheel mode that was found predominantly unstable during in-field squeal measurements as shown in Figure 6-5. Instability due to the (6,R) and (7,R) doublet modes that were also found during the in-field tests will likely not be excited in squeal for the wheel-rail contact conditions depicted in Figure 6-6, i.e. although they are predicted as potentially unstable modes they never have the largest loop gain for any range of longitudinal creepage. Instability due to the (0,C) mode occurring at 111.3 Hz is not relevant to squeal and will instead cause rail corrugation or wheel polygonisation.

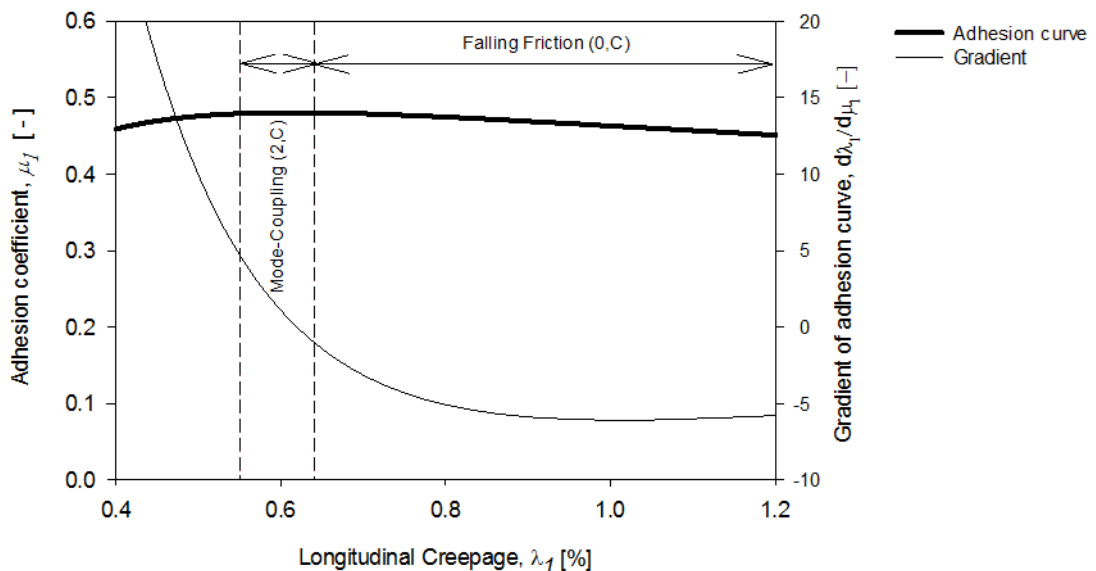


Figure 6-7: Instability regions as a function of the gradient of the adhesion curve

Instability associated with (2,C) doublets occur at a frequency of 4182.2 Hz. This is slightly above the resonance frequency (4178.1 Hz) of the backward travelling wave associated with the (2,C) doublet mode pair. Figure 6-8 plots the magnitude of the denominator of the term $-\mu_1 Y_{31}/Y_{33}$ of the open loop transfer function, i.e. the sum of contact point normal mobility of

the rotating wheel subject to moving load excitation, the contact spring as well as that of the track. The unstable frequency 4182.2 Hz is further indicated in Figure 6-8 by the dashed line. It is clear from Figure 6-8 that the squeal frequency corresponds to an anti-resonance in Y_{33} , which according to Thompson (2009) corresponds to a peak in the normal contact force spectrum and a resonance of the contact-coupled system.

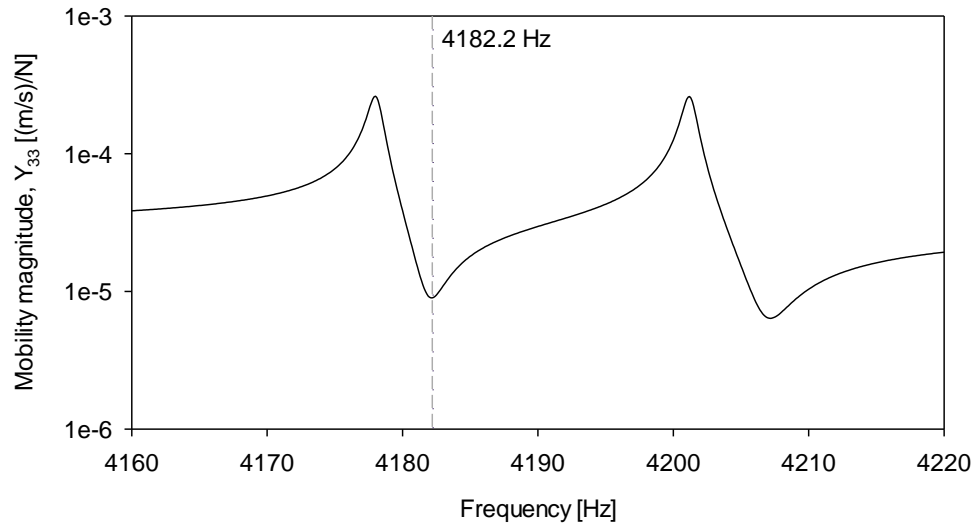


Figure 6-8: Mobility magnitude of Y_{33}

6.5.3 Model results: $k_H = 6 \times 10^8$ N/m

Figure 6-9 shows a stability chart for the modelled wheel for a position 105 mm from the back of flange. For this stability chart the Hertzian contact spring stiffness was selected as 6×10^8 N/m, corresponding to the lower range of wheel loads recorded for the squealing wheels, i.e. 13 kN.

The stability chart in Figure 6-9 shows that three regions can be identified where different wheel modes have the largest loop gain for a given range of longitudinal creepage. In addition to the regions where the (0,C) cosine mode and (2,C) doublet modes have the largest loop gain, the third region predicts the (7,R) doublets with the largest loop gain for longitudinal creepages between 0.53 % and 0.57 %. The fact the current model only predicts squeal associated with the (7,R) doublets for a small range of creepages and for wheel's having significant quasi-static wheel unloading might start explaining the in-field observations that the (7,R) doublets do not squeal very often in the test curve.

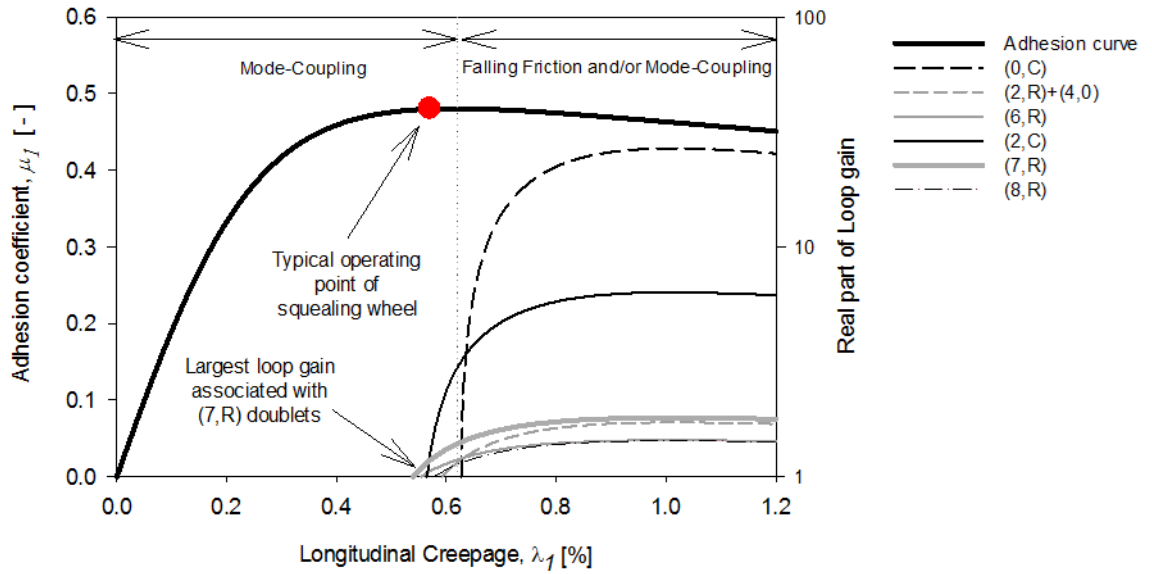


Figure 6-9: Stability chart for a contact position 105 mm from back of flange ($k_H = 6 \times 10^8$ N/m)

Changing the Hertzian contact stiffness changes the magnitude of anti-resonances in Y_{33} , which has a direct impact on the calculated loop gain for the mode coupling term $-\mu Y_{31}/Y_{33}$. Figure 6-10 compares the mobility magnitude for Y_{33} calculated with a normal contact spring stiffness of 8×10^8 N/m and 6×10^8 N/m respectively. The anti-resonances that are associated with instability due to the (2,C) and (7,R) backward travelling waves are additionally encircled in Figure 6-10. The magnitude shift of the anti-resonances changes the loop gain for constant friction by influencing the term $-\mu_1 Y_{31}/Y_{33}$, as well as the rate of change of the loop gain by influencing the term $\frac{Y_{13} Y_{31}}{Y_{33}} \frac{F_0}{V_0} \frac{\partial \mu_1}{\partial \lambda_1}$ that influences the frictional damping. This interplay between the loop gain for constant friction and the rate of change of the loop gain due to a magnitude shift of the anti-resonances of Y_{33} plays a crucial role in selecting the squealing frequency.

The third in-field squeal frequency associated with the (6,R) doublets has not been predicted as an unstable mode with the largest loop gain for any set of operational conditions simulated. Instead it is postulated that a change in wheel diameter might result in the model predicting the (6,R) doublets as unstable instead of the (7,R) doublets. This is based on the experimental deduction in Figure 6-5 that squeal associated with the (6,R) doublets only occurred for wheels with a diameter between 894 mm and 909 mm, whereas squeal associated with the (7,R) doublets occurred for wheels with a diameter between 913 mm and 916 mm which is similar to the modelled wheel diameter of 916 mm.

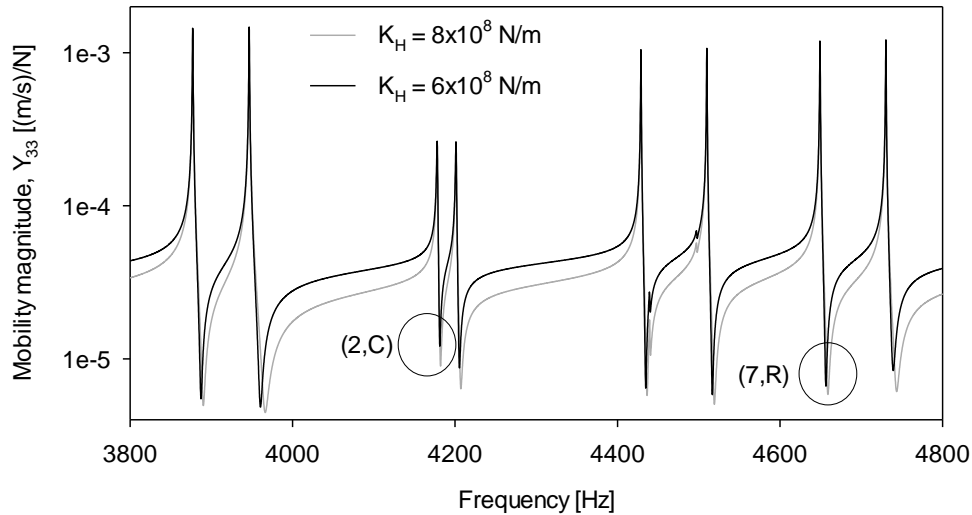


Figure 6-10: Mobility magnitude (Y_{33}) for different Hertzian contact stiffnesses

6.6 WHEEL TYPE B

Following a similar modelling approach, squeal resulting due to unsteady longitudinal creepage was also modelled for wheel Type B. Similar to wheel Type A, instability also showed up for wheel Type B due to coupling of the (2,C) doublet modes in the proximity of the adhesion curve close to the adhesion optimum. For the falling region of the adhesion curve beyond a certain negative gradient the (0,C) mode was also modelled as the predominantly unstable mode for wheel Type B. No other modes were predicted with the largest loop gain, even if the Hertzian contact stiffness was varied in the model. This confirms the experimental findings that squeal due to wheel type B in the test curve was only excited for a single linear varying set of squeal frequencies against wheel diameter.

6.7 DISCUSSION

Railway wheel squeal with longitudinal creepage as the source of instability was modelled. In contrast to international research that does not consider longitudinal creepage to be relevant to squeal, the results of this research demonstrate the importance of longitudinal creepage as a source of instability for squeal. The research further showed that modelling the dynamics of a wheel including the effects of a rotating wheel under moving load excitation is crucial to understanding the instability. This captures the cross-coupling dynamics between the normal and longitudinal degrees of freedom (with respect to the contact patch) that is otherwise zero for a non-rotating sliding wheel.

Both instability due to falling friction and mode-coupling were assessed. The results of the model show that the excitation of squeal due to mode-coupling is limited to the region on the adhesion curve close to adhesion optimum where the positive and negative frictional damping is very small. For wheel Type A the resonances of the contact coupled wheel-rail system associated with the backward travelling waves of the (2,C) and (7,R) doublets could be shown to participate in squeal. In this case the operational conditions associated with longitudinal creepage and the wheel load could be shown to take part in determining which of the potentially unstable modes will have the largest loop gain and will most likely be excited into squeal. For wheel Type B only the resonance of the contact coupled system associated with the backward travelling wave of the (2,C) doublets could be shown to partake in squeal. For the falling region of the adhesion curve, beyond a certain gradient the fundamental torsional resonance of the wheelset will most likely be unstable. Because of the low frequency of the (0,C) mode, the predicted instability is not relevant to squeal and instead relevant to the formation of rail corrugation and wheel polygonisation.

The results of the model based on unsteady longitudinal creepage provide good agreement with experimental findings in terms of the experimentally obtained squeal frequencies as well as being able to predict the dominant squeal mode in the test curve as the mode with the largest loop gain for most operational conditions i.e. the (2,C) mode of both wheel Type A and B.

Based on the above results, the author suggests that a complete model for curve squeal should include longitudinal creepage and the dynamics of the wheel under moving loads. A complete model for curve squeal should also evaluate the existence of squeal for not only falling friction or constant friction, but should include a defined adhesion curve for which a stability map can be generated for different levels of creepage around the adhesion optimum as well as for the falling part of the adhesion curve.

6.8 FREQUENCY DOMAIN MODEL USING COMPLEX EIGENVALUE ANALYSIS

Before the importance of modelling the dynamics of a rotating wheel in relation to squeal due to unsteady longitudinal creepage was clear, the author presented a squeal model based on complex eigenvalue analysis (CEA) using the finite element software MSC Nastran and MSC Marc (Fourie et al. 2018). Similar to the frequency domain model using the Nyquist criterion, the model using CEA was able to accurately predict the experimental squeal frequencies.

The CEA analysis modelled a non-rotating, but longitudinally sliding wheel in contact with the rail. In the finite element (FE) model, friction loaded springs (Ouyang et al. 2005) were used to model the normal and friction contact coupling between the wheel and rail.

A friction-loaded spring represents a friction force due to normal displacements of the contact spring. This is based on the approximation that the normal compression force can be represented as the contact spring stiffness multiplied by the compression of the contact spring. The compression of the contact spring becomes available through the nodal displacements of the contact springs connecting the wheel and rail.

There are generally two approaches used to select the value of the contact spring stiffness. The first consideration is based on the fact that mathematically, the spring connection is equivalent to applying a constraint with the penalty method (Nack 2000 and Lee et al. 2003). Contact conditions are exactly applied when the spring stiffness k_c is infinitely large. However, in the actual numerical analysis, k_c has to be finite to avoid ill-conditioning of the stiffness matrix. Lee et al. (2003) recommend the contact spring stiffness to be in the order of 1 – 100 GN/m. Another consideration is based on selecting the contact spring stiffness based on the actual contact stiffness between the contact bodies (Huang et al. 2006 and Junior et al. 2008).

In the context of railway wheel squeal, the friction-loaded spring approach has been considered by Chen et al. (2008) and in the frequency-domain model presented in Pieringer et al. (2016). Both models included a spring stiffness represented by the actual contact stiffness caused by the local elastic deformation of the wheel and rail i.e. according to Hertzian theory. Whilst Chen et al. only considered saturated lateral creepage, the frequency domain model presented in Pieringer et al. (2016) considered both saturated lateral and longitudinal creepage. No instability was however predicted by the frequency domain model of Pieringer et al. for a resulting creep force acting in the longitudinal direction independent of the friction level; here the coefficient of friction was varied between 0.1 and 0.7. Similar to the results of Pieringer et al. (2016), the initial implementation of complex eigenvalue analysis in Fourie et al. (2018) did not predict any instability for a resulting creep force acting in the longitudinal direction. Fourie et al. set the coefficient of friction to 0.6 and steadily increased the magnitude of the contact normal spring stiffness from a small value until numerical instability was reached. This stepping approach included evaluating the stability of the contact coupled wheel-rail system using a normal contact Hertzian stiffness of 0.8 GN/m and a coefficient of friction of 0.6.

During such simulations the author observed that the (2,C) sine mode, which has a nodal point in the contact longitudinal direction and an anti-node in the contact normal direction without friction-coupling (see Figure 6-11(a)), rotated itself with respect to the contact to allow simultaneous normal and tangential displacement in the contact area when the friction-coupling was considered (see Figure 6-11(b)). This rotation of the (2,C) mode accommodates the tangential displacement of the mode due to normal load variations in the presence of frictional coupling. Figure 6-12 shows the system mode involving the (2,C) cosine doublet mode having

an anti-node at the contact in the contact longitudinal-tangential direction and a node in the contact normal direction.

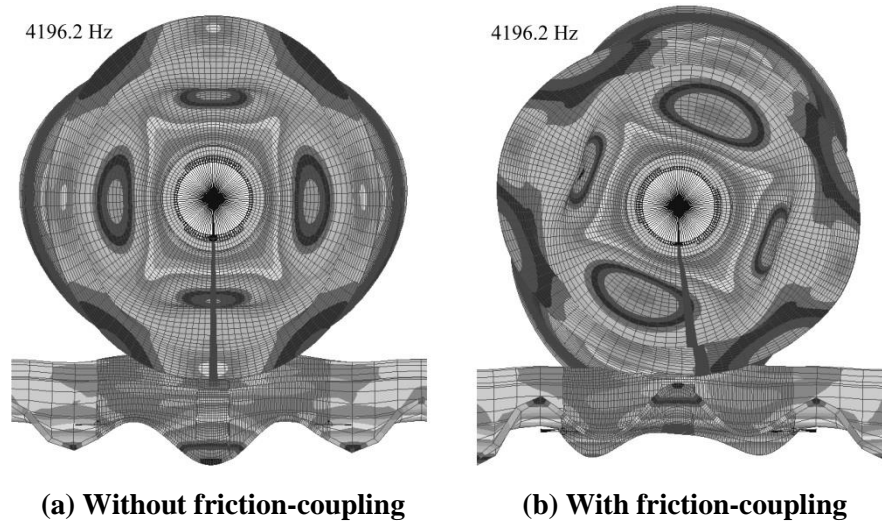


Figure 6-11: System mode involving (2,C) sine doublet mode (Fourie et al. 2018)

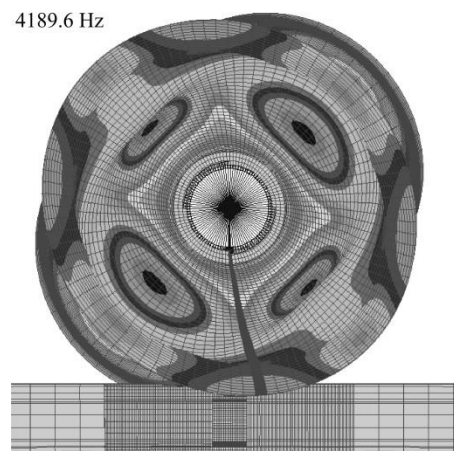


Figure 6-12: System mode involving (2,C) cosine doublet mode (Fourie et al. 2018)

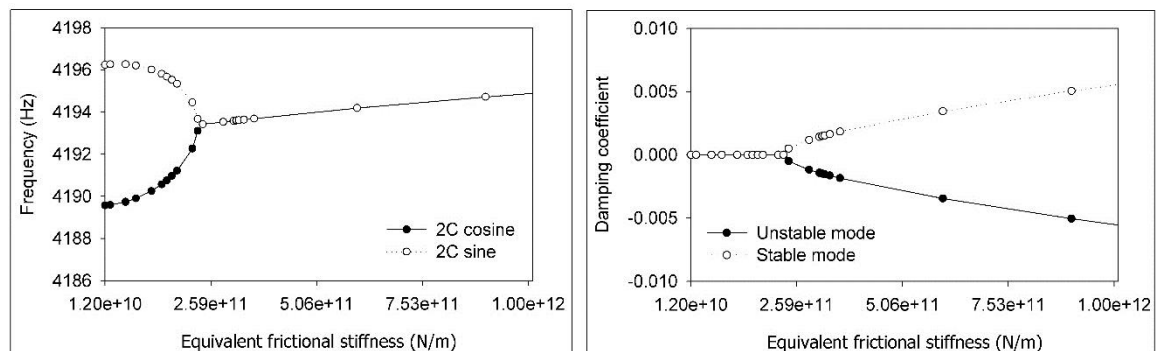
Comparing Figure 6-11(b) and Figure 6-12 it can be seen that the frictional coupling rotates the sine mode to become spatially very similar to the cosine mode, for these otherwise spatially orthogonal modes.

From the work of Huang et al. (2006) it is known that modes should satisfy two conditions for them to merge i.e. become identical in frequency and mode shape. These conditions are (i) that the separation between the frequencies of the two modes of a statically coupled system is sufficiently small, and (ii) that their component-wise mode shapes are compatible. Compatibility implies that the system modes display similar component modal displacements at $\mu = 0$ and can easily become identical when μ is increased.

Because the mode shapes of the (2,C) sine and cosine doublets are identical, but spatially orthogonal, the rotation of the (2,C) sine mode due to the imposed longitudinal friction force is crucial for allowing the two modes to become spatially similar. This mode rotation due to the imposed friction in addition to the inherent closely spaced frequencies of doublet modes means that the criteria for mode merging as discussed by Huang et al. are particularly well fulfilled by doublet modes.

Based on the observation of mode-rotation from the FE model and the criteria for mode-coupling instability, the author hypothesised that the formulation of the friction-loaded spring did not accurately represent the frictional work imposed on the wheel-rail system and decided to keep the normal contact spring stiffness constant, whilst varying the frictional stiffness representing the frictional work.

The results of this analysis showed the coalescing of doublet modes, forming a new pair of a stable and unstable mode. Figure 6-13(a) shows how the (2,C) doublets move closer and closer as a function of the frictional stiffness until they merge. Evident from Figure 6-13(a) is that the modes become coupled at 4193 Hz. Figure 6-13(b) displays the level of damping of the stable and unstable modes. Initially the damping of both modes is zero as the system is stable, but it grows positively and negatively respectively once the system becomes coupled.



(a) Frequency

(b) Damping coefficient

Figure 6-13: Coalescing modes as a function of equivalent frictional stiffness

6.8.1 Validity of model

Based on the results of the frequency-domain model using the Nyquist criterion, it becomes clear that the CEA frequency-domain model doesn't accurately capture the physics of squeal due to unsteady longitudinal creepage although it can accurately predict the unstable frequencies. The CEA frequency-domain model will not be considered further in this work as it cannot represent a rotating wheel in contact with a stationary rail. In hindsight, varying the frictional stiffness most probably simulates a much higher friction coefficient than practical in-field. Modal rotation of the radial modes to allow simultaneous normal and longitudinal displacement with respect to the contact, as was shown for the (2,C) sine mode, could be important for a more accurate squeal model. In contrast, the frequency-domain model using the Nyquist criteria only represents the dynamics of the wheel based on a single frequency response function and hence cannot allow mode rotation due to the imposed friction-coupling. For now this mode rotation is not considered further, although it could prove to be important. On the other hand, it is also highly probable that such mode rotation is not present for a wheel rotating past a stationary forcing point.

6.9 DISCUSSION

Railway wheel squeal due to mode-coupling instability with longitudinal creepage as the energy source was modelled. In contrast to international research that does not consider longitudinal creepage to be relevant to squeal, the results of this research demonstrate the importance of longitudinal creepage as a source of instability for squeal. The research further showed that crucial to the instability was modelling the dynamics of a wheel including the effects of a rotating wheel under moving load excitation. This captures the cross-coupling dynamics between the normal and longitudinal degrees of freedom (with respect to the contact patch) that is otherwise zero for a non-rotating wheel.

The results of the model based on unsteady longitudinal creepage using the Nyquist criterion provide good agreement with experimental findings in terms of the experimentally obtained squeal frequencies as well as being able to predict the dominant squeal mode in the test curve as the mode with the largest loop gain i.e. the (2,C) mode.

Conglomerating the results in Chapter 6, a complete model for curve squeal should include longitudinal creepage and the dynamics of the wheel under moving loads.

Based on the results of the frequency-domain model using the Nyquist criterion, it becomes clear that the CEA frequency-domain model doesn't accurately capture the physics of squeal due to unsteady longitudinal creepage although it can accurately predict the unstable

frequencies. The CEA frequency-domain model will not be considered further in this work as it cannot represent a rotating wheel in contact with a stationary rail.

7 FREQUENCY DOMAIN MODEL FOR RAILWAY WHEEL SQUEAL RESULTING FROM UNSTEADY SPIN CREEPAGE

The work summarised in this chapter is a contribution towards a future squeal model that will be able to comprehensively predict squeal and models the excitation of squeal due to unsteady spin creepage occurring in the region of the wheel's flange throat. In this model the time varying part of the spin creep moment is modelled as a feedback loop and tested for stability with the Nyquist criterion.

7.1 INTRODUCTION

For flange contact squeal excited at the outer rail, on-track measurements provide strong evidence that the mechanism of instability can be linked to mode-coupling due to the presence of simultaneous vertical and lateral rail accelerations that are out-of-phase (Jiang et al. 2015a). This phase lag is necessary to transfer the energy from one direction to the other and generate the instability (Hoffmann et al. 2002). In Chapter 6, mode-coupling was identified as the instability mechanism for squeal excited due to unsteady longitudinal creepage at the inner rail. Crucial to the instability was modelling the dynamics of a wheel including the effects of the rotating wheel suffering moving load excitation. The moving load nature of the rotating wheel causes a non-zero coupling between the longitudinal and the radial/vertical vibration at the contact which is otherwise zero for a non-rotating, sliding wheel. This zero coupling between the longitudinal and radial vibration for a non-rotating wheel is due to the sine and cosine components of wheel vibration being independent for a non-rotating wheel. This is similarly true for the coupling between spin vibration and radial/lateral vibration at the wheel-rail contact that is non-zero for a rotating wheel, but zero for a non-rotating, sliding wheel.

This non-zero coupling between the spin and vertical/lateral dynamics of a rotating wheel, with respect to the contact, suggests that the dynamics of the rotating wheel might be important for squeal due to unsteady spin creepage excited in the flange root. The current chapter presents a frequency domain model for the excitation of flange contact squeal due to unsteady spin creepage with constant friction. The effect of frictional damping due to either a positive or negative gradient of the adhesion curve is not included in the current model and instead only constant friction is considered.

The aim of this chapter is to capture the physics behind flange contact squeal using a frequency domain model based on a time varying spin moment reacted in the flange throat contact area including the dynamics of the rotating wheel. Although previous squeal models have included spin creepage (Thompson and Monk-Steel 2003, Huang et al. 2008, Zenzerovic 2017), it has

not been combined with the dynamics of a rotating wheel in previous work. With this context in mind, this chapter does not aim to validate the squeal model based on squeal occurring in a specific curve; instead the model aims to capture some previously published/unpublished experimental findings related to flange contact squeal. At this point it is also worthy to mention that by increasing the contact angle a more classical normal/tangential mode-coupling instability may also occur (Thompson et al. 2016 and Ding et al. 2018) and that it would be difficult to demonstrate in practise the actual source of instability for flange contact squeal.

7.2 MODELLING OF WHEEL SQUEAL DUE TO UNSTEADY SPIN CREEPAGE

The self-excited vibration between the wheel-rail contact forces/moments and their responses can be described as a feedback loop. Combining the equations for contact dynamics, wheel dynamics and rail dynamics give a loop gain for the tangential contact force/moment. If the loop gain encircles the point (+1,0) on the Nyquist plane, the system is unstable (De Beer et al. 2000).

From Thompson and Monk-Steel (2003), for a case where only spin creepage is important in producing squeal, and assuming constant friction, the loop gain for the potentially unstable spin creep moment m_3 is given by

$$H(\omega) = -\beta_3 \mu_0 \frac{Y_{36}}{Y_{33}} m_3 = -\beta_3 \mu_0 \frac{\alpha_{36}}{\alpha_{33}} m_3 \quad (\text{Equation 23})$$

where the indices 3 and 6 describe the normal direction and a moment about the normal axis with respect to the contact patch and described in Figure 7-1. $\alpha_{ij} = \alpha_{w,ij} + \alpha_{r,ij} + \alpha_{c,ij}$ is the sum of the wheel ($\alpha_{w,ij}$), track ($\alpha_{r,ij}$) and contact spring ($\alpha_{c,ij}$) receptances. Receptance refers to the ratio of the output displacement to a harmonically varying unit input force at a given frequency. β_3 is the rolling friction coefficient in the spin direction and can be calculated with the CONTACT software (Vollebregt 2017) as in Thompson and Monk-Steel (2003). The rolling friction coefficient in the spin direction β_3 represents the contribution of spin creepage to creep saturation.

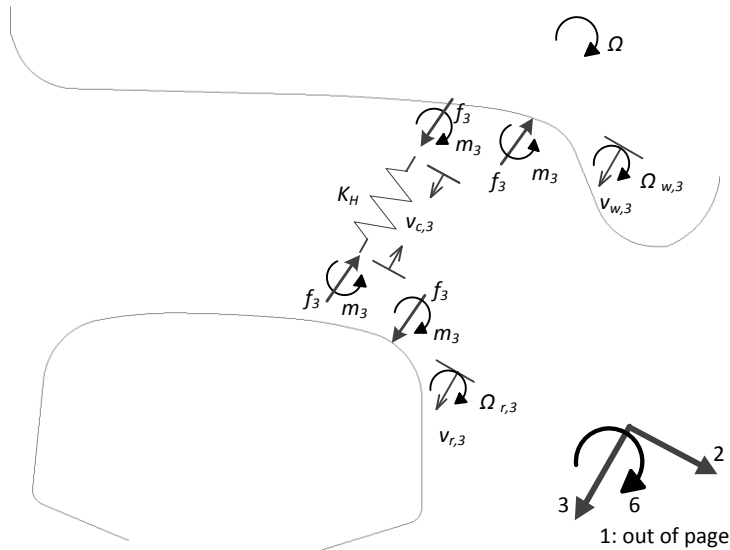


Figure 7-1: Sign conventions at wheel-rail interface: Normal and spin directions

7.2.1 Wheel model

The wheel model defined in Section 5.3 was also used in the model due to unsteady spin creepage. The eigenfrequencies and eigenmodes of the non-rotating wheel up to 10 kHz were calculated using a real eigenvalue analysis in MSC NASTRAN.

Modal parameters of the stationary wheel were calculated from the finite element (FE) model. The equivalent modal parameters of the rotating wheel (which is excited and observed in a fixed contact point) are expressed as a function of the rotational speed and the original stationary status modal parameters.

The normal point and normal/spin cross receptances for a contact point on the wheel in the wheel flange throat having a contact angle of 30° (with respect to the horizontal) was calculated using modal summation including the effects of wheel rotation. This was done using a frequency resolution of 0.1 Hz and a vehicle speed of 60 km/h. From Thompson (1993), the normal and normal/spin cross receptances of the rotating wheel as seen at the contact patch can be calculated using Equations 24 and 25:

$$\alpha_{w,33}(\omega) = \sum_{m,n} \left\{ \frac{\psi_{mn3}\psi_{mn3}}{2m_{mn}} \left(\frac{1}{d_+(\omega)} + \frac{1}{d_-(\omega)} \right) \right\} \quad (\text{Equation 24})$$

$$\alpha_{w,36}(\omega) = \sum_{m,n} \left\{ \frac{\psi_{mn1}\psi_{mn3}}{2m_{mn}} \left(\frac{-i}{d_+(\omega)} + \frac{i}{d_-(\omega)} \right) \right\} \quad (\text{Equation 25})$$

where ψ is the mode shape amplitude of mode (m, n) , m_{mn} is the modal mass of the corresponding mode and d_{\pm} are given by Equation 18.

The eigenmodes with two and more nodal diameters occurring between 0 and 6 kHz are assigned a modal damping ratio according to the measured damping ratios shown in Table 6-1. Damping ratios of eigenmodes with $n \geq 2$ and occurring above 6 kHz were not determined experimentally and are assigned a damping ratio of 1×10^{-4} . Eigenmodes with zero and one nodal diameter were assigned a modal damping ratio, ζ , using the approximate values according to Equation 19.

In addition the (1,R) mode was assigned a damping ratio of 1 since this mode appears too strongly in the frequency response function (FRF) when the influence of the axle is disregarded (Thompson 2009).

The mode shape components at the contact point are available from the FE model only in the x , y and z directions (x vertical, y lateral, z along the track) (see Figure 7-2). This has to be converted to the coordinate system 1-2-3 local to the contact as shown in Figure 7-1, before performing the modal summation. Knowing the mode shape components of the wheel at two closely spaced nodes in the longitudinal direction (A and B in Figure 7-2), allows the rotational mode shape component θ_6 to be estimated at node B using the finite-difference technique (Duarte and Ewins 2000). Figure 7-3 and Figure 7-4 respectively show the rotational contact point receptance α_{66} and the normal/spin cross receptance α_{36} at node B, including the effects of wheel rotation.

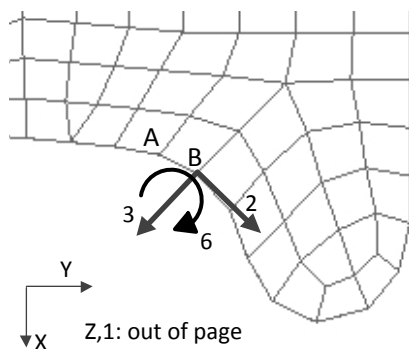


Figure 7-2: Coordinate system: Global (FE model) vs. Local

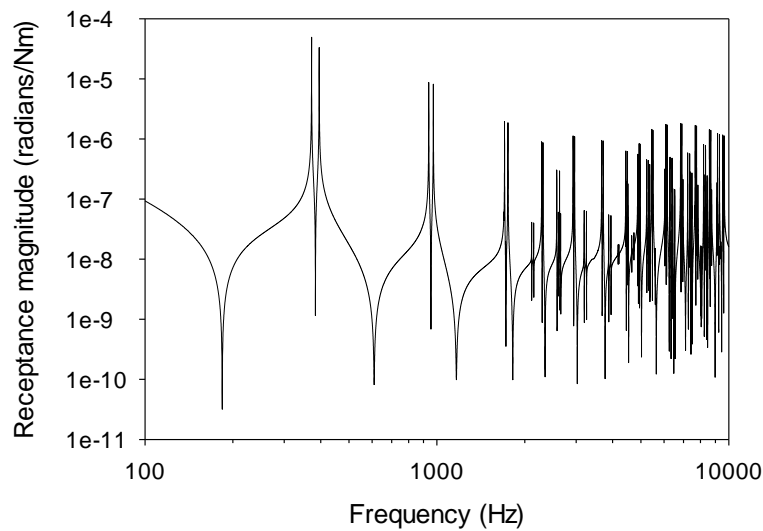


Figure 7-3: Rotational receptance α_{66} of rotating wheelset at 60 km/h

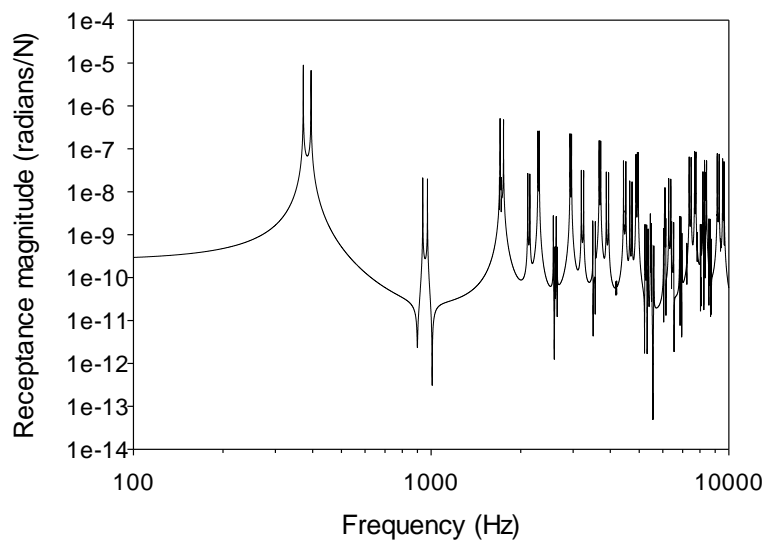


Figure 7-4. Normal/Rotational cross receptance α_{36} of rotating wheelset at 60 km/h

7.2.2 Rail model

Using a generalized Nyquist criterion, Ding et al. (2016) found that rail dynamics play an important role when constant friction is considered. The inclusion of the rail dynamics shows that mode-coupling instability can occur due to coupling between the tangential component and normal component of a single wheel mode. When the rail is assumed as rigid, instability only occurred as a coupling between two different wheel modes. Similarly to unsteady longitudinal creepage, it is anticipated that the coupling of two wheel modes give rise to the instability for

unsteady spin creepage. In this regard the dynamics of the rail is not considered and assumed rigid in the current model even though the track dynamics will cause higher damping of the modes due to rolling damping.

7.2.3 Contact spring

In the contact zone only the normal contact spring is considered. Thus the normal force fluctuates because of the compression or extension of the contact spring. The fluctuation in the normal force leads to fluctuations in the friction force which lead to an asymmetric matrix. This is the reason for possible mode-coupling instability. For the current model, the equivalent Hertzian contact spring stiffness, K_H , was assumed to be 1×10^9 N/m, corresponding to a wheel load of 25 kN and calculated using the kinematic simulation software RsGeo (Kik 2010) for contact occurring in the flange throat of the wheel.

7.3 RESULTS

Assuming a rigid rail and ignoring the vertical/spin cross mobility of the contact spring, $H(\omega)$ simplifies to:

$$H(\omega) = -\beta_3 \mu_0 \frac{\alpha_{w,36}}{(\alpha_{w,33} + \alpha_{c,33})} \quad (\text{Equation 26})$$

Because $\beta_3 \mu_0$ is constant for a given contact scenario, it is only necessary to plot $-\alpha_{w,36}/(\alpha_{w,33} + \alpha_{c,33})$ to indicate instability. Figure 7-5 shows the results of the stability analysis in the form of a Nyquist plot. There are several unstable modes, as a number of loops encircle the point (+1,0). The points at which these loops cross the real axis give the potential squeal frequencies. The eight most unstable frequencies are shown in the Nyquist contour with a '+'. To determine the unstable frequency corresponding to each loop, the real part of the open loop transfer function, referred to as the loop gain, is plotted against frequency in Figure 7-6. The peak with the highest amplitude occurs at 2980.9 Hz, which is slightly above the resonance frequency (2963.4 Hz) of the forward travelling wave associated with the (3,1) doublet mode pair. The first peak in Figure 7-6 occurring at 213.6 Hz and that has not been labeled corresponds to the first anti-resonance in the normal frequency response of the wheel.

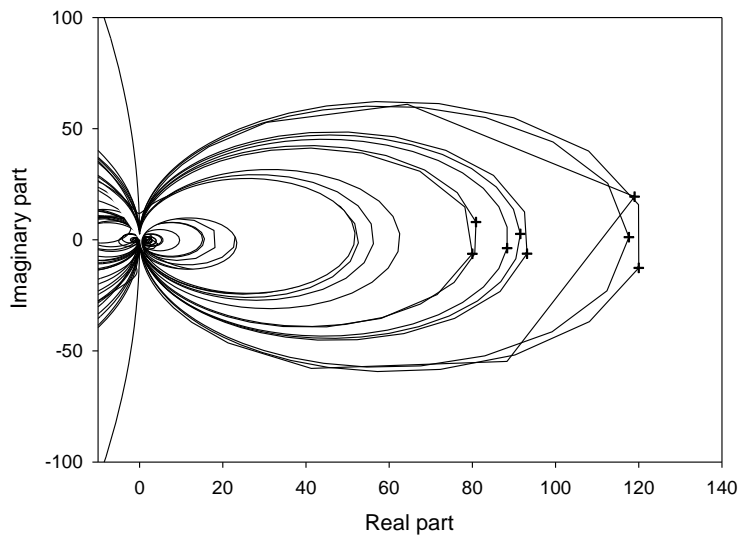


Figure 7-5: Nyquist plot of open loop transfer function

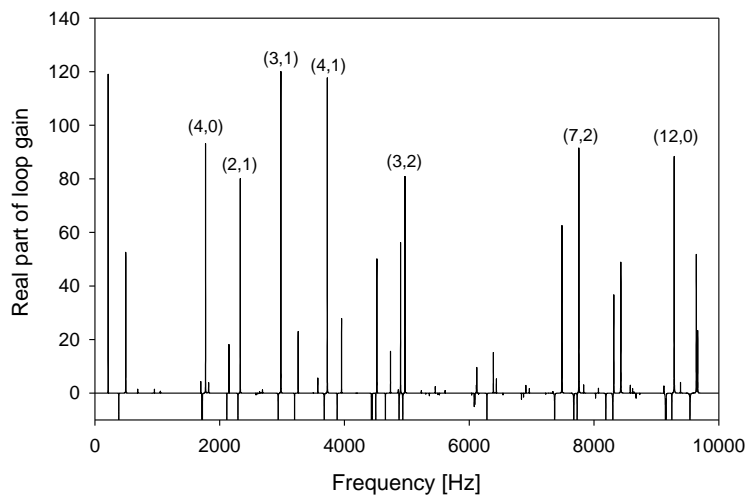


Figure 7-6: Spectrum of real part of loop gain

Figure 7-7 plots the magnitude of the denominator of the open loop transfer function, i.e. the sum of contact point normal receptance of the rotating wheel and the contact spring receptance. The unstable frequency 2980.9 Hz is indicated in Figure 7-7 by the dashed line. It can be seen from Figure 7-7 that the squeal frequency corresponds to the anti-resonance in α_{33} , which

according to (Thompson 2009) corresponds to a peak in the normal contact force spectrum and a resonance of the contact-coupled system.

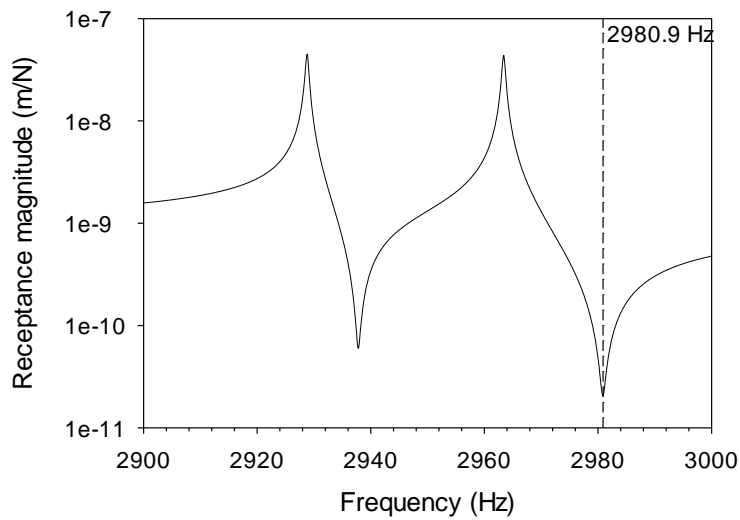


Figure 7-7: Denominator of open loop transfer function

The mode shapes of the (3,1) doublet modes are shown in Figure 7-8 for a wheel slice at the contact point. It is evident from Figure 7-8(a) that the (3,1) cosine doublet mode has a large mode shape component at the wheel flange in the normal direction. The (3,1) sine doublet shown in Figure 7-8(b) has a large rotational mode shape component at the wheel flange. This implies that mode-coupling instability for contact in the wheel flange is excited due to the coupling of doublet wheel modes in the presence of wheel rotation, where the one mode has a large normal displacement in the wheel flange and the other a large rotational displacement about the contact normal direction. The normal/rotational cross coupling dynamics of the rotational wheel are responsible for the phase lag between the normal and rotational vibration necessary for the non-vanishing energy input into the rotational vibration.

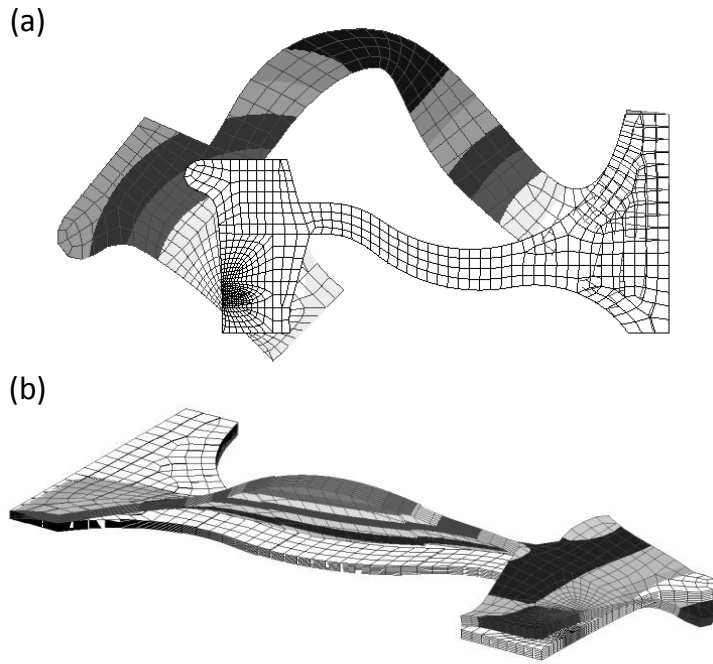


Figure 7-8: (3,1) Doublet modes (a) Cosine doublet (b) Sine doublet

7.4 SENSITIVITY ANALYSIS

To ascertain the results in Section 3.5, i.e. that both wheels underneath empty and loaded wagons are prone to flange contact squeal in the absence of large flange forces, the squeal model was updated to include a normal Hertzian spring stiffness of 1.5×10^9 N/m. This spring stiffness corresponds to the contact conditions of a wheel having a load of 150 kN and being underneath a loaded ore wagon. The Hertzian spring stiffness of 1.0×10^9 N/m previously modelled corresponds to the contact conditions in the flange throat of the wheel being underneath an empty ore wagon with a 25 kN wheel load.

Table 7-1 compares the results of the model with the two different normal contact conditions. Only the results of the seven doublet mode pairs with the largest loop gain according to Figure 7-6 are shown. It is clear from Table 7-1 that increasing the wheel load will increase the unstable frequency predicted for each doublet wheel mode pair. In addition, the results show that the loop gain associated with unstable modes below approximately 3000 Hz decreases whilst the loop gain associated with wheel modes occurring above 3000 Hz increases for the modelled stiffness change. This affects the wheel mode having the largest loop gain (indicated with bold values in Table 7-1) and that will most likely form the squeal limit cycle.

Table 7-1: Stability results for empty and loaded contact conditions

Wheel mode	Unstable frequency* Hz	Loop gain*
(4,0)	1773.7 (1781.3)	92.6 (59.0)
(2,1)	2330.3 (2340.1)	78.2 (64.1)
(3,1)	2980.8 (2991.3)	120.0 (103.2)
(4,1)	3725.7 (3737.4)	117.7 (123.8)
(3,2)	4969.9 (4973.8)	80.9 (100.4)
(7,2)	7757.5 (7760.2)	89.9 (132.4)
(12,0)	9285.2 (9288.8)	88.4 (126.6)

* Values in brackets correspond to a spring stiffness of 1.5×10^9 N/m

For the loaded contact condition, the unstable frequency with the largest loop gain (7760.2 Hz) corresponds to the contact coupled mode involving the forward travelling wave associated with the (7,2) doublet mode pair. The mode shapes of the (7,2) doublet modes are shown in Figure 7-9 for a wheel slice in the contact point. It can be seen from Figure 7-9(a) that the (7,2) cosine doublet mode has a large mode shape component at the wheel flange in the normal direction. The (7,2) sine doublet shown in Figure 7-9(b) has a large rotational mode shape component at the wheel flange. This once more confirms that mode-coupling instability for contact in the wheel flange throat is excited due to the coupling of doublet wheel modes in the presence of wheel rotation, where the one mode has a large normal displacement in the wheel flange and the other a large rotational displacement about the contact normal direction. The normal/rotational cross coupling dynamics of the rotational wheel are responsible for the phase lag between the normal and rotational vibration necessary for the non-vanishing energy input into the rotational vibration.

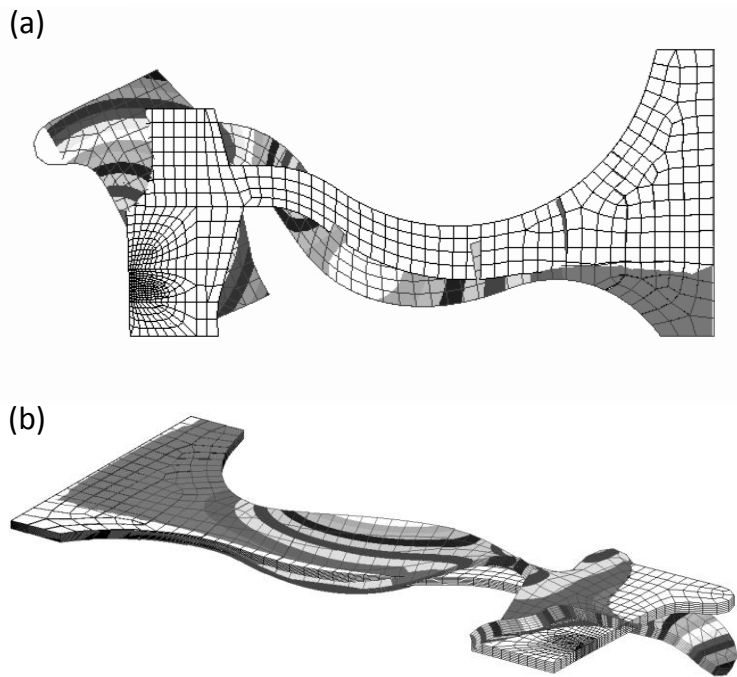


Figure 7-9: (7,2) Doublet modes (a) Cosine doublet (b) Sine doublet

Judging from the on-track measurements presented in Figure 3-29, the dominant squeal modes arising due to unsteady spin creepage is likely to occur at frequencies significantly exceeding the upper frequency limit of 10 kHz used in the model. It can thus be anticipated that for the modelled wheel type doublet modes having frequencies exceeding 10 kHz will have the largest loop gains in the stability analysis. The purpose of the current chapter is however not to provide a validated model for squeal due to unsteady spin creepage, but rather to capture the physics causing the instability. The reader should however be aware that doublet wheel modes having ultra-high frequencies or audible-sensitive frequencies can result in squeal dependent on the wheel type. For instance flange throat squeal reported in Curley et al. (2015) and Jiang et al. (2015a) had a dominant frequency close to 2 kHz. It should also be borne in mind that the inclusion of lateral and longitudinal creepage occurring simultaneously with spin creepage might alter the dominant squeal frequency as well. This will be the subject of future research.

7.5 DISCUSSION

Railway wheel squeal due to mode-coupling instability with spin creepage as the source of instability was modelled. The results of this research demonstrate the importance of spin creepage as a source of instability for squeal. The research further showed that crucial to the instability was modelling the dynamics of a wheel including the effects of a rotating wheel subject to moving load excitation. By including the effects of wheel rotation, the cross-coupling

dynamics between the normal and spin degrees of freedom (with respect to the wheel-rail contact) that is otherwise zero for a non-rotating wheel, are captured.

The results of the model based on unsteady spin creepage provide good agreement with previous on-track measurements, showing squeal resulting from contact between the rail gauge corner and wheel flange throat are caused by mode-coupling instability. Although the model is not validated against on-track measurements, it captures the physics of flange throat squeal and paves the way towards a future complete squeal model that is capable of predicting squeal comprehensively.

Mode-coupling instability for contact in the wheel flange is excited due to the coupling of doublet wheel modes in the presence of wheel rotation. The one doublet mode should have a large normal displacement in the wheel flange and the other a large rotational displacement about the contact normal direction. The normal/rotational cross coupling dynamics of the rotational wheel subject to moving load excitation is responsible for the phase lag between the normal and rotational vibration necessary for the non-vanishing energy input into the rotational vibration.

In addition, the model based on unstable spin creepage showed that the effect of increased axle load on squeal is that it will likely shift the dominant squeal mode to a different doublet mode pair of the wheel.

Finally it is important to take note that flange contact squeal can be excited at ultra-high frequencies or at frequencies where human hearing is very sensitive. This is likely a function of wheel design.

Based on the above results, the author recommends that a future complete model for curve squeal should include spin creepage and the dynamics of a rotating wheel subject to moving load excitation.

8 SQUEAL MITIGATION

The ultimate goal of squeal research and developing validated squeal models is to use the models and insight gained to identify the most feasible mitigation measure(s) to eliminate squeal in a particular situation. This is no different for the current research that studied squeal originating from the inner trailing wheel of self-steering bogies in large radius curves. The key motivation behind the current research was to eliminate squeal through the most effective and long term sustainable solution.

Various technical measures are available to combat curve squeal. Only if the exact underlying mechanism of squeal is known in a particular situation (through extensive experimental testing or a validated model or both), can the best solution for squeal mitigation be identified off hand without trial-and-error testing of the known mitigation measures. Some of the known/proposed mitigation measures include top-of-rail friction modification, gauge face lubrication, wheel and rail damping treatments, changes to rail transverse profiles, rail surface coatings or impregnation as well as improved bogie curving behaviour (UIC 2013, Thompson et al. 2016).

The application of friction modifiers to combat curve squeal has demonstrated to be very effective in eliminating squeal and in general is the first solution tested by railways when faced with a squeal noise ordinance. In spite of the proven effectiveness of top-of-rail friction modification, it has proven only site dependent success (Oertli 2005, Anderson 2008). This was also the first mitigation measure tested to combat squeal in the Elands Bay test curve. Although the in-field trial with top-of-rail friction modification was proven to be successful in mitigating squeal in the test curve (see Chapter 3), top-of-rail friction modification is however a maintenance intensive activity and is thus not desirable as a sustainable solution.

Improved curving behaviour using self-steering bogies is often listed as the solution of choice when discussing squeal mitigation measures of the future (see for e.g. UIC 2013). This is because the improved steering performance associated with these special bogie designs will most likely eliminate the large creepages necessary for squeal generation. The noise ordinance that motivated the current research does however demonstrate that self-steering bogies might not necessarily be the holy grail for squeal mitigation as widely believed. This is because self-steering bogies are very sensitive to geometrical and maintenance tolerances, that if not met, result in impaired steering of these bogies that might in return result in large creepages and squeal.

As demonstrated in Chapters 4 and 5, squeal in the test curve results from asymmetric wheel wear between the different wheels in a bogie that is directly caused by a tracking error that exist between the wheelsets in the squealing bogies. The combination of a wheelset tracking error and the resulting asymmetric wheel wear in the flange root causes the Scheffel self-steering bogies to over-steer in the test curve. This leads to high longitudinal creepage in the squealing wheel-rail contact that results in self-excitation of wheels depending on the magnitude of the creepage. The asymmetric wheel flange wear between the leading and trailing outer wheels is a direct consequence of the design wheel and rail profile pair making two-point contact in the wheel flange throat/rail gauge corner contact area. To improve the curving behaviour of squealing bogies in problematic curves, one has to consider solutions that will be effective in the short and medium to long terms.

It is anticipated that a short term solution will address the curving behaviour of squealing bogies only in problematic curves where noise is the primary concern. A long term solution must address the root cause(s) of the impaired curving behaviour and it is anticipated that such a solution must address the health of the entire bogie fleet through improving manufacturing tolerances of wheelsets and/or bogies and possibly a new wheel-rail profile combination for the entire ore line.

Except for the above two mitigation measures, changing the dynamic behaviour of the wheel and/or track through added damping treatments or design changes is also discussed based on additional curve squeal simulations.

8.1 IMPROVED CURVING BEHAVIOUR – SITE SPECIFIC

A possible solution to improving the curving ability of squealing bogies in the forward/squealing direction is to increase the rolling radius differential of the leading wheelset. This can be done by designing an outer rail profile that would promote conformal contact or by grinding the outer rail with the ore line target profile shifted 5 mm inwards to the gauge side of the track. Shifting the outer rail profile inwards moves the wheel-rail contact point closer to the wheel flange compared to similar lateral displacements for the standard ore line target profile. This would enhance the rolling radius differentials for smaller lateral displacements. Similarly, the conformal outer rail profile would also enhance the achievable rolling radius differences.

It is anticipated that promoting the steering ability of the leading wheelset will cause the squealing bogies to obtain equilibrium curving positions at smaller lateral displacements of both the leading and trailing wheelsets, hence leading to lower creepages.

8.1.1 Rail profiles

A graphical comparison of the ore line target rail profile and the proposed conformal high leg rail profile is shown in Figure 8-1.

The rolling radius difference functions of a wheelset with Transnet Freight Rail No 21 wheel tread profiles on different rail profile pairs are shown in Figure 8-2. The rail profile pairs considered are (i) the test curve measured low and high leg profiles, (ii) both high and low legs with the ore line target profile, (iii) the low leg with the ore line target profile and the high leg with the ore line target profile shifted 5 mm inwards towards the gauge side of the track as well as (iv) the low leg with the ore line target profile and the high leg with the proposed conformal target.

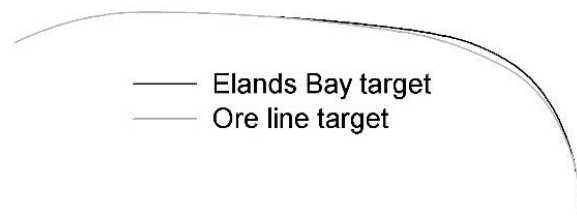


Figure 8-1: Ore line target vs. proposed conformal target

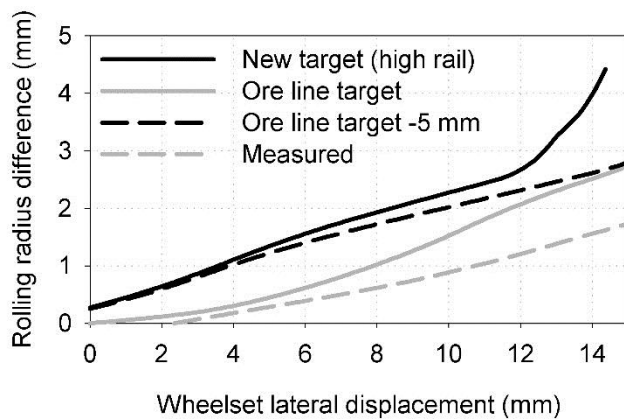


Figure 8-2: Rolling radius difference functions: Transnet Freight Rail No 21 wheelset

From Figure 8-2 it can be seen that the test curve measured high leg profile significantly reduces the achievable rolling radius difference function compared to the target ore line profile. This impacts negatively on the curving of bogies. Also evident from Figure 8-2 is that

the inwards shifted target rail profile significantly increases the rolling radius difference function compared to the ore line target for lateral displacements between 0 mm and 12 mm. This significantly improves wheelset steering at smaller lateral displacements. The conformal high leg rail profile achieves similar rolling radius differences compared to the 5 mm inwards shifted ore line target, but increases the rolling radius differences significantly for lateral displacements exceeding 12 mm.

8.1.2 Bogie curving performance

The simulated curving performance of the squealing bogie travelling in the forward direction with the different high rail profiles is summarised in Table 8-1. The scenarios are listed as 5, 6 and 7, sequential to the already simulated curving scenarios listed in Table 4-1.

Table 8-1: Simulation scenarios

Scenario	Coefficient of friction	Travel direction*	Outer rail profile
5	0.6	Forward	Ore line target
6	0.6	Forward	Ore line target 5 mm
7	0.6	Forward	Conformal target

* Forward is defined as the direction of travel producing squeal during the field tests.

Figure 8-3 to Figure 8-6 summarise the vehicle dynamics results with the different high rail profiles. For completeness, the results of scenarios 1 to 4 of Chapter 4 simulating the curving behaviour of wagon 60 250 577 in combination with the test curve measured rail profiles are reproduced in these figures. Figure 8-3 shows that all three of the suggested high rail profiles allow the worn wheel profiles of the bogie to make use of the bogie's self-steering capabilities. This significantly improves the curving ability of the bogie compared to the squealing scenario. The improved curving ability of the squealing bogie associated with Scenarios 5, 6 and 7 eliminates the large longitudinal creepages at the squealing wheel necessary for vibrational self-excitation of this wheel (see Figure 8-6). Figure 8-5 further shows that because the bogie self-steers with the three suggested high rail profiles, the angles-of-attack of the wheelsets are significantly reduced compared to the squealing scenario (Scenario 1).

Of the three outer rail profiles that eliminate squeal, it is recommended that the high rail of problem curves be ground to the 5 mm inwards shifted ore line target rail profile. In addition to the strong possibility of eliminating squeal from the test curves, it will likely also reduce the level of occurrence and magnitude of flanging noise. The proposed conformal target is not

considered from a squeal perspective because of the possibility of wheel-rail contact occurring at large rolling radius differences.

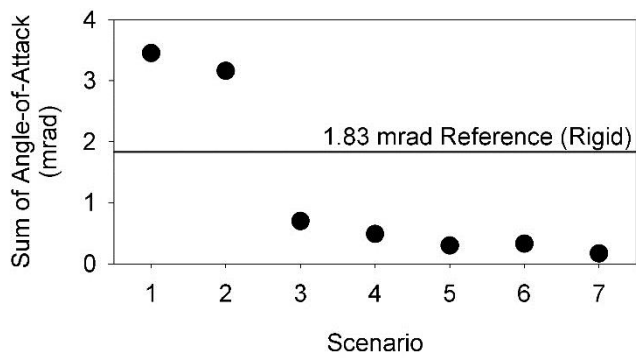


Figure 8-3: Bogie curving performance for different scenarios

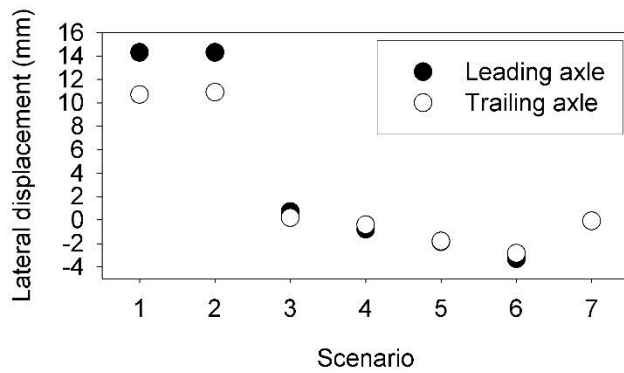


Figure 8-4: Wheelset lateral displacement results

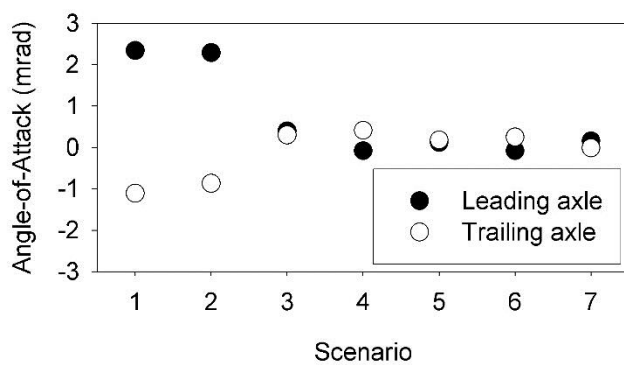


Figure 8-5: Angle-of-Attack results

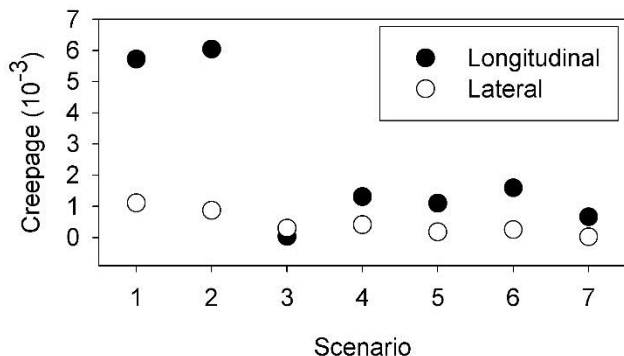


Figure 8-6: Creepages at squealing wheel-rail contact

8.2 IMPROVED CURVING BEHAVIOUR – LONG TERM

8.2.1 Wheelset tracking error

Figure 8-7 shows a distribution of the wheelset tracking error measured on tangent track for a 342-wagon empty ore train during November 2012. A similar distribution is likely to exist for the entire CR13/14 ore wagon fleet.

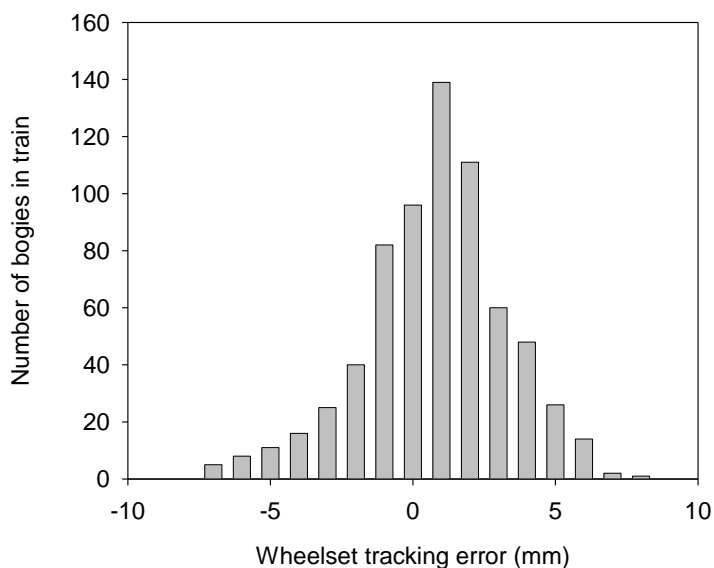


Figure 8-7: Distribution of wheelset tracking error for 342-wagon empty ore train

Strict quality control on the manufacturing tolerances associated with wheelset symmetry and welding of the bearing adapters into the bogie will likely reduce the width of the normal distribution and the maximum tracking error values. The exact root cause of the large tracking error will have to be determined going forward. Whilst addressing this root cause, the

problem associated with the current fleet will exist for years to come until the entire population of problem wheelsets have worn to condemning limits and bogies overhauled. Whilst strict quality compliance is a necessary step going forward to improve the steering performance of the bogie fleet, a workable and cost effective solution is still required in the interim to eliminate squeal until the tracking error of the entire fleet is brought within acceptable limits.

8.2.2 Conformal wheel-rail pair

The different worn shape of wheels in the flange throat area and the mismatch that this creates between the four wheels in a bogie needs to be better controlled to eliminate the asymmetric wear that contributes to the excitation of squeal. The best way to control wheel wear in the flange throat contact area is through conformal flange contact with the rail gauge corner (Tournay 2001, Fröhling 2002 and Kalousek 2005). In return this leads to a reduced variation in rolling radius difference functions across the wheel fleet, because the wheels better maintain their shape. Controlling the rolling radius differences at large lateral displacements through conformal wheel/rail profiles is important to prevent large traction forces that are generated by rolling radius excess or deficiency (Kalousek 2005).

A new conformal wheel profile for South Africa's ore line was recently developed by Spangenberg (2016) as a potential rolling contact fatigue mitigation measure although such a wheel profile has not been implemented on the ore line. The design philosophy of the conformal Transnet Freight Rail No 24 wheel profile was (i) to spread the contact widely across the wheel tread to limit concentrated hollow wear and (ii) to increase the steering ability of the wheelset/bogie for large lateral displacements to reduce flange contact for large lateral displacements. The contact distribution of the TFR No 24 wheel profile on the ore line target rail profile is shown in Figure 8-8.

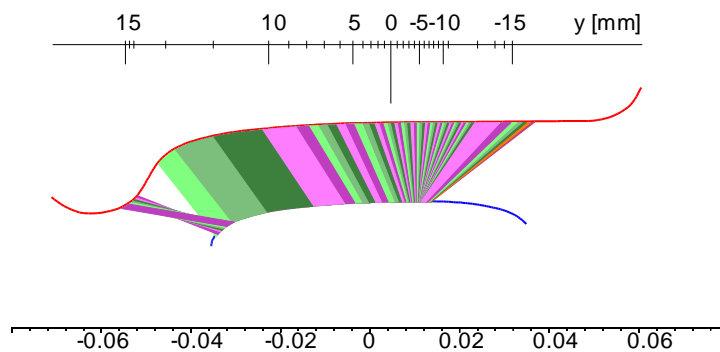


Figure 8-8: Contact distribution of TFR No 24 wheel profile and ore line target profile

The rolling radius difference functions for a bogie with TFR No 24 profiles on the ore line target rail profile having a + 4 mm tracking error is shown in Figure 8-9 for positive lateral displacements. In the left hand test curve this bogie will not have the ability to squeal due to over-steering of the bogie resulting from the wheelset tracking error. Instead the bogie will self-steer.

If the bogie however has a – 4 mm tracking error as shown in Figure 8-10, the probability of squeal increases significantly judging from the Δr vs y functions presented for the leading and trailing wheelsets for four squealing bogies in Figure 3-20 that over-steered in the test curve due to the rolling radius mismatch between wheelsets in a bogie. Compared to the rolling radius difference functions in Figure 8-9, the rolling radius differences in Figure 8-10 has the trailing wheelset curving with a larger rolling radius difference compared to the leading wheelset causing over-steering in a left hand curve. The bogie shown in Figure 8-9 on the other hand will have a high probability to over-steer in a right hand curve.

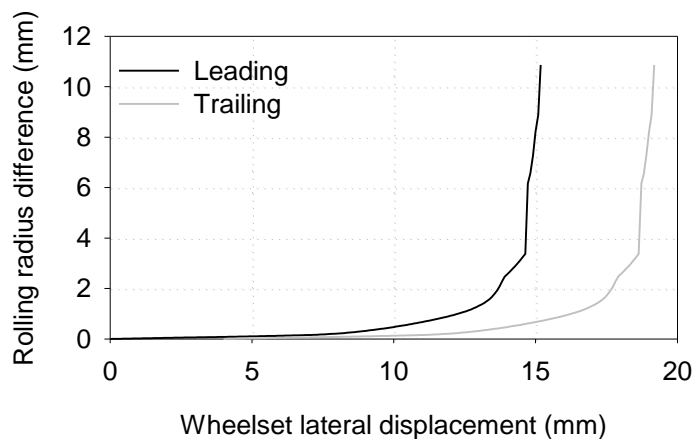


Figure 8-9: Δr vs y functions for + 4 mm tracking error

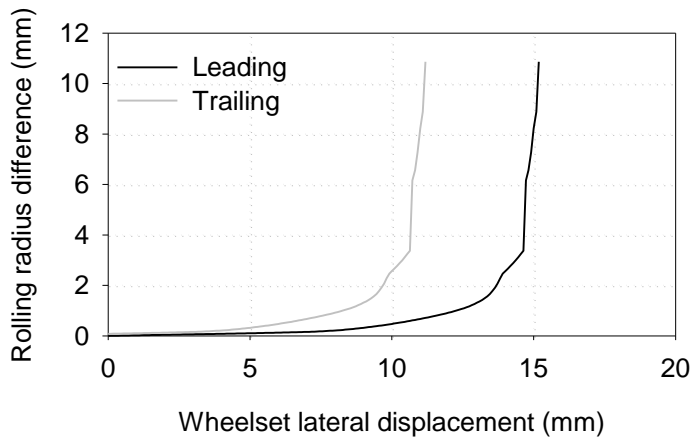


Figure 8-10: Δr vs y functions for - 4 mm tracking error

Judging from the above qualitative analysis, even if the conformal wheel-rail pair controls the worn shape of the wheel in the flange throat contact area very close to the design, the bogie will still have a high probability to squeal. This means that the site specific rail profile increasing the rolling radius difference function of the wheelset at intermediate lateral displacements will from part of the medium term strategy to control squeal when the TFR No 24 wheel profile is introduced and until the geometric tolerances related to the bogie wheelset tracking error can be reduced to within acceptable limits. The increase in the rolling radius difference at intermediate lateral wheelset displacements for the TFR No 24 wheel profile in combination with the outer rail profiled to a 5 mm inwards shifted ore line target profile is shown in Figure 8-11.

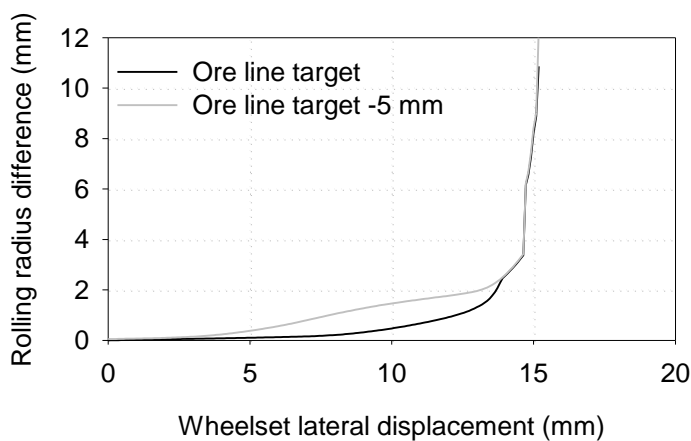


Figure 8-11: Rolling radius difference functions: Transnet Freight Rail No 24 wheelset

To eliminate the high rolling radius differences for large lateral displacements of the TFR No 24 wheelset, the TFR No 24 wheel profile still requires some multi-disciplinary optimisation in the flange root to limit the rolling radius difference to acceptable limits whilst maintaining a conformal wheel-rail profile design. This will be the subject of future work.

8.3 CHANGING WHEEL AND/OR TRACK DYNAMIC BEHAVIOUR

To evaluate the influence of changing the dynamic behaviour of the wheel and/or the track, the frequency domain squeal model based on the Nyquist criterion was used.

The parameters that were varied included the modal damping ratios of the wheel, the material damping of the rail (to simulate added damping treatments) as well as the stiffness and damping of the rail pad. The geometries of the wheel and rail were left unchanged.

Only the vertical dynamics of the rail was considered for parameter variation studies. The vertical rail pad stiffness per unit length was modelled as 150 MN/m², 300 MN/m² and 1000 MN/m². The rail pad damping factor was varied between 0.2, 0.3, 0.4 and 0.5. The rail damping loss factor was varied between 0.02, 0.2 and 0.5. In all cases only a single variable was varied to determine the effect of that variable on the squeal model.

8.3.1 Wheel damping

The frequency domain squeal model estimated that the damping ratio of the (2,C) wheel mode of wheel Type A needs to be increased from 1.2×10^{-4} to 7.0×10^{-4} in order to eliminate squeal. It is important to note that the damping treatment should also increase the damping ratios of all other potential squeal frequencies to be effective. If the damping treatment only increases the damping ratio of the (2,C) wheel mode, a different mode pair will become unstable.

Wheel damping is however not a feasible solution due to the associated cost of fitting wheel dampers to the entire wagon fleet.

8.3.2 Rail damping

Varying the rail damping loss factor showed minimal influence over the loop gain calculated for the different potential unstable modes. This illustrates that squeal in the test curve will not be eliminated by adding additional damping treatments to the rail.

8.3.3 Rail pad properties

Modelling different rail pad properties, i.e. rail pad stiffness and damping, had no effect on the loop gain calculated for the different potential unstable modes. This shows that squeal in

the test curve will not be eliminated by changing either the stiffness or damping associated with the rail pads.

From the results of the sensitivity analysis, it is evident that changing the properties of the track in the test curve by adding rail dampers or changing the properties of the rail pads will have no impact on the occurrence of squeal.

8.4 DISCUSSION

Mitigation measures can broadly be divided into local (site specific) and global (vehicle specific) solutions. Site specific solutions are desirable in situations where only a small portion of curves along the line are responsible for squeal, because this eliminates the need to treat large fleets of vehicles that pass the site. Thus, although wheel damping treatments has shown a high probability of eliminating squeal, the economics of the solution makes it undesirable. Top-of-rail friction modification has proven successful in eliminating squeal from the test curve. This solution is however not desirable due to the constant and dedicated maintenance it requires. Grinding the high rail of problem curves with a new target rail profile is the desired solution to mitigate squeal in the short to medium term, until the wheelset tracking error of the entire wagon fleet can be brought to within acceptable and practically achievable limits. Grinding the high rail of problem curves with a new target profile is an economically viable and sustainable solution, because profile grinding is already performed 3 or 4 times per annum on the entire line. Profile grinding is performed on the line to control rolling contact fatigue and not because the rail profiles change significantly in between grinding campaigns.

9 CONCLUSIONS AND RECOMMENDATIONS

9.1 CONCLUSIONS

9.1.1 Source of instability for squeal

Low frequency audible wheel squeal in the test curve could uniquely be attributed to the trailing inner wheel of Scheffel self-steering bogies underneath empty freight wagons. The key kinematic parameter influencing the generation of inner wheel squeal was lateral displacement of the wheelsets leading to high levels of longitudinal creepage. The high levels of longitudinal creepage result from the contact conditions of some worn wheels on worn rail profiles, resulting in large rolling radius differences between the inner and outer wheels in the curve.

Vehicle dynamics simulations have shown that the combination of worn wheel and rail profiles cause affected Scheffel self-steering bogies underneath empty freight wagons to over-steer in the test curve. This occurs when the the trailing wheelset (squealing wheelset) has much larger rolling radius differences compared to the leading wheelset for similar lateral displacements. Over-steering causes both wheelsets of the bogie to displace laterally towards the outside of the curve causing high levels of longitudinal creepage. This occurs because of a tracking error between the wheelsets in the bogie causing the two sets of diagonally opposite wheels to wear differently. The tracking error exacerbates the flange throat wear on one pair of diagonally opposite wheels, whilst it reduces the probability of flange throat wear on the other pair of diagonally opposite wheels. Because the current ore line wheel-rail profile pair is designed to make two-point contact in the rail gauge corner/wheel flange throat contact area the one pair of diagonally wheels that protrudes the most into the flangeway will wear conformal. This causes the large rolling radius difference between the leading and trailing wheelset that results in an over-steering bogie and large longitudinal creepage at the trailing wheelset.

This research also highlights the importance of spin creepage as a possible source of instability for outer wheel squeal. It is important to take note that flange contact squeal can be excited at ultra-high frequencies or at frequencies where human hearing is very sensitive. This is likely to be a function of the wheel design. Experimental results presented for a 1000 m radius curve have shown that the likelihood of flange contact squeal diminishes for increased rolling stock axle loading. This is because increased flange rubbing with high flange forces, as is likely to occur for higher axle loads, introduce positive damping to the wheel-rail contact. This positive damping reduces the amplitude of flange contact squeal or eliminates it

completely. Instead flange rubbing with high flange forces causes broadband flange rubbing noise. Here it is important to distinguish between contact occurring solely between the rail gauge corner and wheel flange throat or additionally between the rail gauge and wheel flange faces. It is expected that wheel-rail profile pairs making severe one-point contact in the gauge corner will especially be subject to flange throat squeal.

9.1.2 Mechanism of instability: Unsteady longitudinal creepage

Railway wheel squeal with longitudinal creepage as the source of instability was modelled. In contrast to international research that does not consider longitudinal creepage to be relevant to squeal, the results of this research demonstrate the importance of longitudinal creepage as a source of instability for squeal. Both instability due to falling friction and mode-coupling were assessed. The study demonstrates that the measured phenomenon of inner wheel squeal is consistent with mode-coupling instability and more specifically the coupling of doublet modes of the wheel.

The results of the model show that the excitation of squeal due to mode-coupling is limited to the region on the adhesion curve close to adhesion optimum where the positive and negative frictional damping is very small. For the falling region of the adhesion curve, beyond a certain gradient the fundamental torsional resonance of the wheelset will be unstable. Because of the low frequency of the (0,C) mode, the predicted instability is not relevant to squeal and instead relevant to the formation of rail corrugation and wheel polygonisation.

Squeal could be shown as originating from mode-coupling instability due to the coupling of the modes in a doublet due to the moving load nature of the wheel. For wheel Type A the resonances of the contact coupled wheel-rail system associated with the backward travelling waves of the (2,C) and (7,R) doublets could be shown to participate in squeal. In this case the operational conditions associated with longitudinal creepage and the wheel load could be shown to take part in determining which of the potentially unstable modes will have the largest loop gain and will be excited into squeal. For wheel Type B only the resonance of the contact coupled system associated with the backward travelling wave of the (2,C) doublets could be shown to participate in squeal.

The results of the model based on unsteady longitudinal creepage provide good agreement with experimental findings in terms of the experimentally obtained squeal frequencies as well as being able to predict the dominant squeal mode in the test curve as the mode with the largest loop gain for most operational conditions i.e. the (2,C) mode of both wheel Type A and B.

Based on the above results, the author recommends that a complete model for curve squeal should include longitudinal creepage and the dynamics of the wheel under moving loads. It is also recommended that a complete model for curve squeal should also evaluate the existence of squeal for not only falling friction or constant friction, but should include a defined adhesion curve for which a stability map can be generated for different levels of creepage around the adhesion optimum as well as for the falling part of the adhesion curve.

9.1.3 Mechanism of instability: Unsteady spin creepage

The study demonstrates that the measured phenomenon of outer wheel squeal is highly likely to be consistent with mode-coupling instability and more specifically the coupling of doublet modes of the wheel.

Crucial to the instability was modelling the dynamics of a wheel including the effects of a rotating wheel subject to moving load excitation. Including the moving load nature associated with wheel rotation captures the cross-coupling dynamics between the normal and spin degrees of freedom (with respect to the contact patch) that is otherwise zero for a non-rotating, sliding wheel.

The results of the model based on unsteady spin creepage provide good agreement with previous on-track measurements showing squeal resulting from contact between the rail gauge corner and wheel flange throat are most likely caused by mode-coupling instability. Although the model is not validated against on-track measurements, it captures the physics of flange throat squeal and paves the way towards a future squeal model that is capable of predicting squeal comprehensively.

Based on the above results, it is recommended that a complete model for curve squeal should include spin creepage and the dynamics of a rotating wheel.

9.1.4 Mitigation: Squeal due to unsteady longitudinal creepage

Possible mitigation measures for squeal due to unsteady longitudinal creepage include top-of-rail friction modification, wheel damping as well as avoiding over-steering of the affected bogies in the test curve.

Over-steering of affected Scheffel bogies can be avoided in the short term should a rail profile be implemented that promotes the steering of the bogies in affected curves and that promotes the self-steering capabilities of affected bogies. In the long term the wheelset tracking error of the ore line bogie fleet need to be reduced to within defined tolerances. Such tolerances still have to be defined.

Whilst wheel damping and improving the tracking error of problem bogies are global solutions, top-of-rail friction modification as well as rail grinding can be applied locally to affected sites. Of the four proposed solutions, grinding the high rail of affected curves with an alternate high leg rail profile is the most economical and least maintenance intensive solution and is hence desired in the short term. Railhead profile grinding is already performed 3 to 4 times per annum on this line to control rolling contact fatigue and will hence fit in perfectly with a maintenance regime that is already in place on the ore line.

9.2 RECOMMENDATIONS

9.2.1 Mitigation

It is recommended that the high rail of problem curves be ground to the 5 mm inwards shifted ore line target rail profile as a short to medium term solution. In addition to the strong possibility of eliminating squeal from the test curves, it will likely also reduce the level of occurrence and magnitude of flanging noise. The proposed conformal target is not considered because of the possibility of wheel-rail contact occurring at large rolling radius differences. Before the TFR No 24 wheel profile is implemented on the line, the flange throat contact area of the wheel-rail profile pair design must be addressed to limit the rolling radius difference to acceptable limits whilst still maintaining a conformal profile design.

A 5 mm inwards shifted rail profile has already been successfully implemented in the test curve. The author will plan a follow-up measurement campaign in the test curve early 2019 to evaluate the success of the profile to combat squeal in the test curve.

9.2.2 Squeal model

It is envisaged that the current squeal model will be updated in the near future to evaluate the combined effects of lateral, longitudinal and spin creepage including the dynamics of a rotating wheel subject to moving load excitation. This will include varying the contact position as well as the direction and magnitude of the resultant creepage to draw stability maps for the different contact conditions. Evaluating the different values of creepage for a given creep direction is crucial as it has been shown in the current research that the level of creepage in addition to the gradient of the adhesion curve determines the dominant unstable mode for a given range of creepage.

9.2.3 Future work

It is the author's opinion that a wealth of information can be unlocked should the opportunity exist in future for more detailed in field squeal investigations. The data from detailed field investigations is invaluable to validate squeal models or at least provide the opportunity for a

qualitative comparison between models and measurements. This is especially true if researchers want to unlock all the hidden secrets of squeal, the secrets that make squeal appear chaotic rather than deterministic.

In the author's ten years' working in the railway environment in South-Africa, squeal resulting from the self-steering bogies operating on South-Africa's heavy haul lines were the only squeal that has been observed from trailing rolling stock. No squeal originating from other freight wagons using either self-steering bogies or three piece freight bogies have been observed from numerous train's passing in numerous curve radii even for curves down to a 120 m curve radius. Concerning South Africa's electric locomotive fleet, only one locomotive type of the 12 operational types of electric locomotives has been observed to squeal. Interestingly this locomotive also squeals due unsteady longitudinal creepage, but only during wet weather conditions at maximum traction when the adhesion demand significantly exceeds the available adhesion between the wheel and rail. Concerning South Africa's diesel-electric locomotive fleet, only two of the nine operational diesel-electric locomotive classes have been observed to squeal. Interestingly these two locomotive types are the worst curving locomotives in Transnet's entire locomotive fleet as determined during curving force measurements and most likely squeals due to unsteady lateral creepage in small radius curves. On the general freight lines where no squeal occurs in small radius curves, these curves are generally plagued with corrugation possibly pointing to instability at inaudible frequencies. Going forward the author would like to contribute to the modelling of squeal/corrugation by determining what the selection criteria is for instability occurring at high and low frequencies. For instance Balekwa (2017) has shown experimentally that the corrugation wavelength on small radius curves on a 211 km railway line in South Africa are most likely caused by the (1,0) mode of the wheelset of the locomotive type operational on this line. Thus studying squeal and corrugation in parallel with a model capable of predicting low and high frequency instability might yield valuable insights in future.

10 REFERENCES

- Akay, A. 2002. Acoustics of friction. *J Acoust Soc Am*, Vol 111, No 4, pp.1525-1548.
- Anderson, D. Wheatley, N. Fogarty, B. Jiang, J. Howie, A. and Potter, W. 2008. Mitigation of curve squeal in Queensland, New South Wales and South Australia. *Proceedings of Conference on Railway Engineering*, Perth, 7-10 September 2008. Railway Technical Society of Australasia, pp 625-636.
- Balekwa, B.M. 2017. *Corrugation wavelength fixing mechanisms and its relationship to train and track geometry parameters*. Master's thesis. University of Johannesburg. South Africa.
- Bleedorn, T.G. and Johnstone, B. 1977. Steerable steel wheel systems and wheel noise suppression. IEEE Industry Application Society Annual Meeting. Paper 37-E, pp 957-963.
- Chant, C. 2007. *The world's railways*. Grange Books. Hoo.
- Chen, G.X. Xiao, J.B. Liu, Q.Y. and Zhou, Z.R. 2008. Complex Eigenvalue Analysis of Railway Curve Squeal. Eds Schulte-Werning, B. et al. *Noise and Vibration Mitigation for Rail Transportation Systems, NNFM*, Vol 99, pp 433-439.
- Chen, G. Pingbo, W. Huayan, D. and Zhongrong, Z. 2010. Comparative study on the complex eigenvalue prediction of brake squeal by two finite element modelling approaches. *Chinese Journal of Mechanical Engineering*, Vol 23, No 3, pp 383-390.
- Chiello, O. Ayasse, J.B. Vincent, N. and Koch, J.R. 2006. Curve squealing of urban rolling stock – Part 3: Theoretical model. *J Sound Vib*, Vol 293, pp 710-727.
- Collette, C. 2012. Importance of wheel vertical dynamics in the squeal noise mechanism on a scaled test bench. *Journal of Shock and Vibration*, Vol 19, pp 145-153.
- Curley, D. Anderson, D.C. Jiang, J. and Hanson, D. 2015. Field trials of gauge face lubrication and top of rail friction modification for curve noise mitigation. Eds Nielsen, J.C.O. et al. *Noise and vibration mitigation for rail transportation systems, NNFM*, Vol 126, pp 449-456.
- De Beer, F.G. Janssens, M.H.A. Kooijman, P.P. and Vliet, W.J. 2000. Curve squeal of railbound vehicles (part 1): frequency domain calculation model. *Proceedings of Internoise*, Nice, France, 27-31 August 2000, Vol 3, pp 1560-1563.

- De Beer, F.G. Janssens, M.H.A. and Kooijman, P.P. 2003. Squeal noise of rail-bound vehicles influenced by lateral contact position. *J Sound Vib*, Vol 267, pp 497-507.
- Ding, B. Squicciarini, G. and Thompson, D.J. 2016. Effects of rail dynamics and friction characteristics on curve squeal. *J Phys: Conf Ser*, Vol 744, No 1, 012146
- Ding, B. Squicciarini, G. Thompson, D.J. and Corradi, R. 2018. An assessment of mode-coupling and falling-friction mechanisms in railway curve squeal through a simplified approach. *J Sound Vib*, Vol 423, pp 126-140.
- Dittrich, M.G. and Jansen, H.W. 2015. Proposals for improved methods for curve squeal and braking noise. Eds Nielsen, J.C.O. et al. *Noise and vibration mitigation for rail transportation systems, NNFM*, Vol 126, pp 595-602.
- Duarte, M.L.M. and Ewins, D.J. 2000. Rotational degrees of freedom for structural coupling analysis via finite-difference technique with residual compensation. *Mech Syst Signal Process*, Vol 14, No 2, pp 205-227.
- Ehrich, F.F. 2010. Self-excited vibration. *Harris' shock and vibration handbook*. Eds Piersol, A.G. and Paez, T.L. 6th ed. McGraw-Hill, New York, pp 5.1 – 5.25.
- European Commission. 2011. *White paper – Roadmap to a single European transport area – Towards a competitive and resource efficient transport system*. COM(2011) 144 final. Brussels.
- Fingberg, U. 1990. A model of wheel-rail squealing noise. *J Sound Vib*, Vol 143, No 3, pp 365-377.
- Fourie, D.J. 2011. *Mechanisms influencing railway wheel squeal generation in large radius curves*. Master's Thesis. University of Johannesburg.
- Fourie, D.J. Gräbe, P.J. Heyns, P.S. and Fröhling, R.D. 2018. Analysis of railway wheel squeal due to unsteady longitudinal creepage using the complex eigenvalue method. Eds Anderson, D. et al. *Noise and Vibration Mitigation for Rail Transportation Systems, NNFM*, Vol 139, pp. 57-69.
- Fröhling, R.D. 2002. Strategies to control wheel profile wear. *Vehicle System Dynamics*, Vol 37 (Supplement 1), pp 490-501.
- Glocker, C. Cataldi-Spinola, E. and Leine, R.I. 2009. Curve squealing of trains: Measurement, modelling and simulation. *J Sound Vib*, Vol 324, pp 695-702.

- Grassie, S.L. Gregory, R.W. and Johnson, K.L. 1982. The dynamic response of railway track to high frequency longitudinal excitation. *J Mechan Eng Sci*, Vol 24, No 2, pp 97-102.
- Grassie, S.L. and Kalousek, J. 1993. Rail corrugations: Characteristics, causes and treatments. *J Rail and Rapid Transit*, Vol 207, No 1, pp 57-68.
- Heckl, M.A. and Abrahams, I.D. 2000. Curve squeal of train wheels, Part 1: Mathematical model for its generation. *J Sound Vib*, Vol 229, pp 695-707.
- Hettasch, G. and Spangenberg, U. The influence of maintenance-induced variations in bogie geometry on hollow-wear rates of ore line wagon wheels. *Proceedings of the 11th International Heavy Haul Association Conference (IHHA 2017)*, Cape Town, South Africa, 2-6 September 2017, pp721-727.
- Hoffmann, N. Fischer, M. Allgaier, R. and Gaul, L. 2002. A minimal model for studying properties of the mode-coupling type instability in friction induced oscillations. *Mech Res Commun*, Vol 29, pp 197-205.
- Huang, J. Krousgrill, C.M. and Bajaj, A.K. 2006. Modelling of automotive drum brakes for squeal and parameter sensitivity analysis. *J Sound Vib*, Vol 289, No 1, pp 245-263.
- Huang, Z.Y. Thompson. D.J. and Jones, C.J.C. 2008. Squeal prediction for a bogied vehicle in a curve. Eds Schulte-Werning, B. et al. *Noise and Vibration Mitigation for Rail Transportation Systems, NNFM*, Vol. 99, pp 313-319.
- International Heavy Haul Association (IHHA). 2001. *Guidelines to best practises for heavy haul railway operations: Wheel and rail interface issues*. IHHA. Virginia.
- Jiang, J. Dwight, R. and Anderson, D. 2012. Field verification of curving noise mechanisms. Eds Maeda, T. et al. *Noise and vibration mitigation for rail transportation systems, NNFM*, Vol 118, pp 349-356.
- Jiang, J. Anderson, D. and Dwight, R. 2015a. The mechanisms of curve squeal. Eds Nielsen, J.C.O. et al. *Noise and vibration mitigation for rail transportation systems, NNFM*, Vol 126, pp 587-594.
- Jiang, J. Ying, I. Hanson, D. and Anderson, D. 2015b. An Investigation of the influence of track dynamics on curve noise. Eds Nielsen, J.C.O. et al. *Noise and vibration mitigation for rail transportation systems, NNFM*, Vol 126, pp 441-448.

- Jiang, J. Hanson, H. and Dowell, B. 2016. Wheel squeal: Insights from wayside condition monitoring. *Proceedings of the 12th International Workshop on Railway Noise*, Terrigal, Australia, 12-16 September 2016, pp 28-35.
- Junior, M.T. Gerges, S.N.Y. and Jordan, R. 2008. Analysis of brake squeal noise using the finite element method: A parametric study. *Applied Acoustics*, Vol 69, No 2, pp 147-162.
- Kalker, J.J. 1982. A Fast Algorithm for the Simplified Theory of Rolling Contact, *Vehicle Syst Dyn*, Vol 11, pp 1-13.
- Kalker, J.J. 1990. *Three-Dimensional Elastic Bodies in Rolling Contact*. 1st ed. Kluwer: Dordrecht, Netherlands.
- Kalousek, J. 2005. Wheel-rail damage and its relationship to track curvature. *Wear*, Vol 258, pp 1330-1335.
- Kerr, M. Kalousek, J. Elliot, G. Mau, F. and Anderson, D. 1998. Squeal appeal: Addressing noise at the wheel/rail interface. Ed Ogdanna, W. *Proceedings of Conference on Railway Engineering*, Rockhampton, Australia, 7-9 September 1998, pp 317-324.
- Kik, W. 2010. *AcRadSchiene Version 4.4, To create or approximate wheel/rail profiles*. ArgeCare. Berlin.
- Kinkaid, N.M, O'Reilly, O.M. and Papadopoulos, P. 2003. Review: Automotive disc brake squeal, *J of Sound and Vib*, Vol 267, pp 105-166.
- Koch, J.R. Vincent, N. Chollet, H. and Chiello, O. 2006. Curve squeal of urban rolling stock – Part 2: Parametric study on a ¼ scale test rig, *J Sound Vib*, Vol 293, pp 701-709.
- Kopke, U. Rennison, D. and Southern, C. 2004. RailSquad: A wheel/rail noise emission monitoring system. *Proceedings 14th International Wheelset Congress*, 17-21 October 2004, Orlando, Florida, USA.
- Kraft, K. 1967. Der Einfluß der Fahrgeschwindigkeit auf den Haftwert zwischen Rad und Schiene (The influence of travelling speed on the friction coefficient between wheel and rail). *Archiv für Eisenbahntechnik*, Vol 22, pp 58-78.
- Lee, Y.S. Brooks, P.C. Barton, D.C. and Crolla, D.A. 2003. A predictive tool to evaluate disc brake squeal propensity. Part 1: The model philosophy and the contact problem. *Int J Vehicle Des*, Vol 31, No 3, pp 289-308.

- Liu, X. and Meehan, P.A. 2014. Investigation of the effect of relative humidity on lateral force in rolling contact and curve squeal. *Wear*, Vol 310, No 1-2, pp 12-19.
- Magel, E. and Liu, Y. Study of friction: measurement, analysis and practical implications for the wheel-rail contact. *Proceedings 8th International Conference and Wear of Rail, Wheel Systems*, 15-18 September 2009, Firenze, Italy.
- Maree, J.S. Aspects of resilient rail pads. *Proceedings of the 5th International Heavy Haul Association Conference*, 6-11 June 1993, Beijing, China, pp 433-439.
- Meymand, S.Z. Keylin, A. and Ahmadian, M. 2016. A survey of wheel-rail contact models for rail vehicles. *Vehicle Syst Dyn*, Vol 54, No 3, pp 386-428.
- Monk-Steel, A.D. Thompson, D.J. De Beer, F.G. and Janssens, M.H.A. 2006. An investigation into the influence of longitudinal creepage on railway squeal noise due to lateral creepage. *J Sound Vib*, Vol 293, No 3-5, pp 766-776.
- Nack, V.W. 2000. Brake squeal analysis by the finite element method. *Int J Vehicle Des*, Vol 23, Nos 3-4, pp 263-275.
- Oertli, J. 2005. *Combating curve squeal Phase II: Final report*. International Union of Railways (UIC), Bern.
- Oertli, J. and Hübner, P. 2010. *Railway Noise in Europe – A 2010 report on the state of the art*. International Union of Railways (UIC), Paris.
- Ouyang, H. Nack, W. Yongbin, Y. and Chen, F. 2005. Numerical analysis of automotive disc brake squeal: a review. *Int J of Vehicle Noise and Vibration*, Vol 1, No 3-4, pp 207-231.
- Périard, F.J. 1998. *Wheel-rail noise generation: Curve squealing by trams*. PhD Thesis. Delft University of Technology.
- Pieringer, A. 2011. *Time-domain modelling of high-frequency wheel/rail interaction*. PhD Thesis, Chalmers University of Technology.
- Pieringer, A. 2014. A numerical investigation of curve squeal in the case of constant wheel/rail friction. *J Sound Vib*, Vol 333, pp 4295-4313.
- Pieringer A, Baeza L and Kropp W. 2015. Modelling of railway curve squeal including effects of wheel rotation. In Nielsen JCO, et al. (eds.) *Noise and Vibration Mitigation for Rail Transportation Systems. NNFM*, Springer, Heidelberg 2015. 126: 417-424.

- Pieringer, A. Torstensson, P. Giner, J and Baeza, L. 2016. Investigation of railway curve squeal using a combination of frequency- and time domain models. *Proceedings of the 12th International Workshop on Railway Noise*, Terrigal, Australia, 12-16 September 2016, pp 444-451.
- Polach, O. 2005. Creep forces in simulations of traction vehicles running on adhesion limit. *Wear*, Vol 258, pp 992-1000.
- Reitmann, E. 2013. *Vertical load cross-talk investigation on web-bending vs base-chevron lateral force measurement techniques*. Report No BBG1207. Transnet Freight Rail. South Africa.
- Remington, P.J. 1987. Wheel/rail squeal and impact noise: What do we know? What don't we know? Where do we go from here? *J Sound Vib*, Vol 116, No 2, pp 339-353.
- Republic of South Africa Department of Transport. 2010. *National transportation Master Plan (NATMAP 2050) – Executive Summary*. Republic of South Africa Department of Transport. South Africa.
- Rudd, M.J. 1976. Wheel/rail noise – Part II: Wheel squeal. *J Sound Vib*, Vol 46, No 3, pp 381-394.
- Scheffel, H. 1974. A new design approach for railway vehicle suspension. *Rail Int*, Vol 638, pp 638-651.
- Scheffel, H. 1978. Experience gained by South African Railways with the diagonally stabilised (cross-anchor) bogies having self-steering wheelsets. Paper presented at: *Heavy Haul Railways Conference*. Perth.
- Southern, C. and Alexander, K. 2009. Adelaide Hills Wheel Squeal Project. Engineers Australia. Railway Technical Society of Australasia. SA Newsletter. August 2009.
- Spangenberg, U. 2016. *Reduction of rolling contact fatigue through the control of the wheel wear shape*. PhD Thesis. University of Pretoria.
- Spangenberg, U. Fröhling, R.D. and Els, P.S. 2016. Influence of wheel and rail profile shape on the initiation of rolling contact fatigue cracks at high axle loads. *Vehicle Syst Dyn*, Vol 54, pp 638-652.
- Stanbridge, A.B. Martarelli, M. and Ewins, D.J. 2001. Rotating disc vibration analysis with a circular scanning LDV. *Proceedings of the 19th International Modal Analysis Conference*,

Kissimmee, Florida, 5-8 February 2001. International Society for Optical Engineering, pp 464-469.

Stefanelli, R. Dual, J. Cataldi-Spinola, E. and Götsch, M. 2004. Field measurements on Curve Squealing – The influence of the Wheel Diameter. *Proceedings of CFA/DAGA*, Strasbourg, France, 22-25 March 2004, pp 903-904.

Stefanelli, R. Dual, J. and Cataldi-Spinola, E. 2006. Acoustic modelling of railway wheels and acoustic measurements to determine involved eigenmodes in the curve squealing phenomenon. *Vehicle Syst Dyn*, Vol 44, pp 286-295.

Squicciarini, G. Usberti, S. Thompson, D.J. Corradi, R. and Barbera, A. 2015. Curve squeal in the presence of two wheel-rail contact points. Eds Nielsen, J.C.O. et al. *Noise and vibration mitigation for rail transportation systems, NNFM*, Vol 126, pp 603-610.

Thompson, D.J. 1993. Wheel-rail Noise Generation, Part V: Inclusion of Wheel Rotation. *J Sound Vib*, Vol 161, No 3, pp 467-482.

Thompson, D.J. and Monk-Steel, A.D. 2003. *A Theoretical model for curve squeal*. Institute of Sound and Vibration Research. Research Report. University of Southampton.

Thompson, D.J. 2009. *Railway noise and vibration: mechanisms, modelling and means of control*. 1st ed. Elsevier, Oxford.

Thompson, D.J. Squicciarini, G. and Ding, B. 2016. A state-of-the-art review of curve squeal noise: phenomena, mechanisms, modelling and mitigation. *Proceedings of the 12th International Workshop on Railway Noise*, Terrigal, Australia, 12-16 September 2016, pp 1-27.

Tournay, H.M. 2001. Part 2: Supporting technologies vehicle track interaction. In *Guidelines to best practises for heavy haul operations: Wheel and Rail Interface Issues*. 1st edition. Virginia Beach: International Heavy Haul Association.

Transportation Technology Center, INC. (TTCI). 2010. *Vertical and Lateral Force Measuring Circuit, Installation Information*. TTCI. Pueblo.

UIC. 2013. *Railway noise technical measures catalogue*. International Union of Railways (UIC), Paris.

- Verheijen, E. and Elbers, F.B.J. 2015. Future European noise emission ceilings: Threat or solution? A review based on Swiss and Dutch ceilings. Eds Nielsen, J.C.O. et al. *Noise and vibration mitigation for rail transportation systems, NNFM*, Vol 126, pp 71-78.
- Vermeulen, P.J. and Johnson, K.L. 1964. Contact of nonspherical elastic bodies transmitting tangential force. *Trans. ASME, Series E, Journal of Applied Mechanics*, Vol 31, pp 338-340.
- VI-grade GmbH. 2014. *VI-Rail version 16.0.23615*. Computer software. VI-grade GmbH. Marburg.
- Vincent, M. Koch, J.R. Chollet, H. and Guerder, J.Y. 2006. Curve squealing of urban rolling stock – Part 1: State of the art and field measurements. *J Sound Vib*, Vol 293, No 3-5, pp 691-700.
- Vollebregt, E.A.H. 2017. *User guide for CONTACT, Rolling and sliding contact with friction*. Technical Paper Tr 09-03, Version 17.1. Vortech BV, Delft, The Netherlands.
- Von Stappenbeck, H. 1954. Das Kurvengeräusch der Strassenbahn. Möglichkeiten zu seiner Unterdrückung. *Zeitschrift VDI*, Vol96, No 6, pp 171-175.
- Wang, C. Dwight, R. Wenxu, L. and Jiandong, J. 2016. Prediction on curve squeal in the case of constant wheel-rail friction. *Proceedings of the 12th International Workshop on Railway Noise*, Terrigal, Australia, 12-16 September 2016, pp 428-433.
- Wiebe, E. Sandor, J. Cheron, C. and Haas, S. 2011. *ERRAC Roadmap – WP 01 – The greening of surface transport – Towards 2030 – Noise and vibration roadmap for the European railway sector*. International Union of Railways (UIC), Union des Industries Ferroviaires Européennes (UNIFE). Paris and Brussels.
- Wu, T. and Thompson, D.J. 1999. Analysis of lateral vibration behavior of railway track at high frequencies using a continuously supported multiple beam model. *J Acoust Soc Am*, Vol 106, No 3, 1369.
- Zagrodzki, P. 2009. Thermoelastic instability in friction clutches and brakes – Transient modal analysis revealing mechanisms of excitation of unstable modes. *Int J Solids Struct*, Vol 46, pp 2463-2476.
- Zakhrov, S. 2001. *Part 3: Wheel/Rail Performance*. In: Guidelines to best practises for Heavy Haul railway operations: Wheel and Rail interface issues. International Heavy Haul Association, Virginia.

Zenzerovic, I. Pieringer, A. and Kropp, W. 2015. Towards an Engineering model for curve squeal. Eds Nielsen, J.C.O. et al. *Noise and vibration mitigation for rail transportation systems, NNFM*, Vol 126, pp 433-440.

Zenzerovic, I. 2017. *Time-domain modelling of curve squeal: a fast model for one- and two-point wheel/rail contact*. PhD Thesis, Chalmers University of Technology.

APPENDIX A
RAIL FORCE MEASUREMENTS

A.1 INTRODUCTION

This appendix gives the detail of the strain gauge full-bridges that were used to measure the vertical and lateral track forces. Figure A-1 shows an example of the installed load gauges.

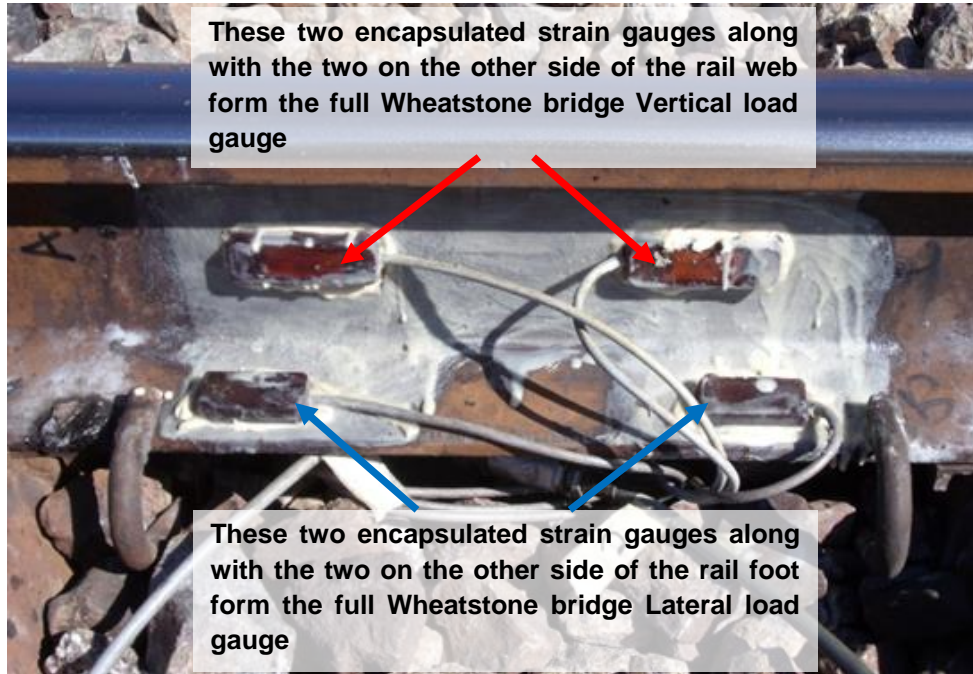


Figure A-1: Installed vertical and lateral load gauges

A.2 Vertical track forces

The vertical force measuring circuit consists of four shear strain gauges connected in a full Wheatstone bridge configuration (see Figure A-2) that is calibrated on-track. This track measuring circuit is configured to cancel out the effect associated with torsional loading due to lateral load or an eccentric vertical load. Figure A-3 shows the installed locations of the four shear strain gauges.

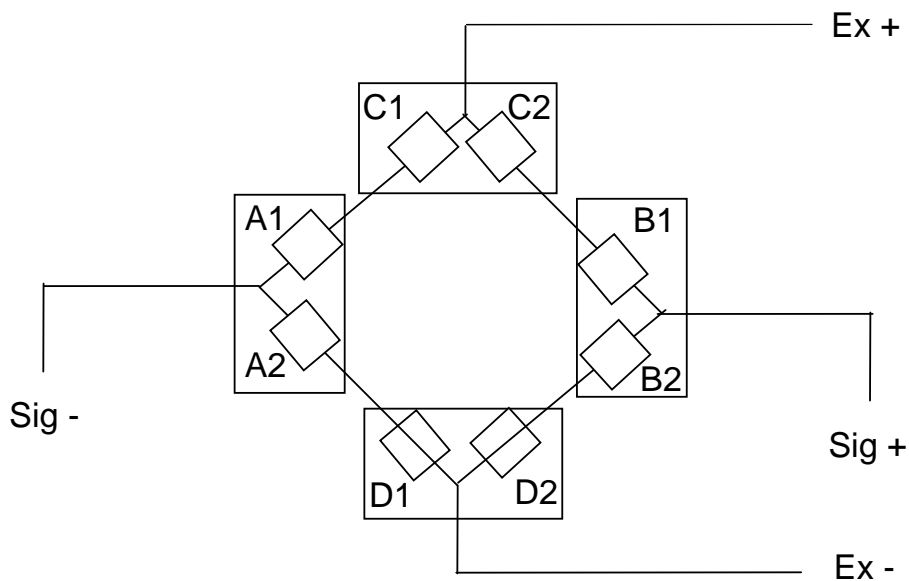


Figure A-2: Vertical (Web chevron method) Wheatstone bridge layout

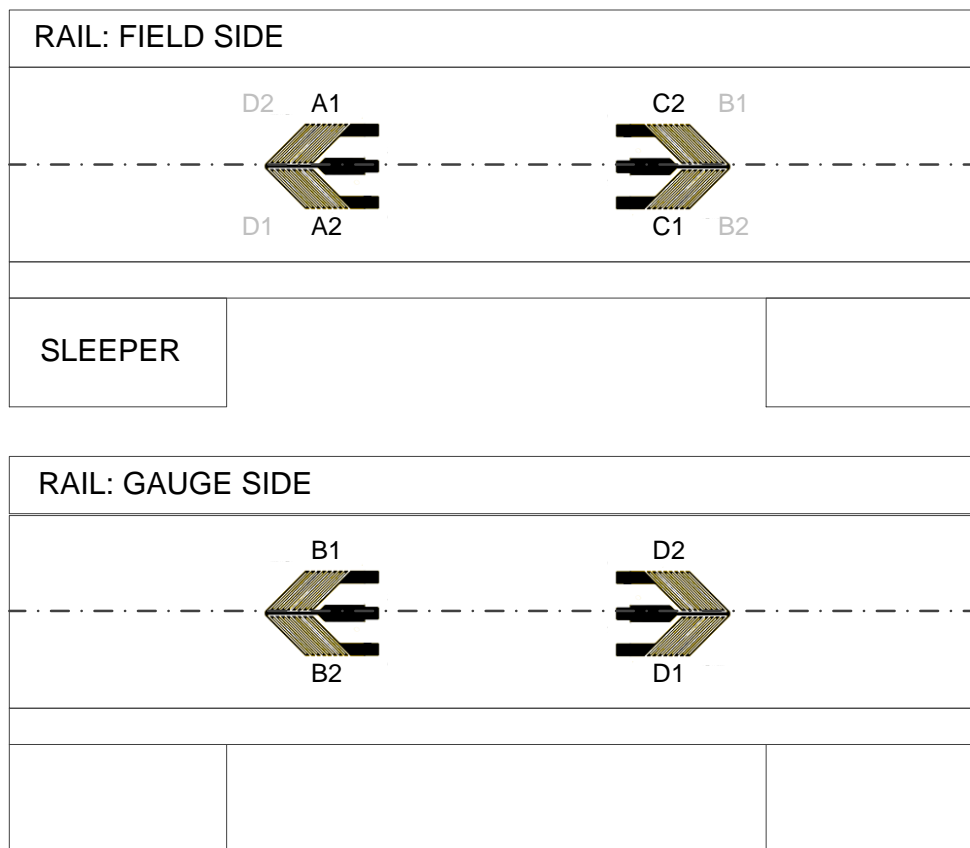


Figure A-3: Strain gauge installation for web chevron method

A.3 Lateral track forces

The lateral force measuring circuit consists of four uni-axial strain gauges connected in a full Wheatstone bridge configuration (see Figure A-4) that is calibrated on-track. This track measuring circuit is configured to measure the strain due to the imposed torsional loading associated with the lateral wheel-rail load and contains a small effect due to an eccentric vertical load. Figure A-5 shows the installed locations of the four uni-axial strain gauges installed at an angle of 45° relative to the rail longitudinal direction.

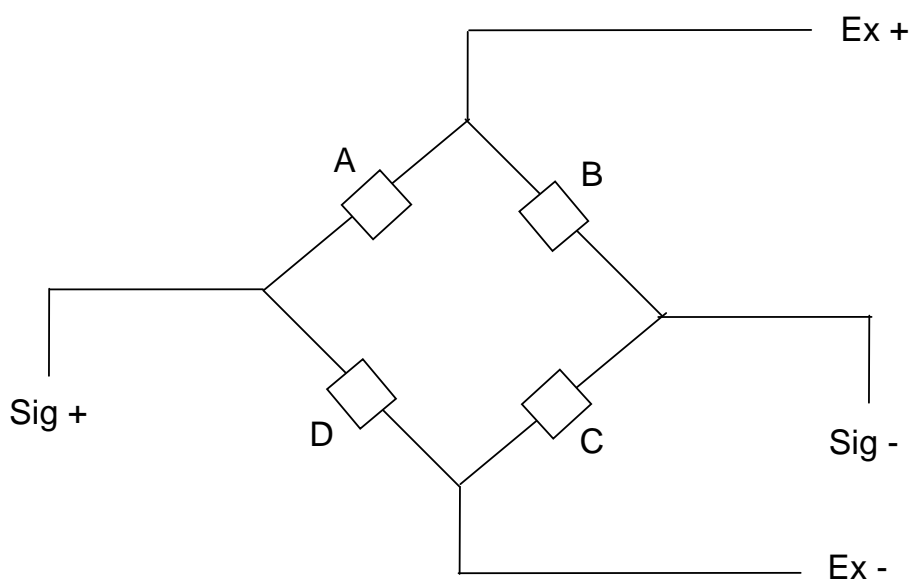


Figure A-4: Lateral (Base chevron method) Wheatstone bridge layout

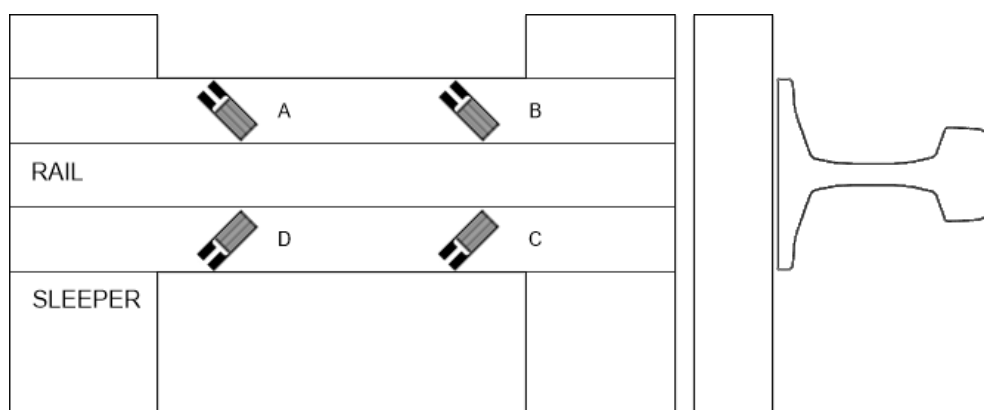


Figure A-5: Strain gauge installation for base chevron method